Wavelet-Automated Recognition System for Power Quality Monitoring

by

Ahmed Mohamed Gaouda

A thesis
presented to the University of Waterloo
in fulfillment of the
thesis requirement for the degree of
Doctor of Philosophy
in
Electrical and Computer Engineering

Waterloo, Ontario, Canada, 2001

Borrower's Page

The University of Waterloo requires the signatures of all persons using or photocopying this thesis. Please sign below, and give address and date.

Abstract

Manufacturing industries are now expected to have substantial increases in flexibility, productivity and reliability as well as increasing quality and value of their products. Automatic Data Processing (ADP), sensitive microprocessor, and power electronic equipment are becoming an essential part to control and automate different assembly lines. However, due to the growing economic pressure, modern electrical equipments are designed to meet their operating limits. This fact means that different equipment manufacturers face a dual responsibility to both desensitize against power disturbances and protect their equipment from power faults. This incompatibility issue, between power system disturbance levels and immunity of equipment, results in a severe impact on the industrial processes, which is known as power quality problem.

To control and improve electric power quality, the sources and causes of any disturbance must be determined. However in order to achieve this, monitoring devices must have the capability to detect, localize those disturbances and further classify and quantify different types of power quality problems for a proper mitigation method.

Different monitoring devices and disturbance analyzers are available that can detect and collect large amount of power quality data. However, there are general problems that exist when dealing with these disturbance analyzers. Off-line analysis is always required. This is due to the design criteria for detection and classification the disturbance. If we utilize the point-by-point comparison technique it is often difficult to build automated recognition system that can on an on-line basis classify the power quality problems such as transient, oscillatory, or non-stationary disturbances. Using this monitoring strategy, one cannot monitor certain class of disturbances or distinguish among similar ones. Furthermore, the selected threshold values (high or low) to be used in detecting different disturbances, may lead to large dimensionality of stored data or undetected important disturbances. The limited capability of Fast Fourier Transform (FFT), while dealing with non-stationary disturbances, is another drawback in the existing monitoring devices.

The goal of this thesis is to overcome the deficiencies that exist in monitoring devices and to design reliable, accurate and a wide-scale power quality monitoring system with superior characteristics. Some of the characteristics in the proposed technique are:

- Fast detection and localization of disturbances that may overlap in time and frequency in a noisy environment.
- On-line classification by extracting discriminative, translation invariant features with small dimensionality, which can represent efficiently the voluminous size of distorted data.
- Analysis of different non-stationary disturbances and measure their indices.
- De-noising ability and high efficiency in data compression and storing.

A wavelet-based power quality automated recognition system is proposed in this thesis. This system will assist in the automated detecting, classifying, and measuring different power system disturbances. This system can overcome the drawback in the existing monitoring devices.

Acknowledgements

First and foremost, I would like to thank and praise Allah almighty for enlightening my way and directing me through each and every success I have or may reach.

I would like to thank the Libyan Ministry of Education for the financial support of this work. I am also indebted to the Canadian Bureau for International Education for their continued assistance through the course of my studies at the University of Waterloo.

I would like to thank my supervisor, Professor Magdy Salama, for his endless encouragement throughout the duration of this research. I would also like to thank members of my doctoral committee, Professor Medhat M. Morcos, Department of Electrical and Computer Engineering, Kansas State University, Professor Aziz Chikhani, Department of Electrical and Computer Engineering, Royal Military College, Professor Dan Stashuk, Department of Systems Design Engineering, University of Waterloo, Professor Claudio Canizares, Department of Electrical and Computer Engineering, University of Waterloo, for their careful reading of the dissertation and valuable comments on my work.

To my friends I would like to express my sincere appreciation, especially Dr. Mansour Sultan and Mr. Salaheddin Kanoun for their invaluable support and suggestions of this dissertation.

My thanks also go to members of the Electrical and Computer Engineering department, especially Wendy Boles for her endless support and help in solving my problems and Gini Ivan-Roth for her everlasting help.

To my mother and father, I would like to extend my profound thanks and appreciation for their deep understanding and moral support. May Allah reward them in this world and in the hereafter.

My wholehearted thanks go to my beloved wife for her love, patience, encouragement, caring and understanding.

Finally, I would like to thank my beloved children for filling my life with fun and pleasantness ever since they were born.

Contents

List of Tables

List of Figures

List of Symbols

$f(t)$	Distorted signal (voltage or current wave form)
N	Number of sampling points
f_{max}	Highest frequency component
f_{sam}	Sampling frequency, $f_{sam} \geq 2f_{max}$
1-D	One dimensional signal "function of single independent variable- time"
2-D	Two dimensional signal "function of two independent variable- time & scale"
$\phi(t)$	Scaling function
$\psi(t)$	Wavelet function
k	Translation factor (shift in time)
j	Scaling factor
c_j	Approximated coefficients of j^{th} resolution level
d_j	Detail coefficients of j^{th} resolution level
c_o	Last approximated coefficients
C_{Signal}	Wavelet coefficients of $f(t)$ at all resolution levels
J	Total number of resolution levels
$h_o(n)$	Scaling function coefficients
$h_1(n)$	Wavelet function coefficients
n	Number of coefficients, $n \in Z$

$H(w)$	Fourier transform of $h(n)$
$< x , y >$	Inner product x and y
A_1	First Approximated version of $f(t)$
D_1	First detail version of $f(t)$
$\Delta\tau$	Distortion duration
x_o	Feature vector
E^2_{Signal}	Energy of the signal in terms of wavelet coefficients
$E^2_{C_o}$	Energy of the approximated coefficients
E^2_{dj}	Energy of the detail coefficients
ΔE	Difference in energy distribution between the distorted signal and the pure one

Chapter 1

Introduction and Objectives

1.1 Introduction

Manufacturing industries are now expected to have substantial increases in flexibility, productivity and reliability as well as increasing quality and value of their products. Automatic Data Processing (ADP), sensitive microprocessor, and power electronic equipment are becoming an essential part to control and automate different assembly lines. However, due to the growing economic pressure, modern electrical equipments are designed to meet their operating limits. This fact means that different equipment manufacturers face a dual responsibility to both desensitize and protect their equipment. This incompatibility issue, between power system disturbance levels and immunity of equipment, results in a severe impact on industrial processes.

Furthermore, the increasing trend towards deregulation pushes generation-transmission-distribution owners to exchange clean power at different ownership locations and to supply high quality power to their customers. With such a multi-ownership generation-transmission-distribution chain, identifying a source of any disturbance, that may affect the customers, becomes a difficult task. This emphasizes the need to identify a baseline of the electric-quality levels at each physical location where the electric power ownership changes.

Monitoring of power quality levels has received a considerable attention in recent years. This interest is even increasing nowadays due to the increasing use of sensitive equipment in customer loads and the impact of the open market trend. In order to monitor power quality problems, traditional disturbance recording systems have been upgraded with real time sampling and analysis features. The ability to extract information rather than data from system response is an important requirement for modern power quality monitors.

Power Quality is the combination of voltage quality and current quality. It is defined according to its effect on different parts of the power system. It is defined as the reliability of the system from the electric utility point of view. Equipment manufacturers defined it as the changes in the characteristics of the power supply. The customers, who are most affected by power quality issues, defined it as any power problem manifested in voltage, current, or frequency deviations that results in the failure or misoperation of their equipment [1-23].

Poor quality of the electric power is normally caused by power line disturbances, shown in Figure 1.1, such as oscillatory and impulsive transients, glitches, sags, swells, over voltages, and harmonic distortion. As indicated in [6], what were considered as an ignored variation in power supply may now bring whole factories to stand-still. A power interruptions or 30% voltage sag lasting mere hundredths of a second, for example, can reset programmable controllers for an assembly line, while adjustable-speed drivers for motorized equipment on the assembly line may themselves be sensitive to voltage harmonics or transients.

It is not easy to make a good estimation of the cost of pollution in the quality of power. According to [6] and [15], poor power quality in the United States causes about $13.3 billion in damage per year. Following a voltage sag, for example, the restarting of the assembly lines may required clearing the lines of damaged work, restarting boilers, and reprogramming automatic controls for a typical cost of $ 50,000 per incident. One glass plant estimates that a five cycle interruption - an outage of less than a tenth of a second- can cost about $ 200,000, and a major computer centre reports that a two second outage can cost some $ 600,000.

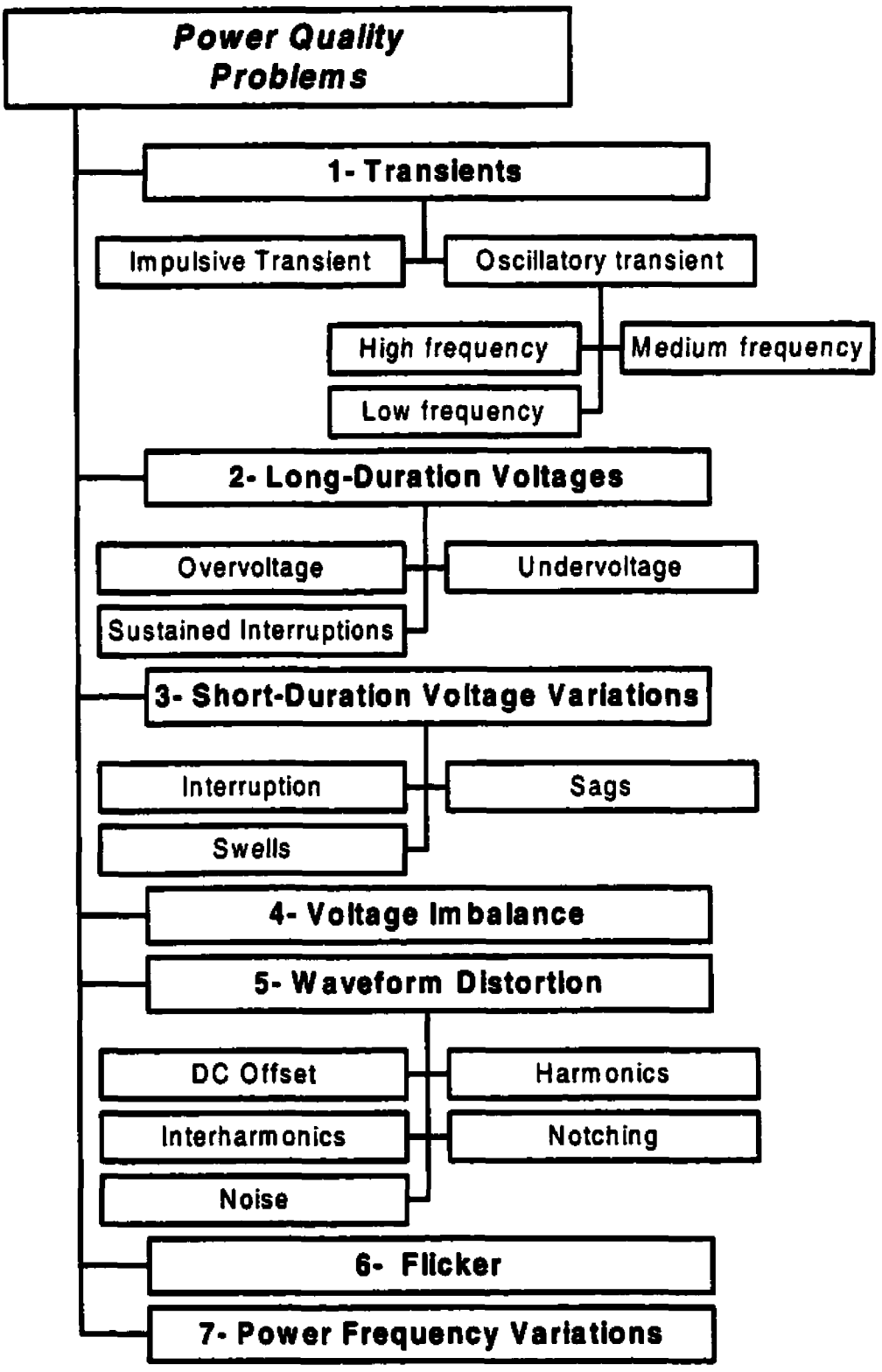

Figure 1.1: Electric power quality problems

Thus, while only a few short years ago, power quality monitoring was a rare feature to be found in instruments, it is becoming much more commonplace in commercially available equipment. The products and services related to power quality now represent a multibillion-dollar market in the United States alone [15].

Power quality monitoring is an important action to quantify the baseline of the electric-quality levels throughout the generation-transmission-distribution chain and customers coupling points. To control and improve electric power quality, the sources and causes of any disturbance must be determined. However in order to achieve this, monitoring devices must have the capability to detect and localize those disturbances and then further classify and quantify different types of power quality problems.

Different monitoring devices and disturbance analyzers are available that can detect and collect large amounts of power quality data. However, there are general problems that exist when dealing with these disturbance analyzers. Off-line analysis is always required. This is due to the design criteria for detection and classification of the disturbance. If we utilize the point-by-point comparison technology it is often difficult to build an automated recognition system that can, on an on-line basis, classify the power quality problems such as transient, oscillatory, or non-stationary disturbances. Using this monitoring strategy, one cannot monitor certain classes of disturbances or distinguish among similar ones. Furthermore, the selected threshold values (high or low) to be used in detecting different disturbances, may either lead to a large dimensionality of stored data or to undetected important disturbances. The limited capability of the Fast Fourier Transform (FFT), when dealing with non-stationary disturbances, is another drawback in existing monitoring devices.

1.2 Research Objectives

The goal of this thesis is to design a sophisticated power quality monitoring system with improved detection characteristics. Some of the characteristics in the proposed technique are:

- Fast detection and localization of disturbances that may overlap in time and frequency in a noisy environment.
- On-line classification by extracting discriminative, translation invariant features with small dimensionality, which can represent efficiently the voluminous size of distorted data.
- Analysis of different non-stationary disturbances and measures of their indices.
- De-noising ability and high efficiency in data compression and storing.

A wavelet-based power quality automated recognition system is proposed in this thesis. This system will assist in the automated detection, classification, and measurement of different power system disturbances. This system can overcome the drawbacks in existing monitoring devices.

1.3 Thesis Layout

Chapter 2 presents a general review of power quality problems and their effects on a power system. Classification of different power quality problems, according to IEEE standard 1159 [16], is reviewed. A summary of the utilized detection techniques in different monitoring devices is also discussed in this chapter. In Chapter 3 a comprehensive survey of the wavelet transform and its application to power systems is discussed. The efficiency of wavelet transform and multi-resolution signal decomposition for transient analyses, system protection, equipment testing, and monitoring power quality problems are discussed. The mathematical background of the wavelet transform and multi-resolution analysis is presented in Chapter 4. The analysis and synthesis procedure for implementing multi-resolution analysis is discussed. This Chapter presents different signal processing techniques that are used to implement wavelet transform and multi-resolution analysis. The property of time-frequency localization and the partitioning of a distorted signal's energy at different resolution levels are also presented in this chapter.

The goal of this thesis is to design a reliable, accurate and wide-scale power quality monitoring system with superior characteristics. Utilizing the wavelet-based techniques to construct the proposed automated recognition system is presented in Chapters 5, 6, 7 and 8. Chapter 5 highlights the procedure to map the distorted signal into the wavelet domain. A wavelet-based procedure to detect and localize any disturbance, in a noisy environment, is presented. In Chapter 6, a new technique is proposed that has the ability to decompose any distorted signal into different building blocks and extract time-frequency features simultaneously from each block. The dimensionality of data is mapped into a small number of interpretable features. These features are proven to be very efficient in auto-classifying different power quality problems that overlap in time and frequency. Chapter 7 presents a new measurement technique that can measure accurately a wide range of different power quality problems. The proposed technique is implemented to measure different parameters in a power system. This chapter also introduces a new wavelet-based procedure to monitor the non-rectangular variation of RMS value in the signal. Chapter 8 is devoted to develop a new procedure that will compress and store the distortion event efficiently. This procedure is based on wavelet analysis, where a small set of wavelet coefficients represents the disturbances will assist in achieving this goal. This procedure will replace the existing technique of storing all sampling points of a disturbance. Finally, Chapter 9 offers the main conclusions of this work and suggests topics for future research.

Chapter 2

Power Quality Problems

2.1 Introduction

A Power Quality Problem is defined as: Any power problem manifested in voltage, current, or frequency deviations that results in the failure or miss-operation of customer equipment. It has been documented in [1] that power-related problems cost U.S. companies approximately $ 26 billion a year in lost time and revenue. As a result there is increasing interest in the power quality problems. The sources of power quality problems are many and in the following sections we will discuss some of these problems.

There are fundamental changes that take place in the loads. Current electronic and power electronic equipment has become much more sensitive than their counterparts 10 or 20 years ago. Furthermore, some of this equipment may generate disturbances and reduce the power quality level of the system. This causes a significant impact on the quality of the power. Such equipment, which utilize *microelectronics*, are responsible for a growing category of loads (residential, commercial, and industrial) that are sensitive to variations of the power supplied. Large-scale integration (LSI) and very large scale integration (VLSI) of modern chips have resulted in faster and more complex components. An additional advantage for such equipment is higher memory per unit surface, with fewer requirements of voltage and power levels, thus reducing energy consumption and ventilation needs. Unfortunately, these types of equipment are becoming more easily disturbed as the voltage level is reduced.

Power electronics have produced a new generation of low-cost, high-capacity equipment, thus expanding its use. Nevertheless, this same equipment is responsible for disturbances in the power system, to which microelectronic equipment is susceptible. It is estimated that the portion of electric energy generated for microelectronic loads that are processed by power electronics will increase from the present level of 10%-20% up to 50%-60% by the year 2010 [6][8][14].

While these changes in the loads are taking place, utilities and industries are continuing to install *capacitor banks* for voltage control and loss reduction. These capacitors have a significant influence on power quality problems, since they are working as a "sink" for high frequency currents and can worsen the situation by increasing harmonic resonance levels in the system.

The open competition power market is another factor that increases the interest in power quality and increases the need for standardization. Electricity is now being viewed as a product with certain characteristics, which have to be measured, predicted, guaranteed, improved, etc. The electric customer can buy electric energy from one company, transmit it through the transmission lines of another company and pay the local utility for the actual connection to the system. It is no longer clear who is responsible for the reliability and the quality of the supply. Designing a system with high quality of supply, for limited cost, is a technical challenge that appeals to many in the power industry.

Finally, the era of digital signal processing techniques and the availability of electronic devices to measure and show waveforms has certainly contributed to the interest of improving power quality and finding its indices. Different techniques can be implemented in hardware and installed on a system to give on-line "real-time" applications.

2. 2 Classifications of Power Quality

In order to be able to classify different types of power quality problems, the characteristics of each type must be known. In general, power quality phenomena are divided into two groups: steady state and non steady state. Different power quality problems are classified as in [2] and [16] and will be discussed below:

2.2.1 Transients

Transients refer to variations in the voltage waveform, which results in over-voltage conditions for a fraction of a cycle of the fundamental frequency. Transients are classified as impulsive or oscillatory.

2.2.1.1 Impulsive transient

It is a sudden change in the steady-state condition of the voltage or current. It is unidirectional in polarity. Impulsive transients are normally characterized by their rise and decay times. The most common cause of impulsive transients is lightning. The general characteristics of impulsive transients are summarized in Table 2.1 and shown in Figure 2.1 [2] and [16].

Table 2.1: Characteristics of impulsive transient and typical causes and solutions

A - Impulsive Transient	Typical Spectral	Typical Duration	
1 - Nanosecond	5 *n* s rise	< 50 ns	
2 - Microsecond	1 μ s rise	50ns – 1 ms	
3 - Millisecond	0.1 ms rise	< 1 ms	
Method of Characterization	Peak magnitude, rise time, duration		
Typical Causes	Lightning, Electro-Static Discharge, Load switching		
Examples of solutions	Surge arresters, Filters, Isolation Transformers.		

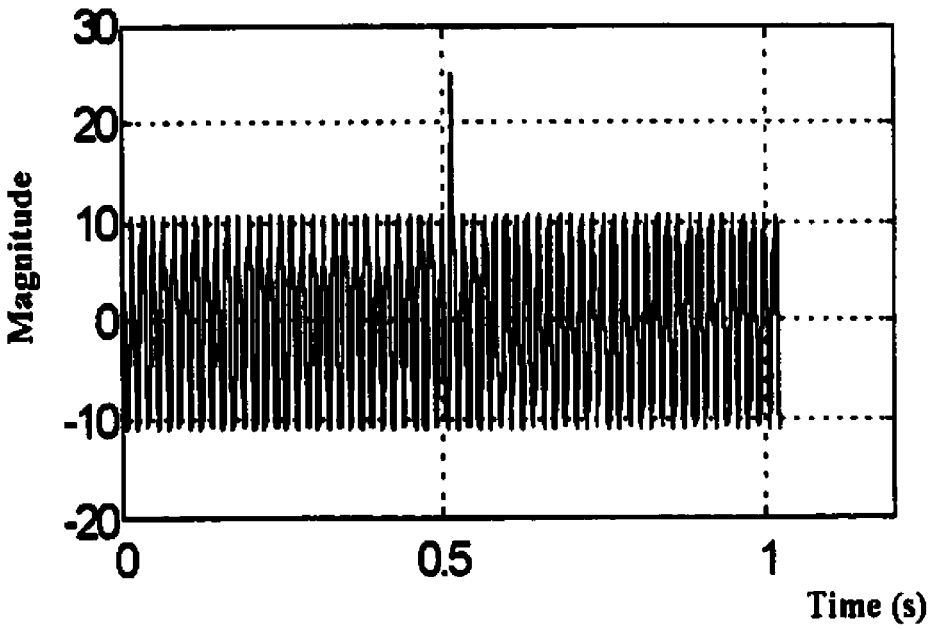

Figure 2.1: Impulsive transient

2.2.1.2 Oscillatory transient

It is a sudden change in the steady-state condition of the voltage or current. It includes both positive and negative polarity values. It is described by its spectral content, duration, and magnitude. Using the spectral content the oscillatory transient is classified into three subclasses:

- High-frequency oscillatory transient
- Medium-frequency oscillatory transient
- Low-frequency oscillatory transient

The general characteristics of different oscillatory transients are summarized in Table 2.2 and shown in Figure 2.2 as indicated in [2] and [16].

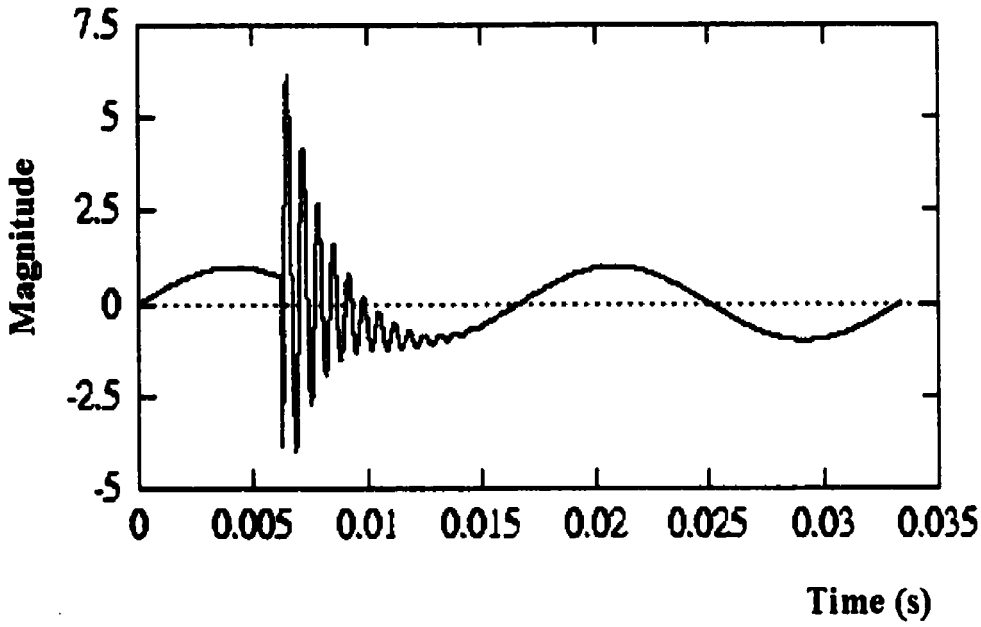

Figure 2.2: Oscillatory transient

Table 2.2: Characteristics of oscillatory transient and typical causes and solutions

B – Oscillatory Transient	Typical Spectral Content	Typical Duration	Typical voltage Magnitude
1 - Low Frequency	< 5 kHz	3 - 50 ms	0.4 pu
2 – Medium Frequency	5.500 kHz	20us	0.8 pu
3 - High Frequency	0.5 - 5 M Hz	5 us	0.4 pu
Method of Characterization	Waveforms, Peak Magnitude, Frequency components		
Typical Causes	Line/Cable switching, Capacitor switching, Load switching		
Solutions	Surge arresters, Filters, Isolation Transformers.		

2.2.2 Long-Duration Voltage Variation

A Long-duration variation is described as a root-mean-square (rms) deviation at power frequencies for a duration longer than one minute. It is caused by load variations on the system or system switching operations. It can be either over-voltage or under-voltage.

2.2.2.1 Over-voltage

Over-voltage is an increase in the rms ac voltage to greater than 110% at the power frequency for a duration longer than 1 minute.

2.2.2.2 Under-voltage

Under -voltage is a decrease in the rms ac voltage to less than 90% at the power frequency for duration longer than 1 minute.

2.2.2.3 Sustained Interruptions

Sustained interruption is a zero supply voltage for duration longer than one minute. The general characteristics of the over-voltage, the under-voltage, and the sustained interruptions are summarized in Table 2.3 as indicated in [2] and [16].

Table 2.3: Characteristics of over voltage, under voltage, and sustained interruptions

PQ Type	Spectral Content	Typical Duration	Typical voltage Magnitude
1- Over-voltage	-	> 1 min	1.1 - 1.2 pu
2 – Under-voltage	-	> 1 min	0.8 - 0.9 pu
3- Sustained Interruption	-	> 1 min	0.0 pu
Characterization	RMS vs Time, Statistics,		
Typical Causes	Motor starting, Load variations		
Solutions	Voltage regulators, Ferroresonance Transformer		

2.2.3 Short-Duration Voltage Variations

This category includes voltage sags, swells, and short interruptions. Each type of variation can be designated as instantaneous, momentary, or temporary, depending on its duration as defined in Table 2.4.

2.2.3.1 Interruption

It is a reduction in the supply voltage or load current to less than 0.1 pu for a period of time not exceeding one minute. The interruptions are measured by their duration since the voltage magnitude is always less than 10% of the nominal. Figure 2.3 shows a voltage interruption in the power signal.

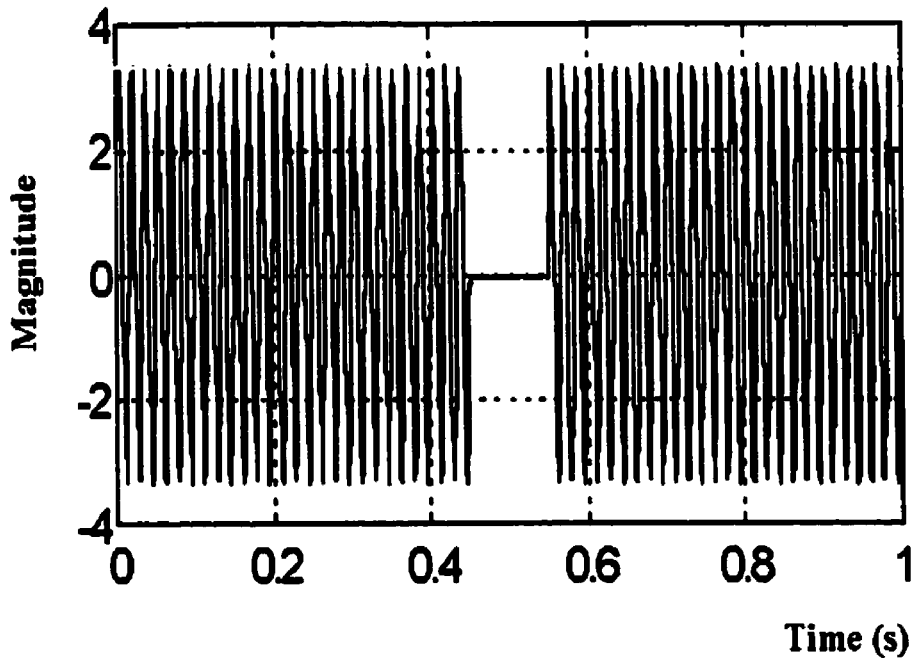

Figure 2.3: Voltage Interruption

2.2.3.2 Sags (dips)

Sag is a decrease in rms voltage or currents to between 0.1 and 0.9 pu at the power frequency for a duration of from 0.5 cycles to 1 minute. Voltage sags are usually associated with system faults but can also be caused by connecting of heavy loads or starting of large motors. Figure 2.4 shows a voltage sag in the power signal.

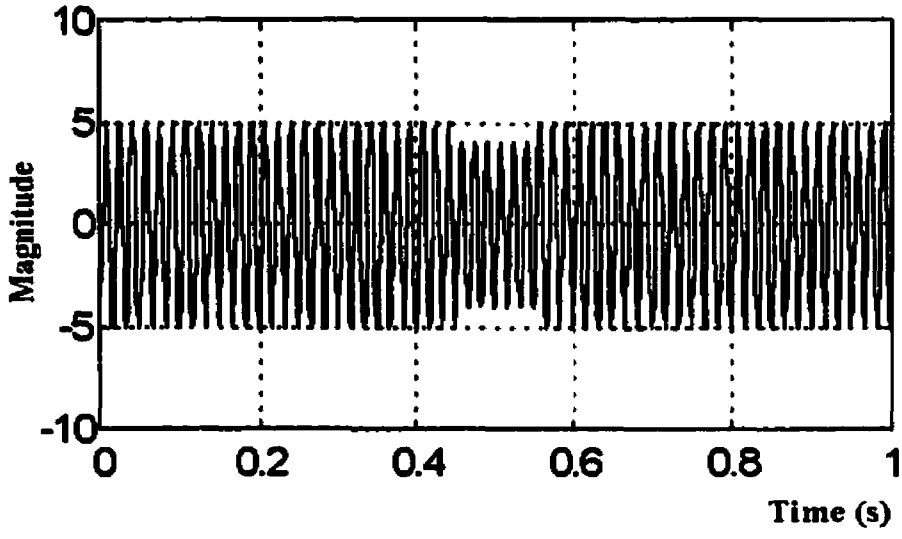

Figure 2.4: Voltage sag

2.2.3.3 Swells

A swell is defined as an increase in rms voltage or current to between 1.1 and 1.8 pu at the power frequency for a duration of from 0.5 cycles to 1 minute. As with sags, swells are usually associated with system fault conditions, but they are not as common as sags. Figure 2.5 shows a voltage swell in the power signal.

The general characteristics of the interruptions, voltage-sag and voltage-swell are summarized in Table 2.4 and shown in Figures 2.3, 2.4 and 2.5 as in [2] and [16].

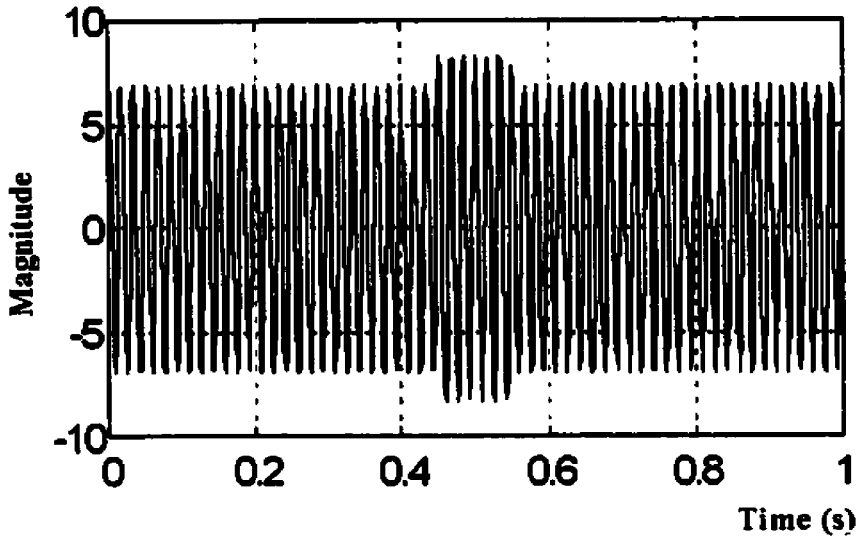

Figure 2.5: Voltage swell

2.2.4 Voltage Unbalance

It is defined as the ratio of either the negative- or zero-sequence component to the positive-sequence component. Single-phase loads on three-phase circuits are the primary source of voltage unbalance.

2.2.5 Waveform Distortion

Waveform distortion is defined as a steady-state deviation from an ideal sine wave of power frequency. It is characterized by the spectral content of the distorted signal. There are five types of waveform distortion:

Table 2.4: Characteristics of voltage sag, voltage swell, and interruptions

Short Duration voltage variation in Electric Power	Spectral Content	Typical Duration	Typical voltage Magnitude
A – Instantaneous			
Sag	-	0.5 - 30 cycles	0.1 - 0.9 pu
Swell	-	0.5 - 30 cycles	1.1 - 1.8 pu
B - Momentary			
1 – Interruption	-	0.5 cycles - 3 s	< 0.1 pu
2 – Sag	-	30 cycles - 3 s	0.1 - 0.9 pu
3 - Swell	-	30 cycles - 3 s	1.1 - 1.2 pu
C - Temporary			
1 – Interruption	-	3 s - 1 min	< 0.1 pu
2 – Sag	-	3 s - 1 min	0.1 - 0.9 pu
3 - Swell	-	3 s - 1 min	1.1 - 1.2 pu
Characterization **Sags and Swells**	RMS vs Time, Magnitude, and Duration		
Typical Causes	Remote System Faults, large loads, and non linear loads for short duration		
Examples of solutions	Ferroresonance Transformers, Energy storage technologies, UPS		
Characterization **Interruptions**	RMS vs Time, Magnitude, and Duration		
Typical Causes	System Protection (Breakers and Fuses), Maintenance		
solutions	Backup Generators, Energy storage technologies, UPS		

2.2.5.1 DC offset:

DC offset is defined as the presence of dc voltage in an ac power system. It occurs as a result of a geomagnetic disturbance or due to the effect of half-wave rectification. DC offset can cause

transformer saturation that can increase the transformer temperature and reduce its life. Direct current may also cause the electrolytic erosion of grounding electrodes and other connections.

2.2.5.2 Harmonic

A harmonic distortion is a sinusoidal voltage or current with frequencies that are integer multiples of the frequency at which the supply system is designed to operate. It originates from non-linear characteristics of devices and loads. Harmonic distortion levels are described by the harmonic spectrum with magnitudes and phase angles of each individual harmonic component. Total harmonic distortion (THD) is used as a measure to calculate the harmonic distortion within the signal. The THD can be calculated as:

$$THD = \sqrt{\sum_{h=2}^{h_{MAX}} (V_h)^2} \Big/ V_1 \qquad (2.1)$$

where V_h is the rms value of harmonic component h of the quantity V. Figure 2.6 illustrates a harmonic distorted signal.

2.2.5.3 Inter-harmonics:

Inter-harmonics are defined as voltages or currents having frequency components that are not multiples of the frequency at which the supply system is designed to operate. The main source of inter-harmonic wave-form distortion are static frequency converters, induction motors, and arcing devices.

The general characteristics of the DC offset, harmonic, and inter-harmonic are summarized in Table 2.5 as in [2] and [16].

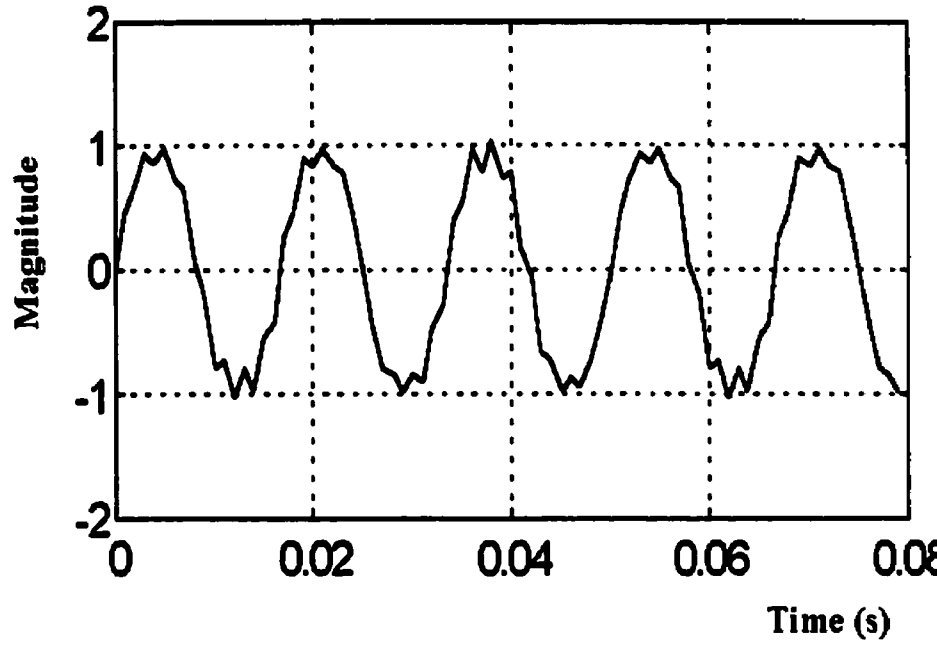

Figure 2.6: Harmonic distorted signal

Table 2.5: Characteristics of DC offset, harmonics, and inter harmonics

Waveform Distortion	Typical Spectral Content	Typical Duration	Typical voltage Magnitude
1 - DC offset		steady state	0 - 0.1 %
2 - Harmonics	0-100th harmonic	steady state	0 - 20 %
3 - Inter-Harmonics	0.6 kHz	steady state	0 - 2%
Method of Characterization	Harmonic Spectrum, Total Harmonic Distortion, Statistics		
Typical Causes	Non-Linear Loads, System Resonance		
Examples of solutions	Active and Passive Filters, Transformers		

2.2.5.4 Notching

Notching is defined as periodic voltage disturbance caused by normal operation of power electronic devices when current is commutated from one phase to another. Figure 2.7 shows a voltage notching in the power signal.

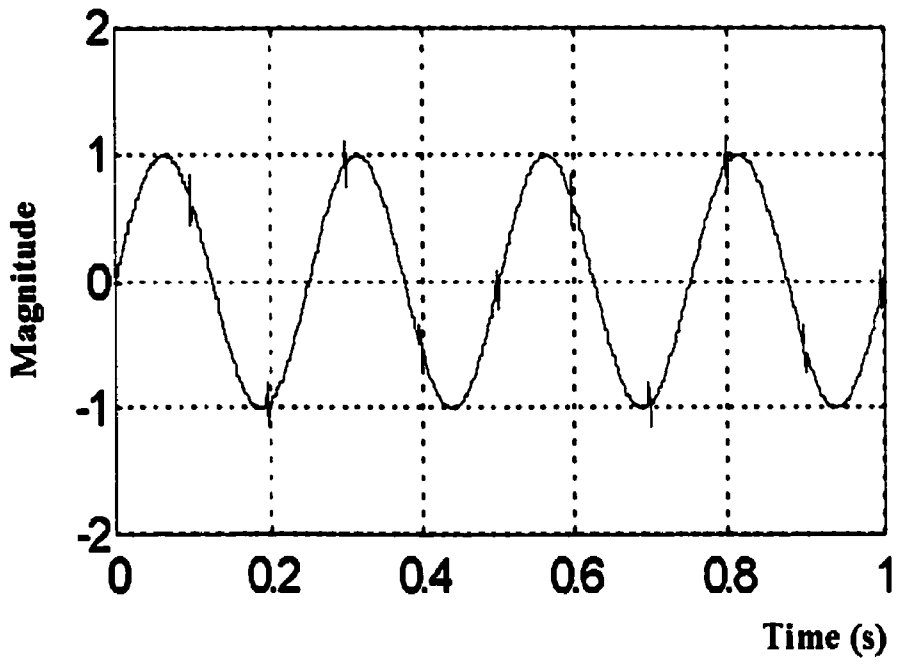

Figure 2.7: Voltage notching

2.2.5.5 Noise

It is defined as unwanted electrical signals with wide-band spectral content lower than 200kHz superimposed upon the power system voltages or currents in the phase conductors, or neutral. It can be caused by power electronic devices, control circuits, arcing equipment, loads with solid-state rectifiers, and switching power supplies. Noise problems are often due to improper grounding that fails to conduct noise away from the power system. Using filters, isolation transformers, and line conditioners can mitigate the noise problem. Figure 2.8 shows a distorting noise superimposed on the power signal.

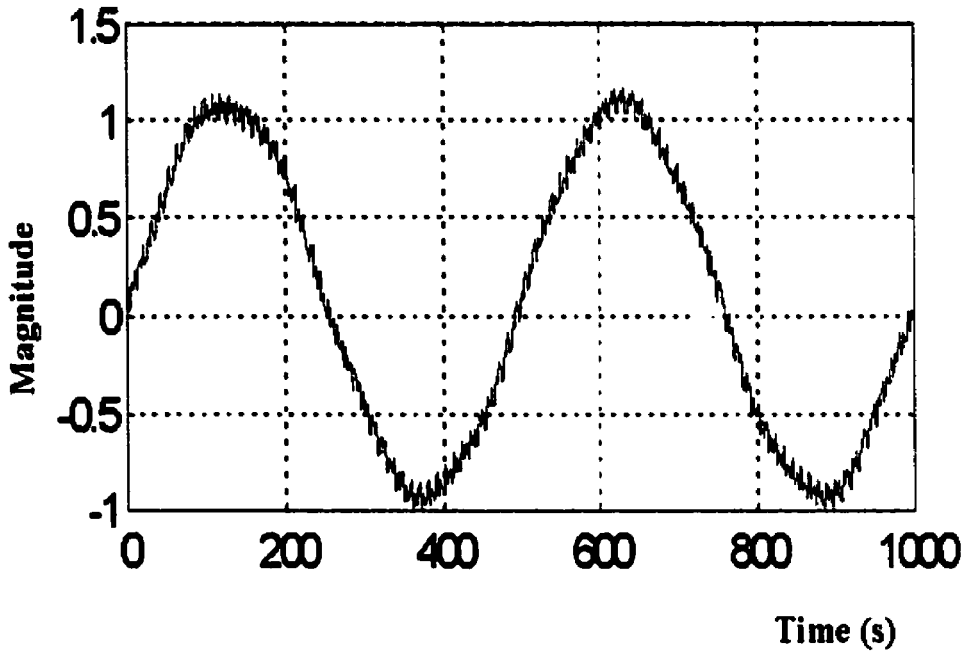

Figure 2.8: Electric noise

2.2.6 Voltage Fluctuation (Flicker)

Voltage fluctuations are systematic variations of the voltage envelope or a series of random voltage changes. Their magnitude do not normally exceed 0.9 to 1.1 pu. The main sources of voltage fluctuations are continuous rapid variations of loads. The continuous variation in the current magnitudes can cause voltage variations that are often refereed to as flicker. One of the most common causes of voltage flickers is the arc furnace. The flicker signal is defined by its rms magnitude expressed as a percent of the fundamental. Figure 2.9 illustrates the voltage flicker wave shape.

2.2.7 Power frequency variation

It is defined as the variation of the power system fundamental frequency from its nominal value (e.g., 50 or 60 Hz). The power frequency is directly related to the rotational speed of the generators. Frequency variations can be caused by faults on the bulk power transmission system, a large block of load being disconnected, or a large source of generation going off line.

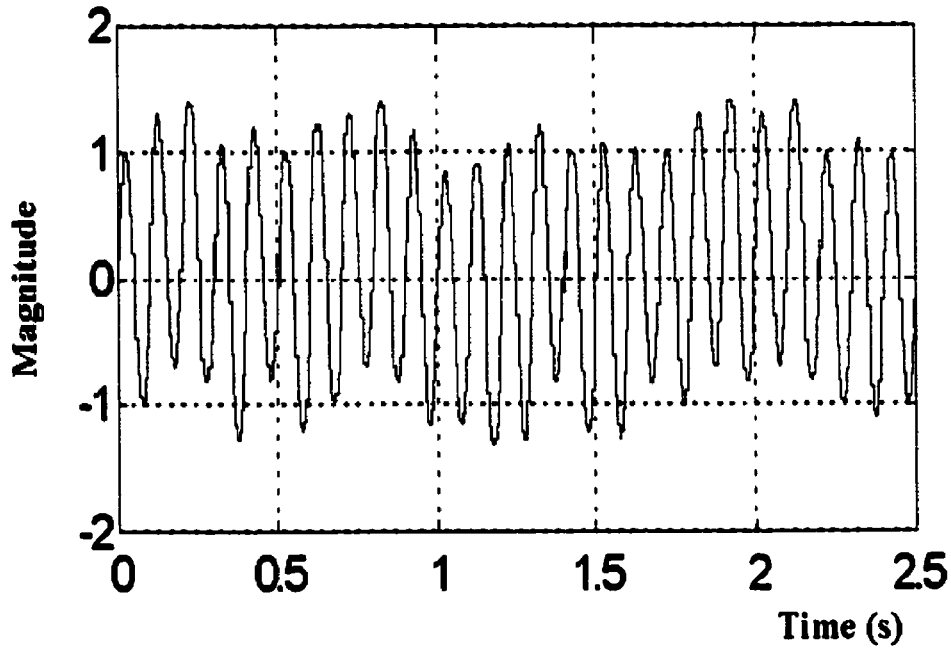

Figure 2.9: Voltage Fluctuation

Table 2.6: characteristics of voltage imbalance, notching, noise, voltage fluctuation, and power frequency variations

PQ type	Typical Spectral Content	Typical Duration	Typical voltage Magnitude
Voltage Imbalance	-	steady state	0.5 - 2.0%
Notching	-	steady state	
Noise	broad-band	steady state	0 - 1 %
Voltage Fluctuations	< 25 Hz	Intermittent (non-stationary)	0.1 - 7%
Power Frequency Variations	-	< 10 s	

2.8 Costs of interruptions

The frequency of interruption and its duration can influence the interruption costs. Reliability of a system is not a single-dimensional quantity. An increase in the number of components in the system can reduce its reliability. A more reliable system is more expensive to build and operate.

The cost of an interruption consists of a number of terms as follows:

1. *Direct costs* which are directly attributable to the interruption. This comes in the form of lost of raw material, lost of production, and salary costs during the non-productive period.

2. *Indirect costs* which is not easy to evaluate. A company can lose future orders when an interruption leads to a delay in delivering product. This might lead the customer to take insurance against loss of its raw material or it might install a battery backup or even move the plant to an area with less supply interruptions. The main problem with the indirect costs is that it cannot be attributed to a single interruption, but to the quality of the whole supply.

3. *Non-material inconvenience* that cannot be expressed in money. A radio station interruption that prevents the listeners from being able to enjoy the broad casting is an example of such inconvenience.

For large industrial and commercial customers an inventory of all direct and indirect costs can be made, and this can be then used in the system design and operation. However, for small domestic customers it is often the non-material inconvenience that has a larger influence on the decision than the direct or indirect costs.

Due to the increasing costs of the power quality problems, different manufactures introduce a wide range of monitoring devices. These devices are implemented to detect and monitor different disturbances that may affect the quality of the power systems. The following section describes different power quality monitoring devices used for measuring a wide range of disturbances, (see Figure 2.10).

2. 9 Review of Monitoring Techniques

The monitoring requirement depends on the type of power quality problem. Some problems require monitoring for several months and others for several hours. The most important monitoring devices are:

2.9.1 Disturbance Analyzers

Disturbance analyzers have been developed specifically for power quality measurements. They typically measure a wide variety of system disturbances from very short duration transient voltages to long variations, outages or under-voltages. As indicated in [2], these devices basically fall into two categories:

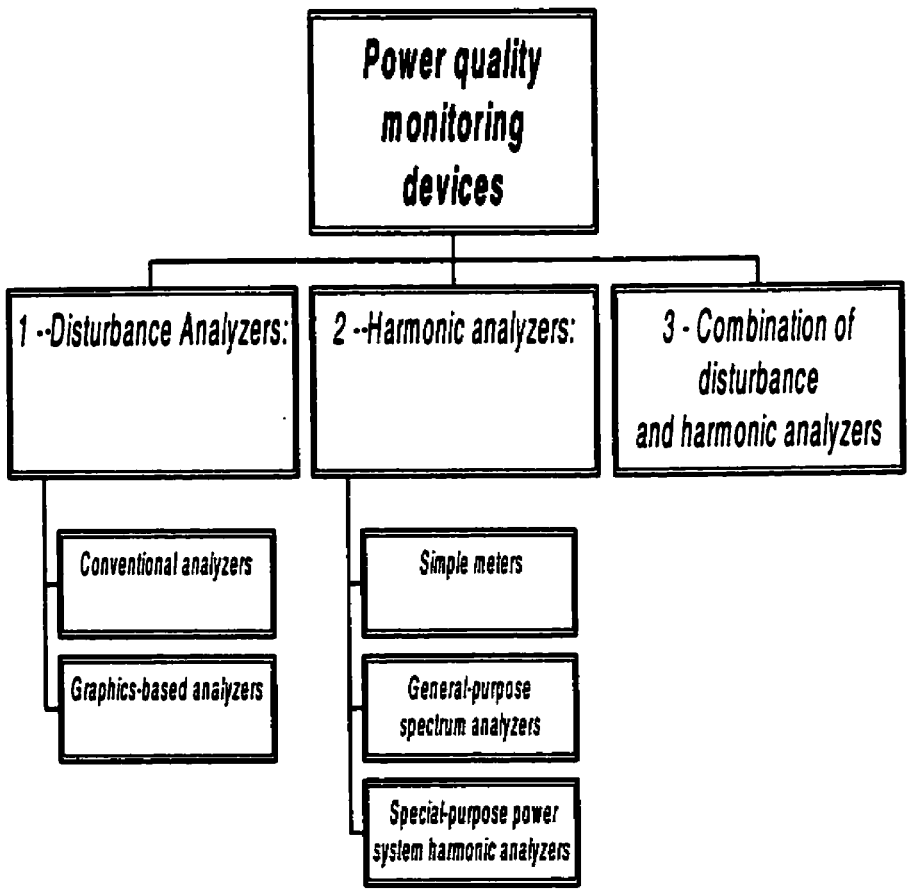

Figure 2.10: Different methods for monitoring power quality levels

1 - Conventional analyzers that summarize events with specific information such as over/under-voltage magnitudes, sags/surge magnitude and duration, transient magnitude and duration, etc.

2 - Graphics-based analyzers that save and print the actual waveform along with the descriptive information, which would be generated, by one of the conventional analyzers.

However, using these devices, it is often difficult to classify the type of the disturbance or transient from the available information. Therefore, to overcome this problem, Graphics analyzers must be used with the conventional one.

2.9.2 Harmonic analyzers

Disturbance analyzers have very limited harmonic analysis capabilities. Fast Fourier Transform (FFT) calculations capability has been added to some disturbance analyzers to obtain a clear picture of the harmonic content within the distorted signal. As indicated in [2], three categories of instruments are considered for harmonic analysis:

1 - Simple meters: for making a quick check of harmonic content, up to the 50^{th} harmonic, as well as the total harmonic distortion (THD) at the problem location.

2 - General-purpose spectrum analyzers: Used for general harmonic signal analysis. They are designed to perform spectrum analysis for a wide range of applications.

3 - Special-purpose power system harmonic analyzers: Designed for power system harmonic analysis. These are based on the FFT with sampling rate specifically designed for determining harmonic components in power signals. They can generally be left in the field and include communications capability for remote monitoring.

2.9.3 Combination of disturbance and harmonic analyzers

The most recent instruments combine limited harmonic sampling with disturbance monitoring. The output is graphically based and the data are gathered over telephone lines into a central database. Statistical analysis can then be performed on the data. It monitors three phase voltages and currents plus the neutral simultaneously, which is very important for diagnosing power quality problems.

2.10 Summary and Comments on Currently Used Monitoring Devices

Different monitoring devices (data loggers) are available that can collect large amount of data. The triggering strategies used by these instruments are based on a set of thresholds. The sensitivity of these loggers depends on a selected threshold level. High threshold levels result in missing desired disturbances and low threshold levels result in capturing a large number of waveforms. Using this monitoring strategy, one cannot monitor certain classes of disturbances or distinguish among similar ones. Off-line analysis is always required which use different disturbance analyzers to extract the disturbances of interest and classify them [2].

There are general problems that exist when dealing with disturbance analyzers to classify different power quality problems. Some of these problems are discussed below:

- The criteria for distortion detection and classification. This method is based on point-by-point comparison of the rms values of sampling points of the distorted signal with its corresponding pure signal. If the difference is larger than a pre-set threshold, then the monitor will start detecting this disturbance. These types of monitors can provide the ability to detect on-line any disturbance, however, it is often difficult to determine on an on-line bases the characteristics of transient, oscillatory, or non-stationary disturbances. Therefore, it is imperative to have the waveform capture capability of the graphic based disturbance analyzers for a detailed off-line analysis of different stored disturbances. For the sake of discussion, the following three

cases present such type of disturbances which need more detailed analysis for classification and can not be classified on an on-line bases using the existing disturbance analyzers:

Case 1: Capacitor Switching phenomena: Figure 2.11 shows a capacitor-switching phenomenon. The frequency content in the signal during the distortion event and its duration are two important features to classify it as an oscillatory transient with low, medium, or high frequency as indicated in IEEE Std.1159 [16]. Using point-by-point comparison, off-line analysis is always required to classify such disturbances.

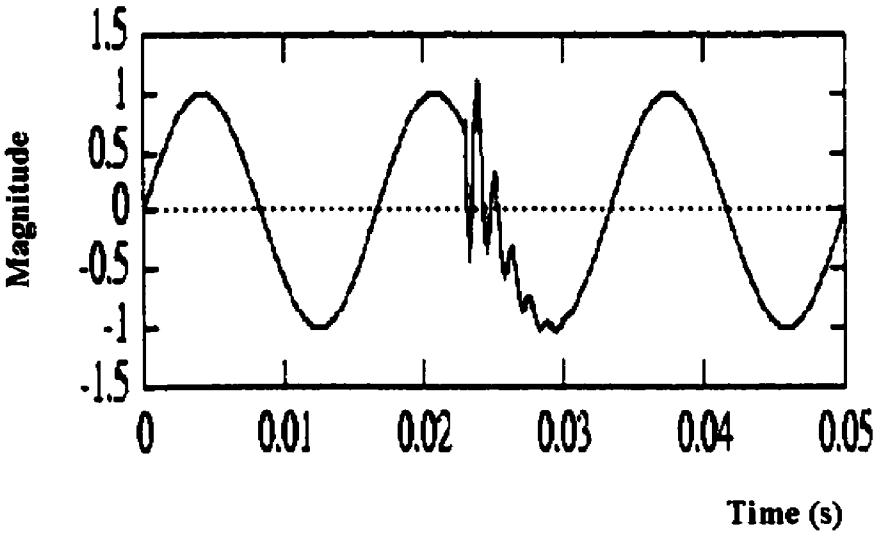

Figure 2.11: Capacitor switching phenomena

Case 2: Two disturbances at the same window: The signal is contaminated with low and high frequency components and a one-cycle sag phenomenon at 0.5s as shown in Figure 2.12. These disturbances can be detected and localized on-line, however, detailed off-line analysis is also necessary to classify them. The Fast Fourier Transform (FFT) will be used to monitor the harmonic content in the signal and point-by-point comparison is needed to detect the sag event. Furthermore, the duration of this disturbance can not precisely determined.

Case 3: Commutation Failure event: Figure 2.13 shows a distortion event detected and localized on the inverter ac-side of HVDC system. This disturbance is due to a commutation failure in the inverter of the HVDC system. Again using existing techniques, which implement point-by-point comparison, this disturbance is classified as a swell phenomenon. However, there is no information that can be extracted during the non-stationary part of the signal (1.012s to 1.051s). This information represents important features to be used to distinguish among similar power quality problems and it can help in identifying the source of the disturbance.

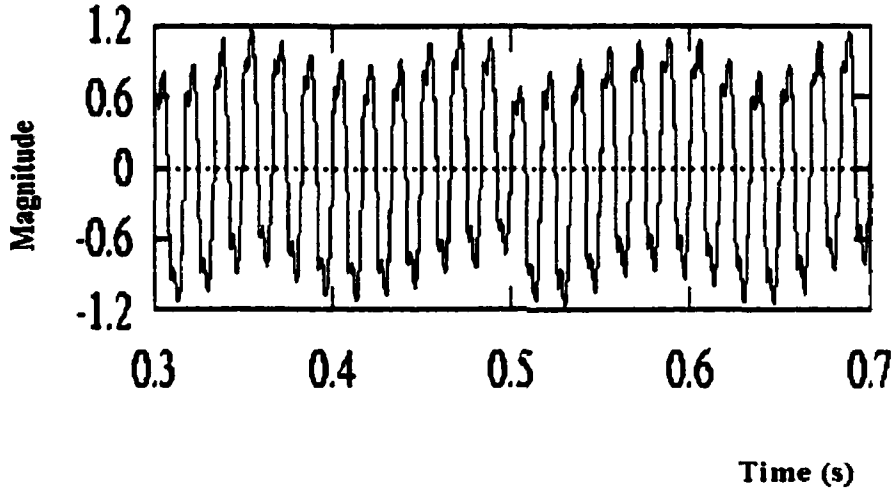

Figure 2.12: Sag event in a harmonic distorted signal

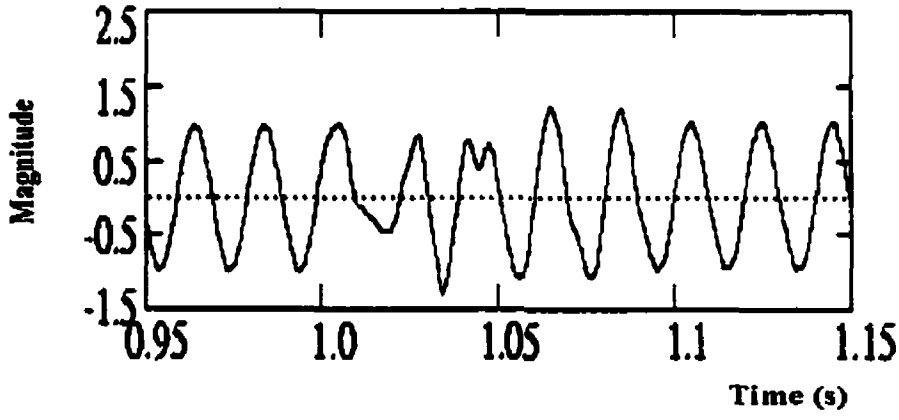

Figure 2.13: Commutation failure at inverter AC side of HVDC system

- The second problem is the large dimensionality of the stored data. This is due to the selected threshold values to be used in detecting different disturbances. Small threshold values will generate large amounts of data and large threshold values will allow certain disturbances to escape from the detection process. It has been documented in [9] that a survey of power quality data of distribution system results in 40MB per day or about 15 GB per year for a modest 200 PQNodes. A major concern arising from the auto-classification of such a large data is the complicity of the discrimination process. The parameters in the discriminate model become highly variable. This leads to a substantial deterioration in performance of traditionally favoured classifiers (Neural net and other pattern recognition techniques). To overcome this problem it is necessary to decrease the number of variables to a manageable size and use an automated technique to classify different power quality problems. All the three signals presented in Figures 2.11 to 2.13 can be captured by the existing devices and stored in high capacity memory; however the engineer must then sort through these data to analyze these disturbances, which is a time consuming job.

- Limited capability of the Fast Fourier Transform (FFT). Some of the power analyzers have add-on models that can be used for computing an FFT to determine the harmonic content in the signal [24-27]. However, the functions e^{jwt} used to analyze the signal are global functions. By this we mean any disturbance on the signal at any point along the $t-axis$ influences every point on the $\omega-axis$. This is due to the selected bases of the transform (sine and cosine functions), which are not localized in time. Therefore, the FFT will not provide any information about the time domain. Time-frequency information is very important, since in power quality analysis we are interested in some particular portion of the signal (distortion event) and we need time-frequency information simultaneously for this particular portion of the signal. To correct this deficiency, a windowing FFT or short time Fourier transform (STFT) is also implemented to get time-frequency information of the distortion event. This can be done by separating the desired portion of the signal by multiplying the original signal by another function (selected window) that has zero magnitude out side the interval desired (windowing the signal for time information) and computes its FFT (for frequency information). However there is a deficiency in STFT that comes from selecting the size of the window. Using a wide window will result in a good frequency resolution and a bad time resolution. This means that we get accurate information on the spectrum of the distortion event but we cannot localize this distortion in time. As the window size gets smaller, we will loose the frequency resolution and obtain a better time resolution. This

means that utilizing the STFT we cannot get time-frequency information simultaneously to classify this disturbance according to IEEE Std.1159.

To illustrate the above fact we will discuss the following example. Using Matlab code, a distorted signal $f(t)$, shown in Figure 2.14, is simulated with the following parameters:

$$f(t) = \begin{cases} \sin(\omega t) & t < t_1 \text{ and } t > t_2 \\ \sin(\omega t) + B * \sin(\omega_C t) * e^{-At} & t_1 \le t \le t_2 \end{cases} \tag{2.2}$$

where, $t_1 = 6.25ms$, $t_2 = 18.15ms$, $f = 50Hz$, and $f_C = 1.5kHz$; and $B = -273.75$ and $A = 600$. The distorted signal is sampled (f_{sam}) at 240 kHz.

The *FFT* has a limited capability to analyze the signal and give time-frequency information. This is due to its use of the global functions e^{jwt} to transform the signal from the time-axis into the frequency-axis. As a result, all information in the time domain, which can help in detecting the starting time t_1 and the duration of the disturbance, is lost. This is illustrated in Figure 2.15.

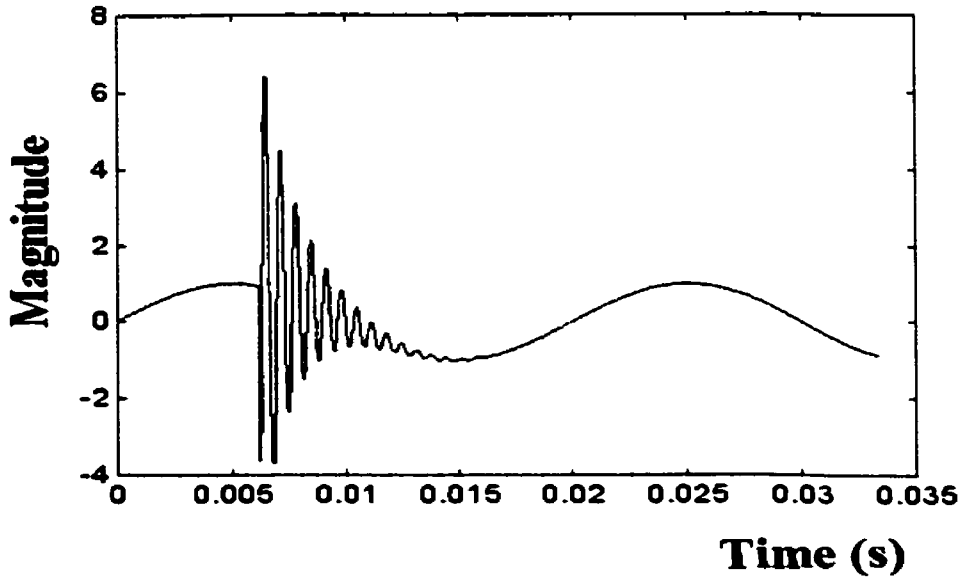

Figure 2.14: Simulated distorted signal

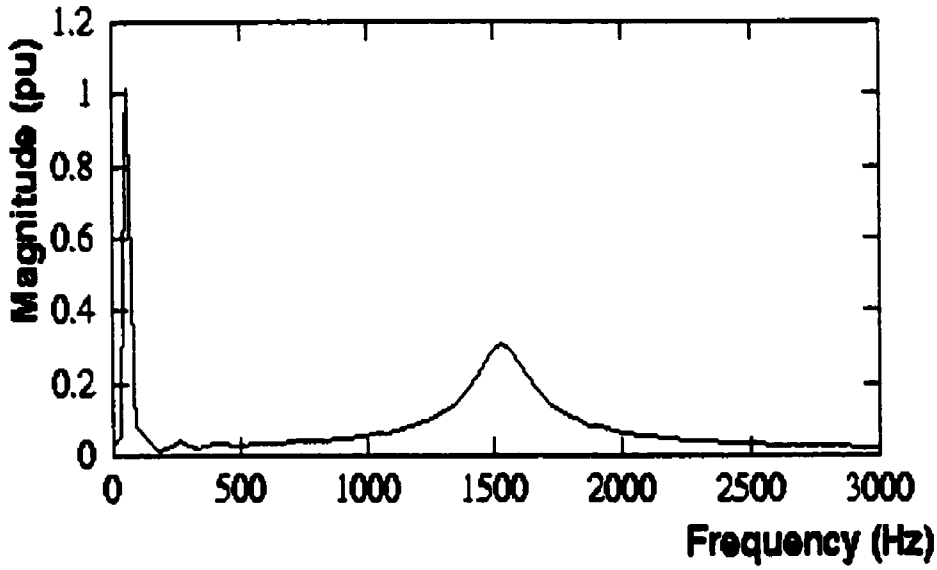

Figure 2.15: Fourier Transform

In order to achieve a high degree of localization, both in time and frequency, a window function with a sufficiently narrow time and frequency window is required; this can be done with the windowing FFT or short-time Fourier transform STFT. This is done by separating the desired portion of the signal (achieved by multiplying the original signal by another function that has zero magnitude outside the desired interval). The FFT of this portion of the signal provides the frequency information. However, the method is limited due to the constraint on the size of the window. Using a wide window will result in good frequency resolution but poor time resolution, and using a narrow window will result in poor frequency resolution but good time resolution. Furthermore, "Heisenberg's uncertainty principle imposes a theoretical lower bound on the area of the time-frequency window of any window function. This principle indicates that the function's feature (frequency component) and the feature's location (position at which that frequency component is found) cannot both be measured to an arbitrary degree of precision simultaneously [24-26].

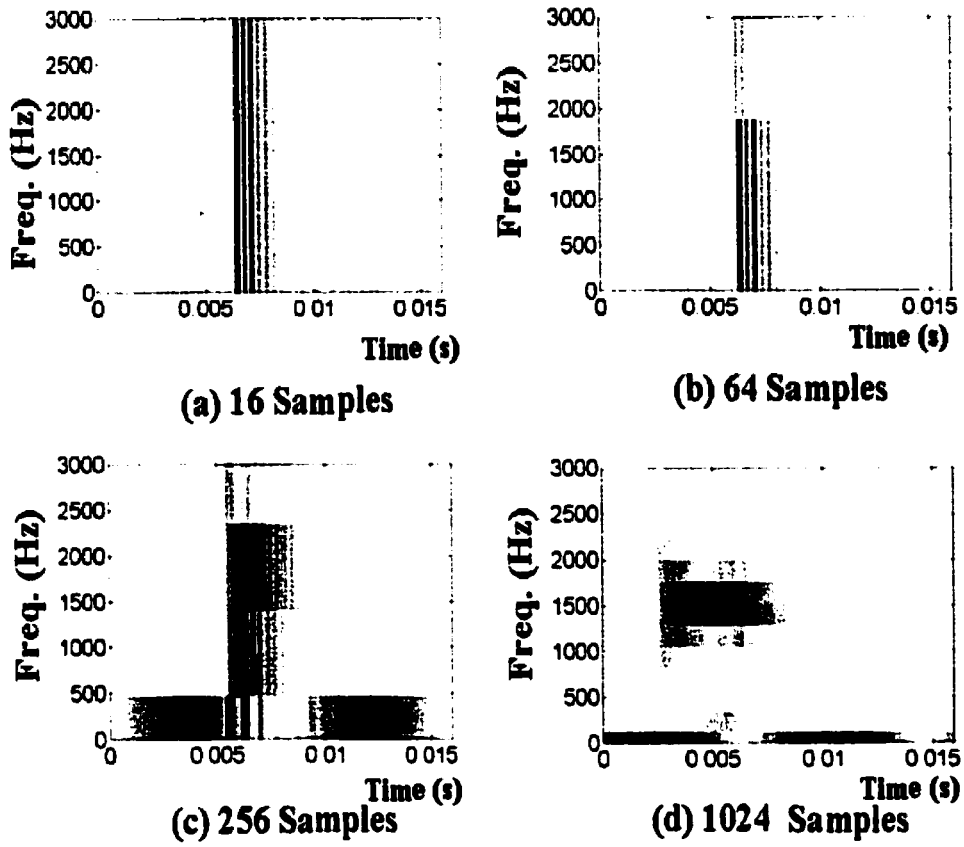

Figure 2.16: Short-time Fourier transform of the distorted signal

Figure 2.16 shows the results of implementing the STFT on $f(t)$ given by Equation 2.2. This example shows that as the size of the window increases (16, 64, 256, and 1024 samples), different time-frequency features of the distortion event will result. Figure2.16a (16 samples window) shows good time resolution regarding the distortion event starting time; however, the duration of this distortion cannot be easily measured. Furthermore, the frequency content of the distortion event shows a poor resolution due to the distribution of the spectrum over the whole frequency band. The frequency resolution increases and the time resolution decreases as the size of the window increases. Figure 2.16d (1024 samples window) shows more accurate localization of the frequency content in the signal but the time resolution becomes blurred. This means that, one should apply the STFT many times using different sized windows in order to get a clear time-frequency information.

To overcome the limitations of the flexible window function capable of operating over a wide frequency range, a Wavelet transform is utilized [24-40]. Using wavelet multi-resolution analysis the signal can be decomposed into different resolution levels. These resolution levels can extract time-frequency information of the signal that can help in designing the wavelet-based automated recognition system.

2.11 Summary

In this chapter, power quality indices are presented as defined by IEEE std. 1159. The sources of such power quality problems are presented and an introduction to different mitigation techniques, for each disturbance, is discussed as indicated in Tables 2.1 to 2.6. The direct or indirect effects of interruptions on customers are presented and the cost of such interruptions is discussed.

A detailed discussion of the existing monitoring devices shows the drawback of utilizing such devices in monitoring different disturbances. The limitation of the utilized tools are illustrated and presented by using simulated signals. The wavelet-based multi-resolution analysis is proposed as a tool that can be implemented to overcome the limitations in the existing monitoring devices. This tool can be utilized to design an automated power quality monitoring system.

Chapter 3

Wavelet Transform and Multi-resolution Analysis For Power System Applications

3.1 Introduction

The wavelet transform is a mathematical tool that cuts up data, functions or operators into different frequency components, and then studies each component with a resolution matched to its scale. For example, in signal analysis, the wavelet transform allows us to view a time history in terms of its frequency components, which means it maps a one-dimensional signal of time, $f(t)$, into a two dimensional signal function of time and frequency [24-40]. The wavelet transform represents the signal as a sum of wavelets at different locations (positions) and scales (frequency bands). The wavelet coefficients essentially quantify the strength of the contribution of the wavelets at these locations and scales.

This chapter is devoted to representing a general introduction to the wavelet transform and its applications in power system areas. Wavelet types, conditions, and efficiency are illustrated. Wavelet and Fourier transforms is presented in Section 3.6. Finally, a review of wavelet applications in power systems and a chapter summary are demonstrated in Sections 3.7 and 3.8.

The mathematical notations and tools that are useful for understanding wavelet theory and multi-resolution analysis will be illustrated in Chapter 4.

3.2 Wavelet and Multi-resolution

A wavelet is a small wave, which has its energy concentrated in time to give a tool for analysing transient, non-stationary, or time-varying phenomena. A wavelet still has oscillating wave-like characteristics but also has the ability to allow simultaneous time and frequency analysis with a flexible mathematical foundation. Different wavelets are shown in Figure 3.1.

The wavelet transform can be accomplished in three different ways namely as: the *Continuous Wavelet Transform* (CWT), the *Wavelet Series* (WS) and *Discrete Wavelet Transform* (DWT). In this research the DWT is implemented where a discritized signal is mapped into different resolution levels. The DWT maps a sequence of numbers into a sequence of numbers much the same way the Discrete Fourier transform (DFT) does.

The discrete wavelet transform (DWT) is sufficient for most practical applications in power systems and for reconstruction of the signal. It provides enough information, and offers an enormous reduction in the computation time. It is considerably easier to implement when compared to the continuous wavelet transform. The discrete wavelet coefficients measure the similarity between the signal and the scaled and translated versions of a scaled wavelet, $\psi_{a,b}$.

On the other hand, multi-resolution analysis (MRA) is used to analyze a signal at different frequencies with different resolutions. The goal of MRA is to develop representations of a complicated signal *f(t)* in terms of several simpler ones and study them separately. This goal will help in achieving two important properties. The first is the localization property in time of any transient phenomena. And the second is the presence of specific frequencies at different resolution levels.

In this research, MRA is implemented as a tool that utilizes the DWT to represent a time-varying signal in terms of its frequency components.

The DWT uses selected wavelets as digital filters with different cut-off frequencies to analyze a signal at different scales. In MRA, the signal is passed through a series of discrete filters "selected mother wavelet" to analyze and localize the high and the low frequencies that embedded in the signal.

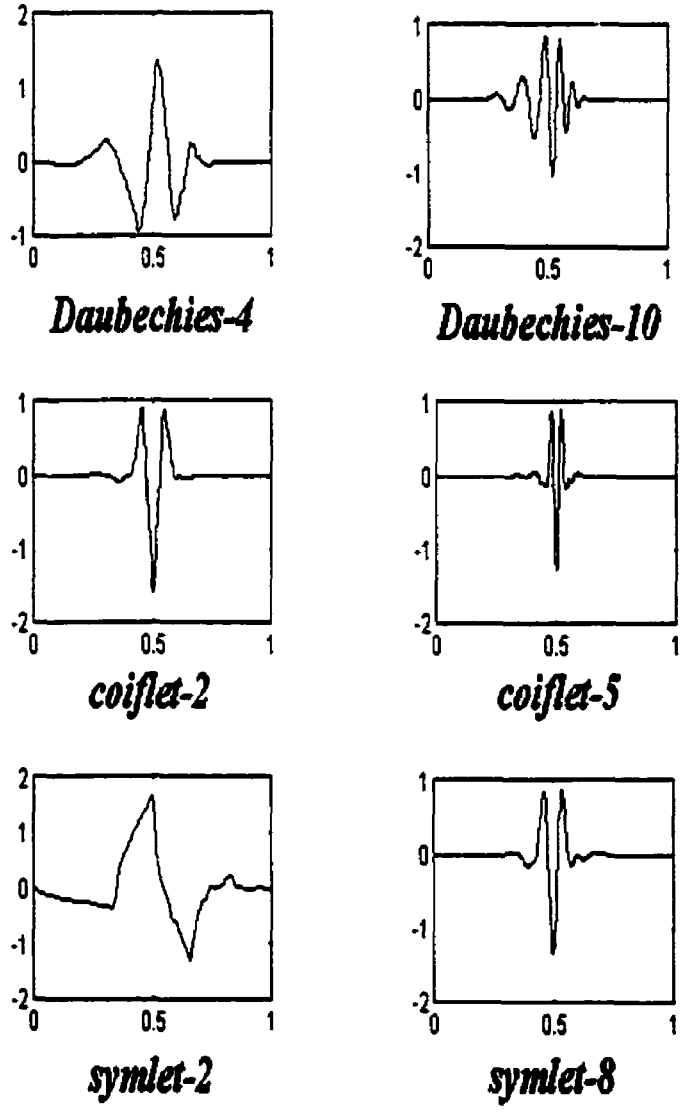

Figure 3.1: Examples of different wavelet functions

3.4 Wavelet Properties

Wavelets have three main properties:

1. They are building blocks to decompose and reconstruct signals. This means complicated signals can be decomposed and represented as simple building blocks in terms of the selected wavelets.

2. The wavelet expansion gives a time-frequency localization of the signal. This means most of the energy of the signal is well represented by a few expansion coefficients that are localized in the time and frequency domains.

3. The calculation of the wavelet coefficients from the signal can be done efficiently. This means that by using orthogonal wavelets, the distorted signal coefficients in the wavelet domain are simply given as the inner product of the signal with the wavelet function, which greatly simplifies the transform algorithm [24-30].

3.5 Wavelet efficiency

Wavelet transforms have been proven to be very efficient in signal analysis. Due to the above-mentioned properties of the wavelet transform, the following advantages can be gained:

1. Wavelet expansion coefficients represent a component that is itself local and are easier to interpret. Therefore, the location of these coefficients can be used to detect and localize any distortion in the signal. Furthermore, the energy of these coefficients will assist in extracting features that can classify the distortion event in terms of its magnitude, frequency components and duration. Detection and Classification of different distortion events will be discussed in Chapters 5 and 6.

2. MRA that decomposes a signal at different resolution levels will allow a separation of components that overlap in both time and frequency. This property will be useful in detecting and classifying multiple distortion events that may take place in the same monitored window. This will be presented in Chapter 6.

3. The wavelet transform coefficients represent the energy of the distorted signal. These coefficients will be used to measure the magnitude of the distorted signal and quantify its quality. This will be presented in Chapter 7.

4. The rapidly drop off in the size of the coefficients, with increasing translation and scaling factors, will assist in representing the distortion event by using only small number of coefficients. This will help in designing an automated recognition system that has the ability to store a large number of distortion events using a small number of coefficients. This efficient storing property will be presented in detail in Chapter 8.

5. MRA and DWT calculations are efficiently performed by digital computers. Discrete wavelet transform (DWT) computation relies on convolution and decimation or interpolation. These operations depend on addition and multiplication. Furthermore, the number of mathematical operations for DWT is in the order of (N) which is lower than that for the Fast Fourier Transform (FFT) algorithm which needs $(N\log(N))$ operations. This computational speed feature of the DWT will help in implementing the automated recognition system on-line and for real time applications.

3.7 Review of Wavelet Applications in Power Systems

Wavelets have been successively applied in a wide variety of research areas such as signal analysis, image processing, data compression and de-noising, and numerical solution of differential equations. The power of wavelets comes from their location at the crossroads of a wide variety of research areas. Recently, wavelet analysis techniques have been proposed extensively in the literature as a new tool for monitoring and analyzing different power system

disturbances. Other researchers proposed wavelet analysis as a new tool in different power engineering areas. Figure 3.2 summarizes the applications of wavelet transform in different power system areas.

The following section summarizes some of the previous work of applying wavelets in a power system, with emphases on the power quality and transient analysis areas [41-67].

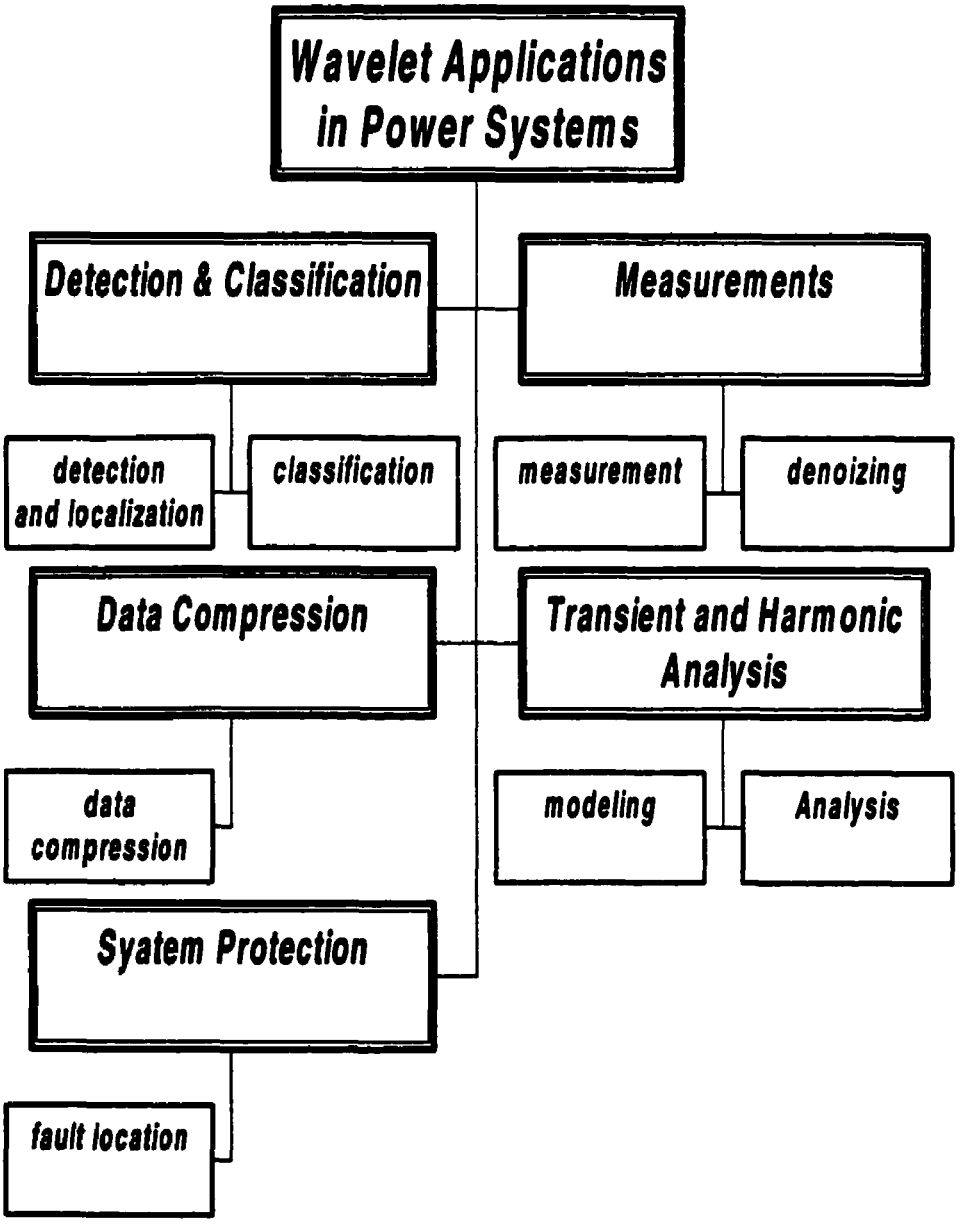

Figure 3.2: Wavelet transform applications in power system

3.7.1 Detection, Localization and Classification

Wavelet multi-resolution signal decomposition was applied to detect and localize different power quality problems. The squared wavelet coefficients were used to find a unique feature for different power quality problems. It was proposed that a proper classification tool might then be used depending on the unique feature to classify different power quality problems [41].

In [42] Wavelet and Fourier transforms were used to detect the number of notches per cycle and the harmonic content in the voltage in order to characterize the operation conditions of a converter. The squared wavelet coefficients (WTC1) of the first resolution level were used to detect and count the number of notches per cycle. However, for this to work the sampling rate should be very high in order to detect the notch impulses and therefore, the number of coefficients (WTC1) will be very large. Furthermore, the magnitude of the squared WTC1 can be affected by the noise content in the signal and other dynamic operation conditions.

In [43] multi-resolution analysis was proposed as a new tool that may be used to detect different disturbances, or to present the state of post-disturbances, and to identify their sources.

In [44] a combination of wavelets and neural nets was implemented to classify a one-dimensional signal embedded in normally distributed white noise. Noise signals were decomposed using the Haar wavelet basis and Daubechies 4 wavelet. A feed forward neural network was trained on the wavelet series coefficients at various scales and the classification accuracy for both wavelet bases was compared over multiple scales, several signal-to-noise ratios, and varying numbers of training epochs. This paper proposed using wavelets to classify the noisy signals and not other power quality problems.

In [45] a wavelet transform approach, using the Morlet basis, was applied to detect and localize different kinds of power system disturbances. However, it could not be easily used to discriminate among different power quality problems.

In [46] multi-resolution signal decomposition was applied to detect and monitor incipient faults during impulsive testing of a transformer. The neutral current was monitored and decomposed into different detailed and smoothed versions to detect any fault during the testing process. The proposed method was found to have many advantages over existing methods.

3.7.2 Measurements

In [47] a new technique was proposed to detect, localize, and estimate automatically the most relevant disturbances in a power system. The proposed method combines the use of the continuous wavelet transform, modulus maxima properties, multi-resolution signal decomposition, and reconstruction by means of the DWT. This technique was used to measure steady state magnitude of a harmonic distorted signal.

In [48] a wavelet-based algorithm was used to measure the power and rms values of a steady-state harmonic distorted signal. The algorithm was applied on simulated and actual sets of periodic data. Frequency separation into the various wavelet levels was discussed using infinite impulsive response (IIR) and finite impulsive response (FIR) filters. The results were compared with that derived by using the Fourier Transform.

3.7.3 Data Compression

In [49] wavelet transformation was applied as a compression tool for power system disturbances. Three simulated transient voltages were generated and reconstructed by using a suitable mother wavelet and by using only 2% of the coefficients. This approach presented the efficiency of the wavelet transform to reconstruct non-stationary power system disturbances.

In [50] the arc furnace current was decomposed into a series of 11 wavelet levels. A good approximation to the original waveform was obtained by adding only five of the wavelet levels.

In [51] wavelet analysis was applied to compress actual power quality data and the compression ratio achieved was in the range of 3-6 with normalized mean square errors of the order of 10^{-16} to 10^{-5}.

In [52] the results of compressing power system disturbances using the discrete wavelet transform and wavelet packets were presented. The wavelet transform offered compression ratios $\leq 10:1$ compared to that by the discrete cosine transform.

3.7.4 Transient and Harmonic Analysis

In [53] the wavelet technique was proposed for analyzing the propagation of transients in power systems. The approach concluded that it is possible to use wavelets to calculate the transient within the system. The advantage of the method depends on the similarity of the existing transient to the selected mother wavelet. The wavelet transform was used to solve the differential equations as an example of the use of multi-resolution analysis.

In [54] Daubechies wavelets have been used for the analysis of power system transients. The method is based on the wavelet companion equivalent circuit of power system components, such as resistors, inductors, capacitors, and distributed parameter lines. This equivalent circuit is developed by applying the wavelet transform on the integral-differential equations of the power system elements.

In [55] the wavelet transform was utilized to model the power system components. This model was used to analyze transient and steady state events in a power system. An actual arc furnace system data was used to illustrate the efficiency of the proposed technique.

3.7.5 System Protection

In [56] wavelets were introduced in the power system-relaying domain. It was shown that wavelets may be employed for analyzing recorded data to study efficiently the faulted network. In this reference, it was also proposed to implement the wavelet transform in real-time protection

devices. The information of the transient period analyzed by the wavelet can help to improve the performance of the protection system.

In [57] the wavelet transform was applied to identify the fault location in transmission systems. The wavelet transform was used to extract the traveling time information accurately for signals traveling between the faulted point and the line terminals. The first two levels of high frequency wavelet transform coefficients were shown to carry information directly related to the location of the transmission line fault. This information was then used to find the location of the fault.

In [58] Morlet wavelets were proposed to discriminate the high-impedance faults from normal switching events under different grounding conditions. The proposed technique shows the feasibility of the method as a potential alternative in the area of power system relaying.

In [59] a wavelet-based method was proposed as a reliable and computationally efficient tool for distinguishing between internal faults and inrush currents of the transformers. The Neural network was proposed to improve the performance of the algorithm.

3.8 Summary

Wavelets have been successively applied in a wide variety of research areas. Recently, wavelet analysis techniques have been proposed extensively in the literature as a new tool to be implemented in different power engineering areas. The wavelet transform analysis was proposed as a new tool for monitoring power quality problems. However, most of the mentioned approaches that dealt with power quality problems did not present a real classification methodology that can be used to classify different power quality problems or design a practical on-line automated monitoring system. Most of the work done in the power quality area, deals with the power quality problem either from the detection and localization point of view or from the data compression frame.

3.9 The Author Contribution to Monitoring Techniques

To overcome the deficiency in proposed monitoring techniques, the author of this thesis, in [60-67] used the wavelet transform and multi-resolution analysis of a distorted signal to design a new technique that can monitor accurately a wide range of power quality problems.

The proposed monitoring system has the ability to detect and localize any disturbances in the system. Using the localization property of the wavelet transform, the first detail version of the signal under analysis is used to detect any disturbance and localize it in time. The duration of the distortion event can be measured in this resolution level. Moreover, the energy of the detail coefficients in this resolution level can be used to give assessment of the noise content in the signal. The de-noising property of the wavelet transform is used to localize the distorted signals in a noisy environment. Detailed information about the application of the detection and localization property of the proposed technique is presented in Chapter 5.

A new technique that uses multi-resolution analysis is proposed that has the ability to decompose any distorted signal into different building blocks and extract time-frequency features simultaneously from each block. The energy of the detail coefficients of each resolution level is used to construct the proposed feature vector. The dimensionality of data is mapped into a small size of interpretable features. Different pattern recognition techniques are implemented on the proposed feature vector to design an on-line automated monitoring system. These features are proven to be very efficient in auto-classifying different power quality problems that overlap in time and frequency. Chapter 6 introduces the proposed auto-classification technique.

Using the signal coefficients in the wavelet domain, a new measurement technique that can measure accurately a wide range of signal characteristics is proposed. Different power quality problems that may overlap in time or frequency domains are measured. The proposed technique is implemented to measure different parameters in a power system under steady state or transient conditions. A new wavelet-based procedure to monitor the non-rectangular variation of the RMS

value in the signal is also introduced. The proposed measuring techniques are presented in Chapter 7.

The reduction in the size of the detail coefficients, due to the decimation property, is used to represent the distorted signal in terms of a small set of coefficients. A complete chapter, Chapter 8, is devoted to develop a new procedure that will compress and store the distortion event efficiently. This procedure is based on wavelet analysis, where a small set of wavelet coefficients that represents the disturbances will assist in achieving this goal. This procedure will replace the existing technique of storing all sampling points of the disturbance.

A general layout of the design procedure of the wide-scale on-line automated power quality monitoring system is presented in Chapter 9.

Chapter 4

Wavelet and Multi-resolution Analysis Mathematical Representation

4.1 General Introduction

The Wavelet transform was proposed in this thesis as a tool to solve power quality problems. Using wavelet properties, detection and localization of any transient distortion within the signal can be achieved. Furthermore, classification of the power quality problem can be obtained and quantification of the distortion level can be measured.

These features can modify the existing monitoring devices and upgrade their ability to be used as an automated on-line base for real-time applications. The Wavelet based multi-resolution analysis is used to decompose any complicated signal and represent it in terms of several simpler ones. Such analysis of any transient event will help in localizing the transient event in the time domain and clarifying the presence of any specific frequency components at different resolution levels.

To achieve our goal and construct an automated wavelet-based monitoring system the mathematical details of the proposed tool is highlighted. The mathematical concepts of the Wavelet transform (WT) and multi-resolution analysis (MRA) are presented in this Chapter. The Analysis and Synthesis procedures of multi-resolution analysis are discussed and applied on selected examples. The time-frequency "scale" plane and localization and partitioning of signal energy at different resolution levels are also presented in this chapter. Appendix A is added as a support for the mathematical derivations that are needed to clarify the main concepts of the wavelet theory.

4.2 General Mathematical Preliminaries

The purpose of this section is to introduce the mathematical notations and tools that are useful to present Wavelet Transform theory. Some definitions of vector spaces and related mathematical relations are introduced and more detailed discussions are presented in Appendix A.

4.2.1 Vector Spaces

The totality of vectors that can be constructed by scalar multiplication, and vector addition form vectors in a given set is called a *vector space*. A set of vectors that is capable of generating the totality of vectors by these operations is said to *span the space*. If the set consist of the least number of vectors that span the space, the set is called a *Basis of the space*. The number of vectors in the basis is called the *dimension of the space*. *n-basis* vectors generate an *n-dimensional* space. Any subset of *r-basis* vectors forms the basis of an *r-dimensional subspace*.

4.2.2 Norms

The concept of the distance is generalized in the case of vectors through the use of norms. The norm of a vector x, $||x||$, is a real non negative number such that:

$$\| x \| = 0 \quad \text{if and only if} \quad x = 0$$

$$\| cx \| = |c| \; \|x\| \quad \text{for all scalars } c \text{ and vectors } x$$

$$\| x_1 + x_2 \| \leq \| x_1 \| + \| x_2 \| \quad \text{for all } x_1 \text{ and } x_2$$

There exist many norms for vectors. Three of the commonly used ones are:

$$\|x\|_1 = \sum |x_i| \tag{4.1}$$

$$\|x\|_2 = \sqrt{\sum |x_i|^2} \tag{4.2}$$

$$\|x\|_\infty = \max_i |x_i| \tag{4.3}$$

4.2.3 Inner Product

It is a scalar "a" obtained from two vectors $f(t)$ and $g(t)$, by an integral. It is denoted as:

$$a = \langle f(t), g(t) \rangle = \int f(t)\, g(t)\, dt \tag{4.4}$$

The length of a vector " *norm*" can be defined in terms of the inner product as:

$$\| f(t) \| = \sqrt{|\langle f(t), f(t) \rangle|} \tag{4.5}$$

4.2.4 Hilbert Spaces

It is a complete inner product space with orthogonal basis, where any signal $f(t) \in L^2(R)$ satisfies the following condition:

$$\int_{-\infty}^{\infty} |f(t)|^2 dt < \infty \tag{4.6}$$

which means that the signal $f(t)$ has finite energy.

4.2.5 Basis

A set of vectors $\phi_k(t)$ spans a vector space F if any element $f(t)$ in that space can be expressed as a linear combination of members of that set. This means that $f(t)$ can be written as:

$$f(t) = \sum_k a_k\, \phi_k(t) \tag{4.7}$$

with $k \in Z$ the set of integers and $a, t \in R$. $\phi_k(t)$ is known as the *expansion set* and a_k is known as the expansion coefficients.

The expansion set $\phi_k(t)$ forms a *basis set* or *basis* if the set of expansion coefficients $\{a_k\}$ are unique for any particular $f(t) \in F$. There may be more than one basis for a vector space. However, all of them have the same number of vectors, and this number is known as the dimension of the vector space.

The expansion set $\phi_k(t)$ forms an *orthogonal basis* if its inner product is zero:

$$<\phi_k(t), \phi_l(t)> = 0 \quad \text{for all} \quad k \neq l \tag{4.8}$$

The expansion set $\phi_k(t)$ forms an *orthonormal basis* if the inner product can be represented as:

$$<\phi_k(t), \phi_l(t)> = \delta(k-l) = \begin{cases} 0 & k \neq l \\ 1 & k = l \end{cases} \tag{4.9}$$

This means that in addition of being orthogonal, the basis is normalized to unity norm.

$$\|\phi_k(t)\| = 1 \quad \text{for all} \quad k \tag{4.10}$$

For an orthonormal basis, the set of expansion coefficients $\{a_k\}$ can be calculated using the inner product,

$$a_k = <\phi_k(t), f(t)> \tag{4.11}$$

Therefore, having an orthonormal basis, any element in the vector space $f(t) \in F$, can be written as:

$$f(t) = \sum_k <\phi_k(t), f(t)> \phi_k(t) \tag{4.12}$$

This expansion formulation is extremely valuable. The inner product of $f(t)$ and $\phi_k(t)$ produce the set of coefficients a_k. This set of coefficients a_k can be used linearly with the basis vectors $\phi_k(t)$ to give back the original signal $f(t)$.

4.3 The Wavelet Transform (WT) and Multi-level representation

The Wavelet Transform is a tool that can cut any signal into different frequency components, and then study each component at a certain resolution level. The WT depends on two sets of functions known as scaling functions and wavelet functions. In order to implement a multi-level presentation of a signal we will start by defining the scaling function and then use it to represent the wavelet function.

4.3.1 The Scaling Function

The scaling function $\phi(t)$ is a function that belongs to the Hilbert space. The scaling set $\phi_k(t)$ is defined as a set of integer translations of a basis scaling function $\phi(t)$, where:

$$\phi_k(t) = \phi(t-k) \quad \text{for } k \in Z \; ; \; \phi_k \in L^2(R) \tag{4.13}$$

and $L^2(R)$ is the Hilbert space, which can be represented by a set of subspaces $\{V_j \mid j \in Z\}$, where Z is the set of integers.

The set of scaling functions $\phi_k(t)$ span the subspace V_0 defined as:

$$V_0 = span_k[\phi_k(t)] = span_k[\phi(t-k), \quad k \in Z\} \tag{4.14}$$

If *f(t)* is a finite energy signal ($f(t) \in L^2(R)$), then an approximated version of $f(t) \in V_o$, can be represented in terms of the scaling function as shown in Figure 4.1 and can be expressed according to Equation 4.7 as:

$$f(t) = \sum_k a_k \phi_k(t) \tag{4.15}$$

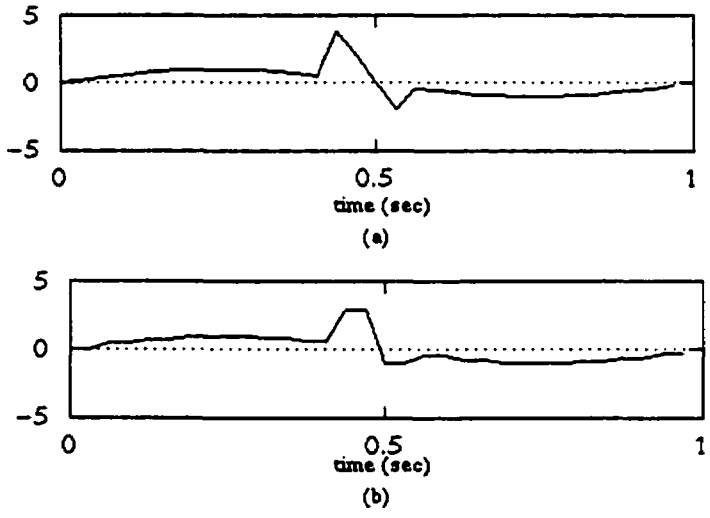

Figure 4.1: Approximation of the input signal, a- the input signal, b- approximation of the input signal using Haar scaling function

Keeping in mined the containment property (See Appendix A), the scaling function $\phi(t)$ can be expressed in terms of a weighted sum of shifted $\phi(2t)$:

$$\phi(t) = \sum h(n)\sqrt{2}\phi(2t-n) \qquad n \in Z \tag{4.16}$$

where the coefficients *h(n)* are a sequence of real or complex numbers called the scaling function coefficients (or the scaling filter coefficients) and the $\sqrt{2}$ maintains the unity norm of the scaling function with the scale of two.

This equation is called the multi-resolution analysis equation. It can be utilized to represent the signal at different resolution levels. This is presented in the following subsection.

4.3.2 Multi-level representation using the Scaling Function

In order to represent a signal *f(t)* at different resolution levels, the used scaling function $\phi(t)$ must be translated and scaled. Therefore, the two dimensional family of scaling function $\phi_{j,k}(t)$ is presented as:

$$\phi_{j,k}(t) = 2^{j/2}\phi(2^j t - k) \tag{4.17}$$

where, j is the scaling factor and k is the translation factor. This two dimensional family can span different subspaces $\{V_j | j \in Z\}$ as:

$$V_j = span_k\{\phi_{j,k}(t)\} = span_k\{2^{j/2}\phi_k(2^j t - k)\} \tag{4.18}$$

for all integers k.

This means that any signal $f(t) \in L^2(R)$ can be approximated and represented at different resolution levels ($f(t) \in V_j$), as:

$$f(t) = \sum_k a_k 2^{j/2}\phi(2^j t - k) \tag{4.19}$$

The multi-level representation of the signal *f(t)* is shown in Figure 4.2. The Haar scaling function is scaled and translated to represent the input signal at five resolution levels.

As the scale j changes in Equation 4.19 changes, more details are added to the approximated version and a more similar version of the original signal can be achieved. These details, which exist in between each of the two approximated versions of the signal, are very important in analyzing and monitoring the original signal. These details can be extracted by using the wavelet function.

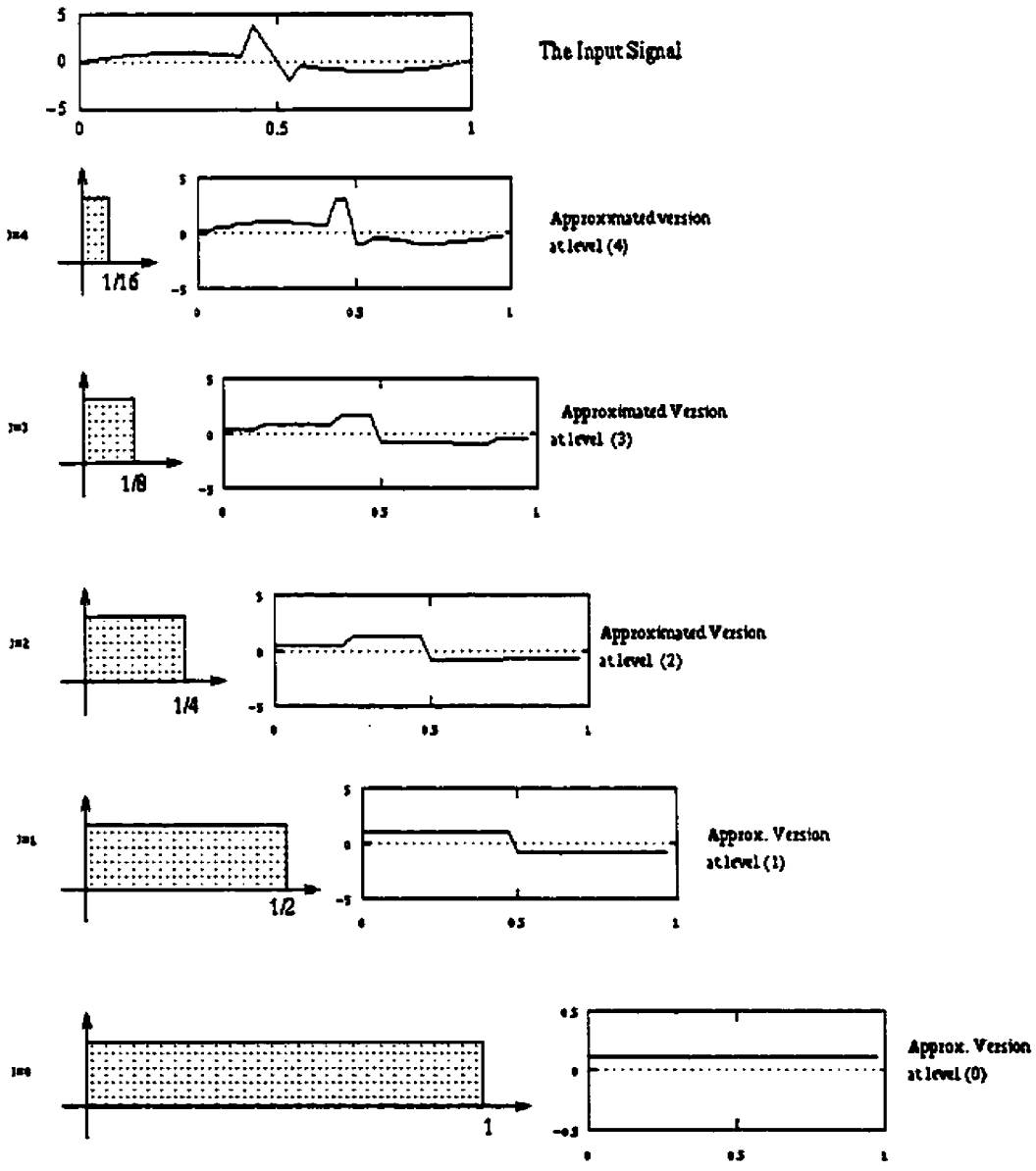

Figure 4.2: Multilevel representation of an input signal using the Haar scaling function

4.3.3 The Wavelet Function

More important features of a signal can be extracted by using a function that spans the difference between various approximated versions obtained using the scaling function $\phi_{j,k}(t)$. This can be achieved by using the wavelet function $\psi_{j,k}(t)$.

As indicated by the containment property (See Appendix A), the subspace V_0 is embedded in the subspace V_1, $V_0 \subset V_1$. In order to move to a finer subspace V_1 from a coarser subspace V_0, one must add another subspace in between, which is known as the complement subspace W_0. This is illustrated clearly in Figure 4.3.

Since these wavelets reside in the space spanned by the next narrower scaling function, then they can be represented by a weighted sum of shifted scaling functions at that space. For example $\psi(t)$ resides in the space W_0, and $W_0 \subset V_1$. Therefore, $\psi(t)$ can be represented by a weighted sum of shifted scaling function $\phi(2t)$. This is illustrated in Figure (4.3) and mathematically can be presented by:

$$\psi(t) = \sum_n h_1(n)\sqrt{2}\phi(2t-n) \qquad n \in Z \tag{4.20}$$

for some set of wavelet coefficients (wavelet filter coefficients) $h_1(n)$, where,

$$h_1(n) = (-1)^n h(1-n) \tag{4.21}$$

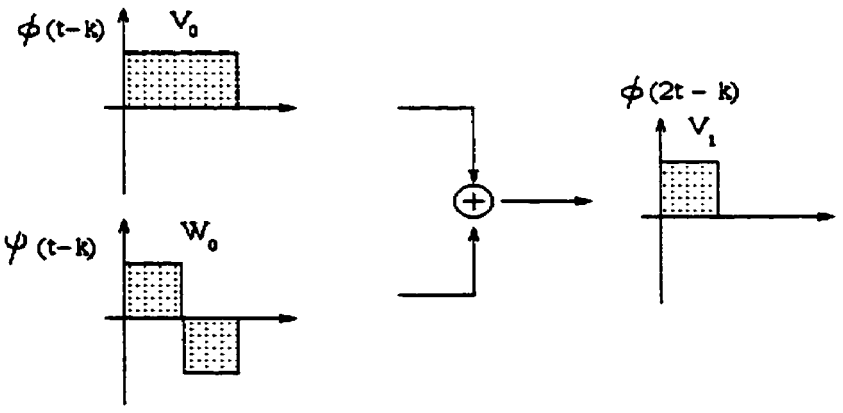

Figure 4.3: Moving to a finer space using the wavelet, $\psi_{j,k}(t)$, and scaling function, $\phi_{j,k}(t)$

Again, the scaled wavelet function can be utilized to extract different details that reside in between different approximated versions of the signal. This will be discussed in the following subsection.

4.3.4 Multi-level representation using the Wavelet Function

As the scaling function $\phi_{o,k}(t)spans V_O$ and $\phi_{1,k}(t)spans V_1$, there are a particular functions which span W_o and W_j. Therefore, as the scaling function $\phi_{j,k}(t)spans V_j$, the wavelet function $\psi_{j,k}(t)spans W_j$. Where W_j is the orthogonal complement V_j. This means that all members of V_j are orthogonal to all members of W_j, $(V_j \perp W_j)$.

Therefore, the space V_j can be represented in terms of a set of subspaces where each subspace can be spanned using the scaling and wavelet functions. This is mathematically represented as:

$$V_j = V_{j-1} \oplus W_{j-1} = V_0 \oplus W_0 \oplus W_1 \oplus W_2 \oplus .... \oplus W_{j-1} \tag{4.22}$$

Therefore, any signal $f(t) \in L^2(R)$ can be represented as a series expansion by using a combination of the scaling function and wavelets function:

$$f(t) = \sum_{k=-\infty} c_k \varphi(t-k) + \sum_{k=-\infty} \sum_{j=0} d_{j,k} \psi(2^j t - k) \tag{4.23}$$

where, c_k are the approximated coefficients of the last approximated version and $d_{j,k}$ are the detail coefficients at different scales.

Equation 4.23 represents the signal $f(t)$ at different resolution levels in terms of one approximated version and different details that exist in between different approximated versions. The first summation gives the approximated version of the signal $f(t)$ in terms of the scaling function. The second summation gives different details that can be extracted in terms of the

wavelet function at different scales. The summation of the approximated version and the different detail versions will represent the original signals *f(t)*.

Figure 4.4 shows the details of the input signal at different resolution levels by using the Haar wavelet function. It is clear form the figure that as the scale changes more resolution is achieved.

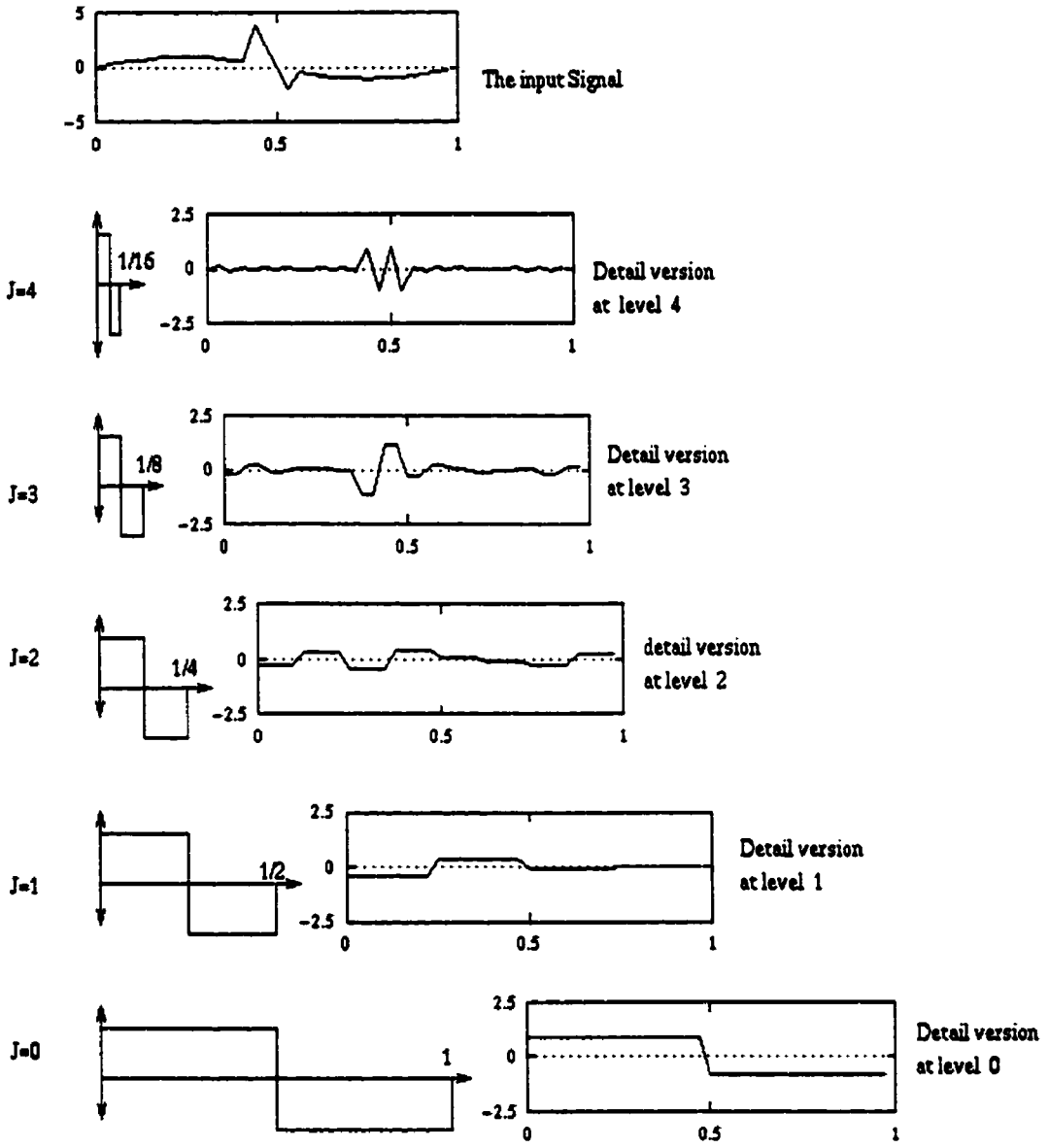

Figure 4.4: Multilevel representation of the input signal using the wavelet function

This led to multi-resolution analysis and its application in monitoring different power quality disturbances that exist in electrical systems.

4.4 Multi-resolution Analysis (MRA)

Multi-resolution analysis (MRA) is used to decompose any signal and represent it at different resolution levels. The goal of multi-resolution analysis (MRA) is to develop representations of a complicated signal *f(t)* in terms of several simpler ones and study them separately. This goal will help in achieving two important properties. The first is the localization property in time of any transient phenomena. And the second is the presence of specific frequencies at different resolution levels. In multi-resolution analysis, the signal is decomposed to find a time-frequency picture of the signal and then reconstructed to get back the original signal. It essentially maps a 1-D signal of time into a 2-D signal of time and frequency. This is explained in Figure 4.5, where a 1-D noisy sinusoidal signal is mapped into the wavelet domain and represented as a 2-D signal as shown in Figure 4.6.

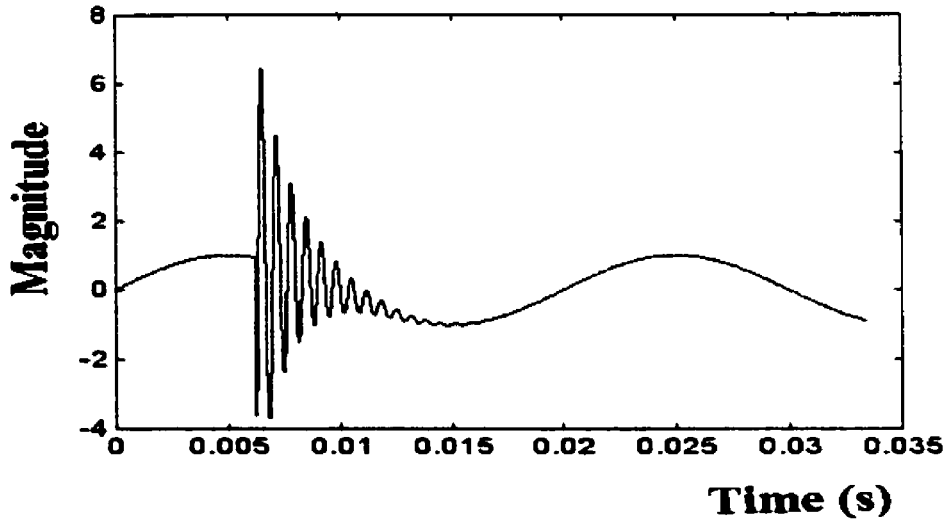

Figure 4.5: One-dimensional signal in time domain

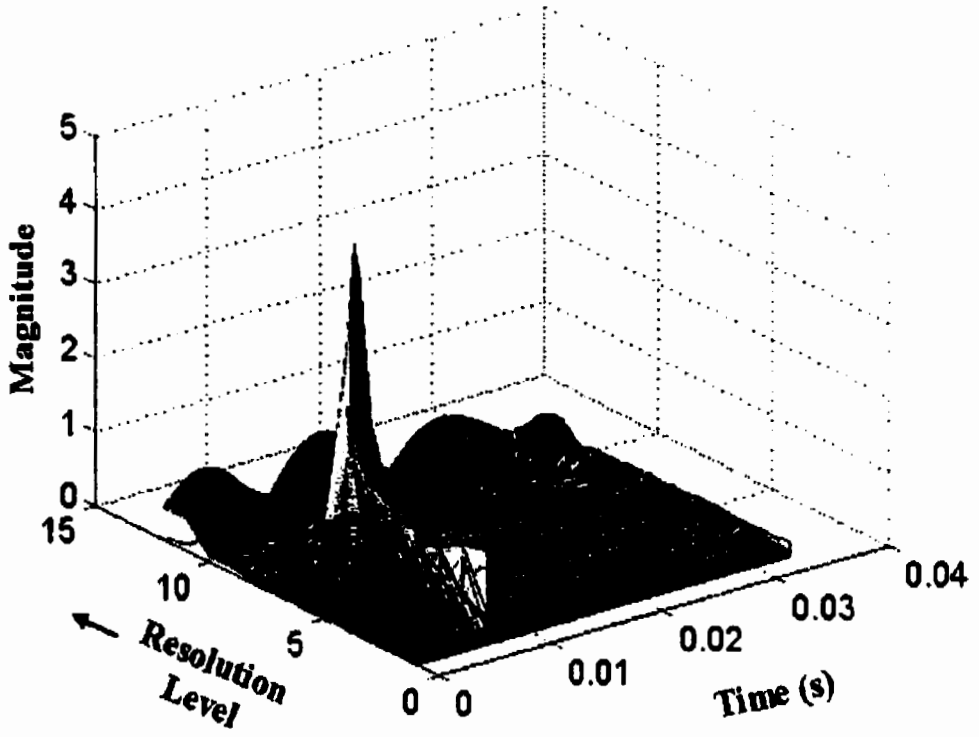

Figure4.6: Mapping one dimensional signal into a two dimensional signal in a wavelet domain

The main advantage of this technique comes from its ability to extract information that overlaps in time and frequency domains. The transient event in the signal is extracted and its energy is distributed at different resolution levels in time and frequency domains simultaneously.

Using the scaling and wavelet functions the signal is mapped into the wavelet domain and analyzed into an approximated and different detail versions. This can be achieved by extracting the approximated coefficients $c_j(k)$ and the detail coefficients $d_j(k)$ as follows:

$$c_j(k) = \langle f(t), \varphi_{j,k}(t) \rangle = \sum_m h(m-2k)\, c_{j+1}(m) \tag{4.25}$$

$$d_j(k) = \langle f(t), \psi_{j,k}(t) \rangle = \sum_m h_1(m-2k)\, c_{j+1}(m) \tag{4.26}$$

The reconstruction process uses the approximated and detail coefficients, $c_j(k)$and $d_j(k)$ at resolution j to reconstruct the coefficients $c_{j+1}(k)$ at the next resolution, $j+1$.

$$c_{j+1}(n) = \sum_k c_j(k)\, h(n-2k) \; + \sum_k d_j(k)\, h_1(n-2l) \tag{4.27}$$

The mathematical derivation of the approximated and detail coefficients for analysis and reconstruction process is presented in Appendix A.

Multi-resolution analysis Equations 4.25 and 4.26, shows that in order to get the expansion coefficients at level j, convolve the expansion coefficients at scale $j+1$ by the scaling filter coefficients $h(n)$ and the wavelet filter coefficients $h_1(n)$ then down sample or decimate the result. This process can be repeated to give a multi-level representation of the signal. On the other hand, to reconstruct the signal from the wavelet coefficients, up-sample the j-scale approximated coefficients $c_j(n)$ and detail coefficients $d_j(n)$, then convolve them with the scaling filter coefficient $h(n)$ and the wavelet filter coefficient $h_1(n)$.

This simplifies the wavelet based multi-resolution process of decomposition/synthesis, which is known by Mallat's algorithm.

4.5 Mallat's algorithm

This algorithm simplifies the implementation of the Discrete Wavelet Transform (DWT). It represents the DWT in terms of convolution and decimation (down-sampling) for the decomposition stage and convolution and interpolation (up-sampling) for the synthesis process.

The Mallat's transform analysis (decomposition) algorithm for the data $c_{j+1}(n)$ is achieved as follows:

- Convolve data with $h(n)$ and decimate to get $c_j(n)$
- Convolve data with $h_l(n)$ and decimate to get $d_j(n)$

The inverse Mallat's transform implements the synthesis (reconstruction) process with the following steps:

- Up sampling by inserting zero between every sample in $c_j(n)$ and $d_j(n)$
- Convolve the up sampled coefficients $c_j(n)$ with the filter $h(n)$.
- Convolve the up sampled coefficients $d_j(n)$ with the filter $h_l(n)$.
- Add the results of the convolution to get the original data $c_{j+1}(n)$

If the sampling rate f_{sam} of the signal is above the Nyquist rate ($f_{sam} \geq 2f_{max}$ where f_{max} is the highest frequency component in the signal), then these samples of the signal can be considered as the scaling coefficients $c_{j+1}(n)$.

Decimation or down sampling is a multi-rate processing which is an efficient technique for changing the sampling frequency of a signal in digital domain and efficiently compressing the data [65-67]. As indicated in the block diagram (Figure 4.7), the sampling rate compression and data reduction in (d_j) are achieved by discarding every second samples resulting from convolving approximated coefficients (c_{j+1}) and the wavelet coefficients $h_l(n)$.

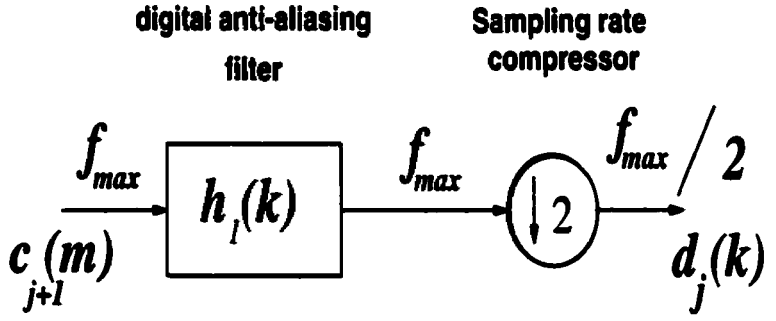

Figure 4.7: Block diagram of decimation by factor 2

Similarly, the approximated coefficients (c_j) are achieved by convolving c_{j+1} by the scaling function coefficients $h_o(n)$ and decimate by two. Since half of the data is discarded (decimation by 2) there is a possibility of losing information (aliasing), however the wavelet and scaling function coefficients ($h_1(n)$ and $h_o(n)$) will work as digital filters that limit the band of the input c_{j+1} and prevent aliasing. This is explained in Figure 4.8, which represent one stage of MRA. The samples of the signal are considered as the set c_{j+1} and decomposed into the sets d_j and c_j. These coefficients can be used to reconstruct an approximated version A_1 and a detailed version D_1 of $f(t)$ at that scale as shown in Figure 4.8a.

Coiflet5 scaling and wavelet functions and their frequency response $H_o(w)$ and $H_1(w)$ are shown in Figure 4.8b. The two functions are working as a low and high pass filters that divide the spectrum of c_{j+1}. The spectrum of $f(t)$, $0 - f_{max}$, will be decomposed into the ($\frac{f_{max}}{2}$ *to* f_{max}) band for d_j and the (0 *to* $\frac{f_{max}}{2}$) band for c_j. The size of the data points will also be reduced to $(N+n-1)/2$ as shown in Figure 4.8c. Where, N is the number of $f(t)$ sampling points and n is the number of filter coefficients (n=30 for coif5). As the scale changes, the shape of the wavelet becomes wider and the steps in time (translation) become larger. This allows representation of less details and or lower resolution. In the second MRA stage, the approximated coefficients (c_j) can be further decomposed into d_{j-1} ($\frac{f_{max}}{4}$ *to* $\frac{f_{max}}{2}$) and c_{j-1}(0 *to* $\frac{f_{max}}{4}$) by convolution and decimation. The decomposition of the approximated coefficients can be continues till no more details can be extracted. The last approximated coefficients c_o will be reached at the final stage of MRA and $f(t)$ can be presented as in Equation 4.23.

In MRA, the first stage divides the spectrum into two equal frequency bands; the second stage sub-divides the lower frequency band into quarters, and so on. In other words, the DWT coefficients for any signal, periodic or non-periodic, can be computed by using a multi-rate filter bank. The total number of the resolutions that can be achieved J depends on the number of sampling points, which can be controlled by the sampling frequency and the window size of the data.

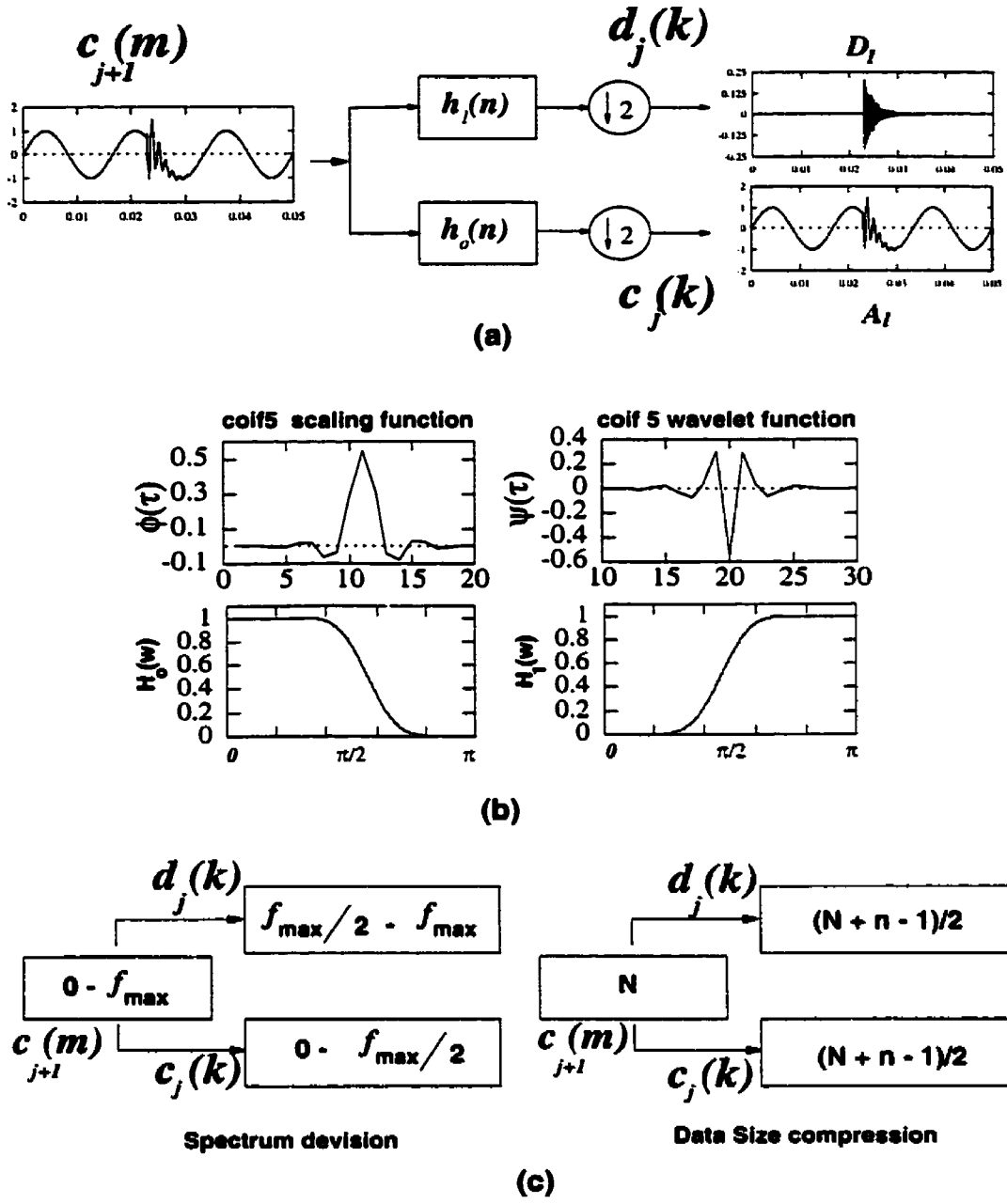

Figure 4.8: One stage of MRA and wavelet filters

a- decomposing into detail and approximated version,

b- Coiflt 5 scaling and wavelet functions and their frequency response,

c- spectrum division and coefficients size compression.

In other words, an analysis filter bank efficiently calculates the discrete wavelet transform (DWT) using banks of digital filters and down-samplers, and the synthesis filter bank calculates the inverse discrete wavelet transform (IDWT) to reconstruct the signal from the transform.

Figure (4.9) shows five-levels of multi-resolution signal decomposition using the Haar scaling and wavelet functions.

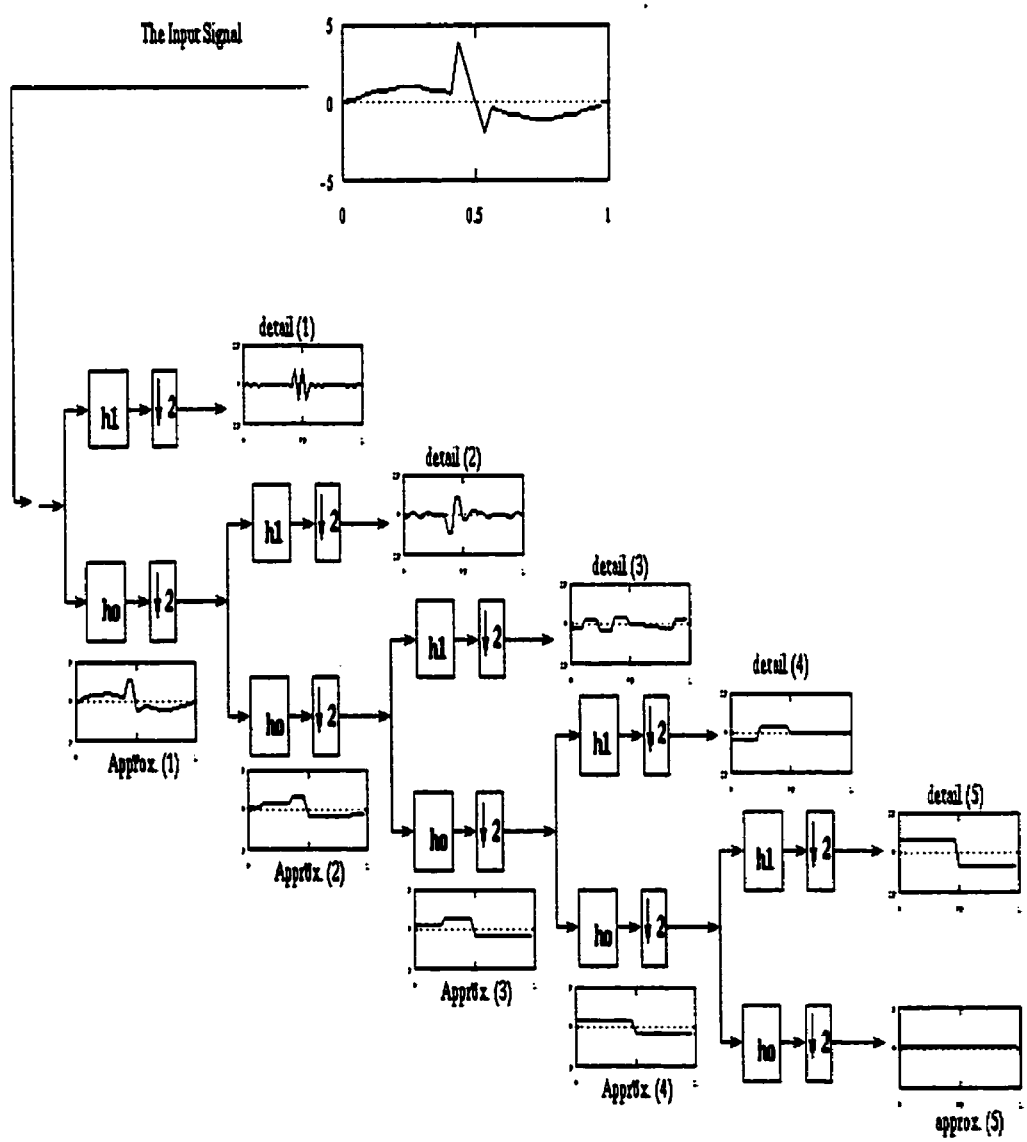

Figure 4.9: Five level multi-resolution signal decomposition

4.6 Parseval's Theorem

If the scaling function and wavelets form an orthonormal basis, there is Parseval's theorem that relates the energy of the signal to the energy in each of the components and their wavelet coefficients of the approximated and detail versions. This means that the norm or energy of the signal can be partitioned in terms of the expansion coefficients [28].

Any function $f(t) \in L^2(R)$ can be presented as a series expansion by using a combination of the scaling functions and wavelets.

$$f(t) = \sum_{k=-\infty} c_k \varphi(t-k) + \sum_{k=-\infty} \sum_{j=0} d_{j,k} \psi(2^j t - k) \tag{4.28}$$

The Parseval's theorem is:

$$\int |f(t)|^2 dt = \sum_{k=-\infty} |c(k)|^2 + \sum_{j=0}^{\infty} \sum_{k=-\infty}^{\infty} |d_j(k)|^2 \tag{4.29}$$

with the energy in the expansion domain partitioned in time by k and in scale by j.

4.7 Summary and Conclusion

The wavelet transform and multi-resolution analysis is a promising tool for satisfying our goal in designing an Automated Recognition System (ARS) for power quality monitoring. It can give good results in monitoring transient or steady state signals or both of them simultaneously.

Implementing MRA any distorted signal can be decomposed into different building blocks that represent the time-frequency information of the distorted signal. The coefficients that represent the signal in the wavelet domain can be used to extract classification features for classifying the different power quality problems.

The scaling property of the selected wavelet function to be used in decomposing the signal will assure the ability of the MRA technique to detect any transient event and localize it in the time and frequency domains.

Selecting orthonormal wavelets, multi-resolution analysis will have the ability to distribute the energy of the distorted signal in terms of the expansion coefficients of the wavelet domain. Therefore, both the expansion approximated and detail coefficients will give an indication about the energy content of the distorted signal in certain time and frequency bands. This feature can be used to classify different power quality problems. From the other side, the energy of the wavelet coefficients can be combined with the localization property to give a measure of the distortion event.

The small values of the expansion coefficients will give us an indication about the resolution levels that contains low energy of the distorted signal and hence can be ignored for data compression purposes. This can reduce the large volume of disturbance data to a manageable size. It will provide a higher quality of information about the disturbance event to be analyzed by the planning engineers.

Furthermore, the expansion coefficients of the highest resolution levels can be ignored for de-noising purposes.

Using these properties of multi-resolution signal decomposition, an automated recognition system can be designed to detect, localize and classify different power quality problems. The wavelet coefficients at different resolution levels can be used to de-noise and compress the data of the distorted event. A complete discussion of the proposed Automated Recognition System will be presented in the following chapters.

Chapter 5

Detection and Localization

5.1 Introduction

In order to improve the electric power quality the sources and causes of disturbances on the distribution system must be determined. However in order to determine the causes and sources of disturbances, one must have the capability to detect and localize those disturbances. This chapter proposes a technique that has the ability to detect and localize any disturbances in a clean or noisy environment. This technique is based on wavelet-multi-resolution analysis (WMRA).

This chapter is organized as follows. Section 5.2 highlights the procedure to map the distorted signal into the wavelet domain. The proposed procedure for disturbance detection and localization is presented in Section 5.3. Section 5.4 describes a wavelet-based procedure to quantify the noise content in the monitored signal while Section 5.5 presents a detection and localization technique for different disturbances in a noisy environment. The applications of the proposed technique are presented in Section 5.6. Finally, the assessment of this chapter is discussed in Section 5.7.

5.2- Mapping Into The Wavelet Domain

Let us assume that a distorted signal $f(t)$ has a finite length and consists of two components. The first component is the 60 Hz pure signal $p(t)$ and the second one is $s(t)$ that represents the distortion event superimposed on the pure signal. Therefore, the distorted signal can be presented as:

$$\underset{Signal}{f(t)} = \underset{pure}{p(t)} + \underset{Distortion}{s(t)} \tag{5.1}$$

Applying multi-resolution analysis, one can decompose the signal $f(t)$ at different resolution levels and present it as a series expansion by using a combination of scaling functions $\phi_k(t)$ and wavelet functions $\psi_k(t)$. This can be mathematically presented as:

$$\underset{Signal}{f(t)} = \sum_k c_o(k)\phi(t-k) + \sum_k \sum_{j=0}^{J-1} d_j(k)2^{j/2}\psi(2^j t-k) \tag{5.2}$$

where, d_j are the detail coefficients that represent different detail versions of the signal $f(t)$ at different resolution levels (scales), and c_o is the last approximated coefficients that represent the last approximated version of the signal $f(t)$ where no more details can be extracted. Since the selected wavelet and scaling functions are orthonormal (orthogonal and normalized), the expansion coefficients c_j and d_j can be computed by the inner product of the signal $f(t)$ and the scaling or wavelet functions.

Since the sampling rate of $f(t)$ are above the Nyquist rate ($f_{sam} \geq 2f_{max}$), then the signal samples can be considered as the approximated coefficients c_{j+1} and used to compute the approximated c_j and detail d_j coefficients as:

$$c_j(k) = \sum_m h_o(m-2k)c_{j+1}(m) \tag{5.3}$$

$$d_j(k) = \sum_m h_1(m-2k)c_{j+1}(m) \tag{5.4}$$

Therefore, using Equations 5.3 and 5.4, the distorted signal $f(t)$ is mapped into the wavelet domain and presented in terms of its expansion (approximated and detail) coefficients as:

$$C_{Signal} = [\, c_o \mid \; d_o \mid d_1 \; \mid \ldots\ldots d_{J-1} \mid \,] \tag{5.5}$$

where c_o are the last approximated coefficients and d_i are the detail coefficients at resolution level i of the distorted signal.

In a similar way, the expansion coefficients of a pure signal C_{pure} can be generated and used as a reference for the purpose of classification and measurements. These coefficients are:

$$C_{pure} = [\, c_{op} \mid \; d_{op} \mid d_{1p} \; \mid \ldots\ldots d_{(J-1)p} \mid \,] \tag{5.6}$$

where c_{op} are the last approximated coefficients and d_{ip} are the detail coefficients at resolution level i of the pure signal.

Therefore, the expansion coefficients C_{dist} that represent the distortion event $s(t)$ are formulated by subtracting Equation 5.6 from Equation 5.5. Therefore,

$$C_{dist} = C_{Signal} - C_{pure} \tag{5.7}$$

$$C_{dist} = [\, c_{od} \mid \; d_{od} \mid d_{1d} \; \mid \ldots\ldots d_{(J-1)d} \mid \,] \tag{5.8}$$

where c_{od} are the last approximated coefficients and d_{id} are the detail coefficients at resolution level i of the distortion event only.

5.2 - Detection and Localization the Distortion

Any changes in the pattern of the signal can be detected and localized at the finer resolution levels. As far as detection and localization is concerned, the wavelet coefficients of the first finer decomposition level of $f(t)$ are normally adequate to detect and localize any disturbance in the signal. These coefficients are:

$$d_j(k) = \langle f(t), \psi_{j,k}(t) \rangle = \sum_m h_1(m-2k)\, c_{j+1}(m) \tag{5.9}$$

For a pure signal, the set of coefficients $d_j(k)$ presented in Equation 5.6 are equal to zero. Any changes in the signal can be detected and localized in time due to the changes in the magnitude of these coefficients. This property is shown in Figure 5.1. An impulsive transient event, Figure 5.1a, is detected and localized due to the changes in the magnitude of the detail coefficients $d_j(k)$ that represent the first detail version D_1.

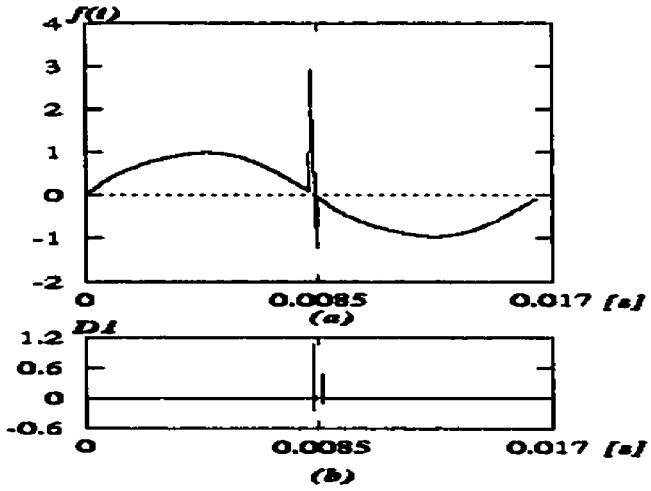

Figure 5.1: Transient detection

a- impulsive transient phenomena,

b- detection and localization of the transient event at the first resolution level.

However, as the transient event magnitude decreases and the noise level increases, the coefficients that represent the noise will merge with those representing the transient event. This will cause a failure in the wavelet detection and localization property. Figure 5.2a shows a harmonic distorted signal where the total harmonic distortion equals to 26.6%. The signal is further distorted with sag to 0.8 p.u. for one cycle. If the noise level is small then the first resolution level D_1 can be used to detect and localize the sag event as shown in Figure 5.2b. However, as the noise level increases, the first resolution level can no longer detect and localize the transient event, Figure 5.2c.

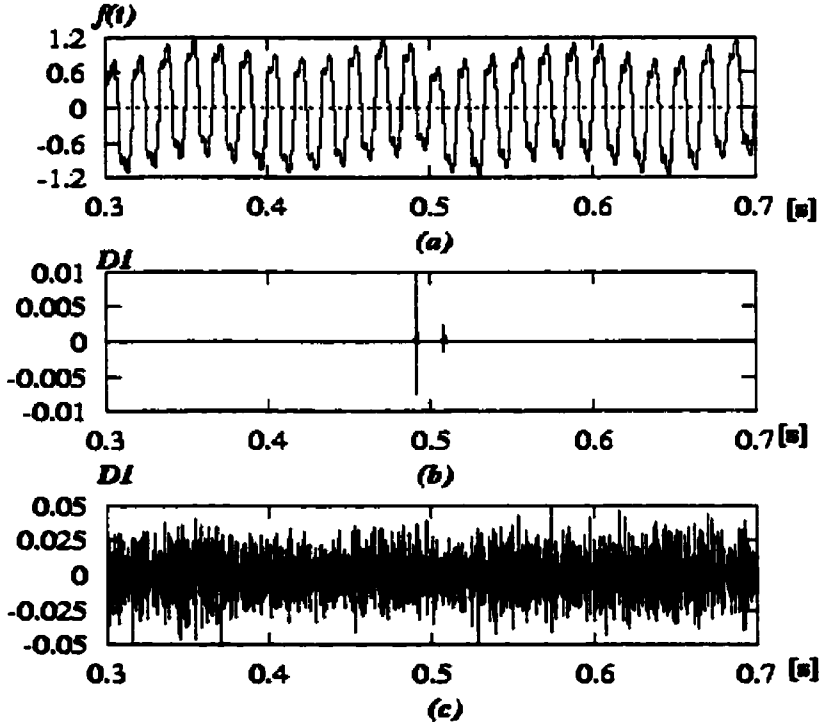

Figure 5.2: Steady state phenomena detection

a- harmonic distorted signal with one cycle sag to 0.8,

b- the highest resolution level with zero noise level,

c- the highest resolution level with 2.0% noise level.

A new technique relying on noise level assessment and an approximated version of the distortion event is proposed to de-noise and localize the transient event and to measure its duration, $\Delta\tau$, in a noisy environment.

5.3 - Noise Level Assessment

In multi-resolution analysis, shown in Figure 5.3, the first stage will divide the spectrum of distortion into a low-pass and high-pass band, resulting in the scaling coefficients and wavelet coefficients at a lower scale $c_{[J-1]d}(k)$ and $d_{[J-1]d}(k)$. The second stage then divides that low-pass band into another lower low-pass band and a band-pass band. The first stage divides the spectrum into two equal parts. The second stage divides the lower halves into quarters and so on.

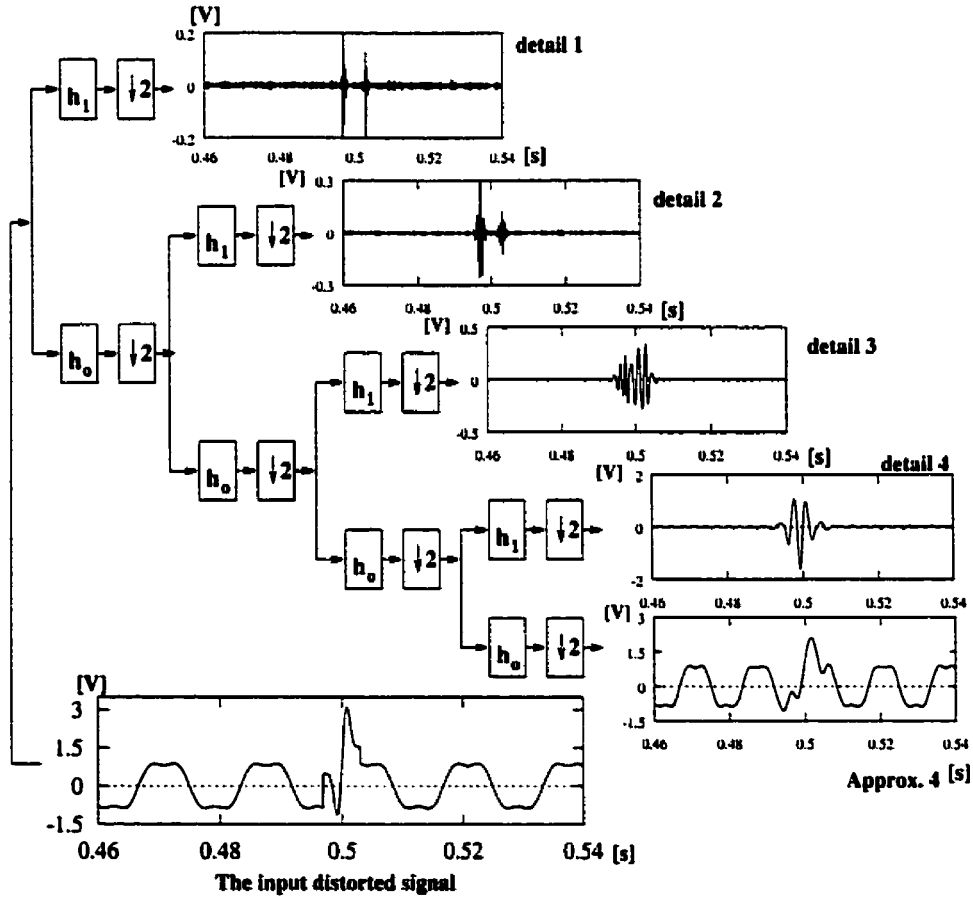

Figure 5.3: Multi-resolution analysis of a distorted signal

The noise is defined as an electrical signal with wide-band spectral content lower than 200kHz superimposed upon the distorted signal [3]. However, the principle noise sources in power system inject their noise components at high frequencies [2] [16]. Therefore, great part of the noise energy is expected to appear at the highest resolution level $d_{(J-1)d}$ as computed in Equation 5.8. This means that the energy of the coefficients $\Delta E_{d(J-1)}$ at the highest resolution level can give a good indication about the energy of the noise superimposed over the signal.

$$\Delta E_{d(J-1)} = \| d_{(J-1)d} \|_2 = [\sum_{k=-\infty}^{\infty} | d_{(J-1)d}(k) |^2]^{1/2} \tag{5.10}$$

For a pure signal,

$$\Delta E_{d(J-1)} = 0 \tag{5.11}$$

The variation of $\Delta E_{d(J-1)}$ with different white noise levels superimposed on a pure signal is presented in Table 5.1.

Table 5.1: Coefficient's energy with white noise level variation in one-second pure signal.

Noise	0.0%	0.25%	0.50%	0.75%	1.0%
$\Delta E_{d(J-1)}$	0.0	0.1521	0.3143	0.4646	0.6345

An assessment of the noise level can be determined as the value of $\Delta E_{d(J-1)}$ goes beyond zero or a certain threshold value of accepted noise level.

5.4 - Detection and Localization in a Noisy Environment

As the noise level increases, $\Delta E_{d(J-1)} > 0$, the distortion event can be localized by reconstructing an approximated version of the distorted signal and ignoring the coefficients that represent the noise. This can be mathematically represented as:

$$s(t) = \sum_{k} c_{od}(k)\phi(t-k) + \sum_{k}\sum_{j=0}^{F} d_{jd}(k)2^{j/2}\psi(2^{j}t-k) \tag{5.12}$$

where $F < J$ and J represents the total number of resolution levels and F represents the subspace index or the highest resolution level to be used to reconstruct $s(t)$. The value of F depends on the noise level content and the energy distribution of the distortion event as indicated in Table 5.1. Squaring the distortion event and applying the following thresholds can accomplish further reduction for any existing harmonic components.

$$m(t) = \begin{cases} 0 & [s(t)]^2 < \theta \\ 1 & [s(t)]^2 \geq \theta \end{cases} \tag{5.13}$$

where

$$\theta = std\,[s(t)^2] \tag{5.14}$$

Utilizing $m(t)$ the starting time τ_{start} and the ending time τ_{end} of the disturbance event can be localized. The duration $\Delta\tau$ is measured and used to categorize the disturbance as instantaneous, momentary, or temporary.

$$\Delta\tau = \tau_{end} - \tau_{start} \tag{5.15}$$

5.5 – Applications and Results

The proposed detection method is applied to detect, localize, and estimate the duration of the following power system disturbances with different noise levels:

5.5.1 Oscillatory Transient phenomenon

The proposed detection technique was applied to detect the duration of the simulated oscillatory transient as indicated by Equation 2.2 and shown in Figure 5.4. As indicated in Section 2.10 neither the STFT technique nor the point-by-point comparison technique can monitor exactly the duration of the oscillatory transient event.

Applying MRA, the First Detail Version D_1 of the distorted signal was used to localize the distortion event in time. Even though, the oscillatory phenomena decayed to small values after 0.015s, the exact ending time of the distortion event was detected around 0.018s. This is clearly shown in Figure 5.5.

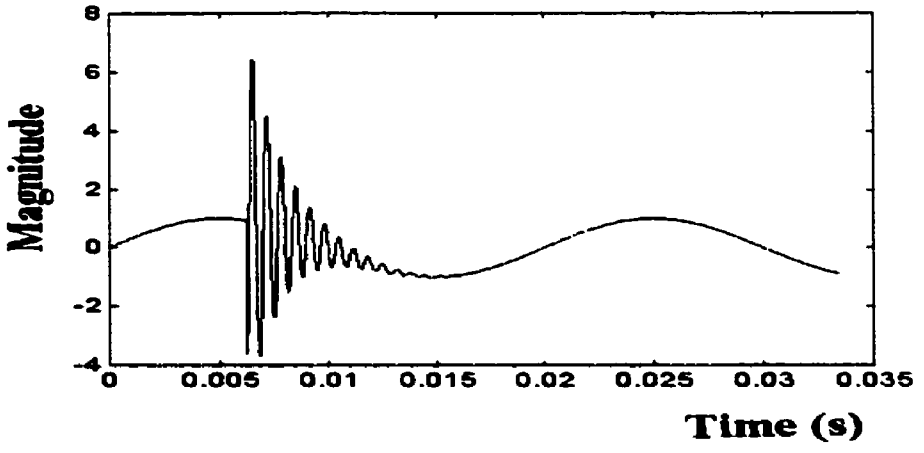

Figure 5.4: Simulated oscillatory distorted signal

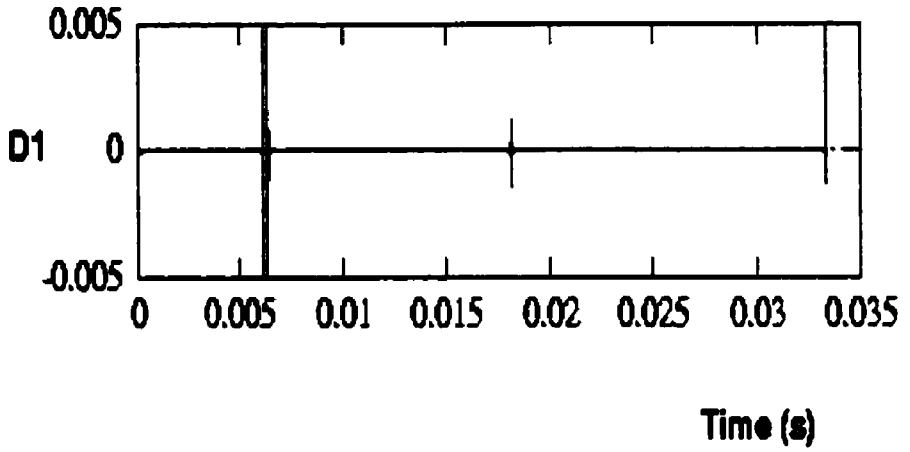

Figure 5.5: The first detail version of the distorted signal

5.5.2 Capacitor Switching Phenomenon

The distorted signal $f(t)$, shown in Figure 5.6a and its zoomed version Figure 5.6b, was simulated with the transient event. The actual starting time of the distortion was 0.4901 s and the ending time was 0.4926 s. The proposed algorithm was used to estimate the time information of the distortion. The distortion event $s(t)$ was synthesized using the wavelet coefficients C_{dist} as shown in Figure 5.6c. The threshold measure Equation 5.14 was applied on $[s(t)]^2$ and $m(t)$ was constructed to estimate the time information of the distortion (Figure 5.6d and 5.6e).

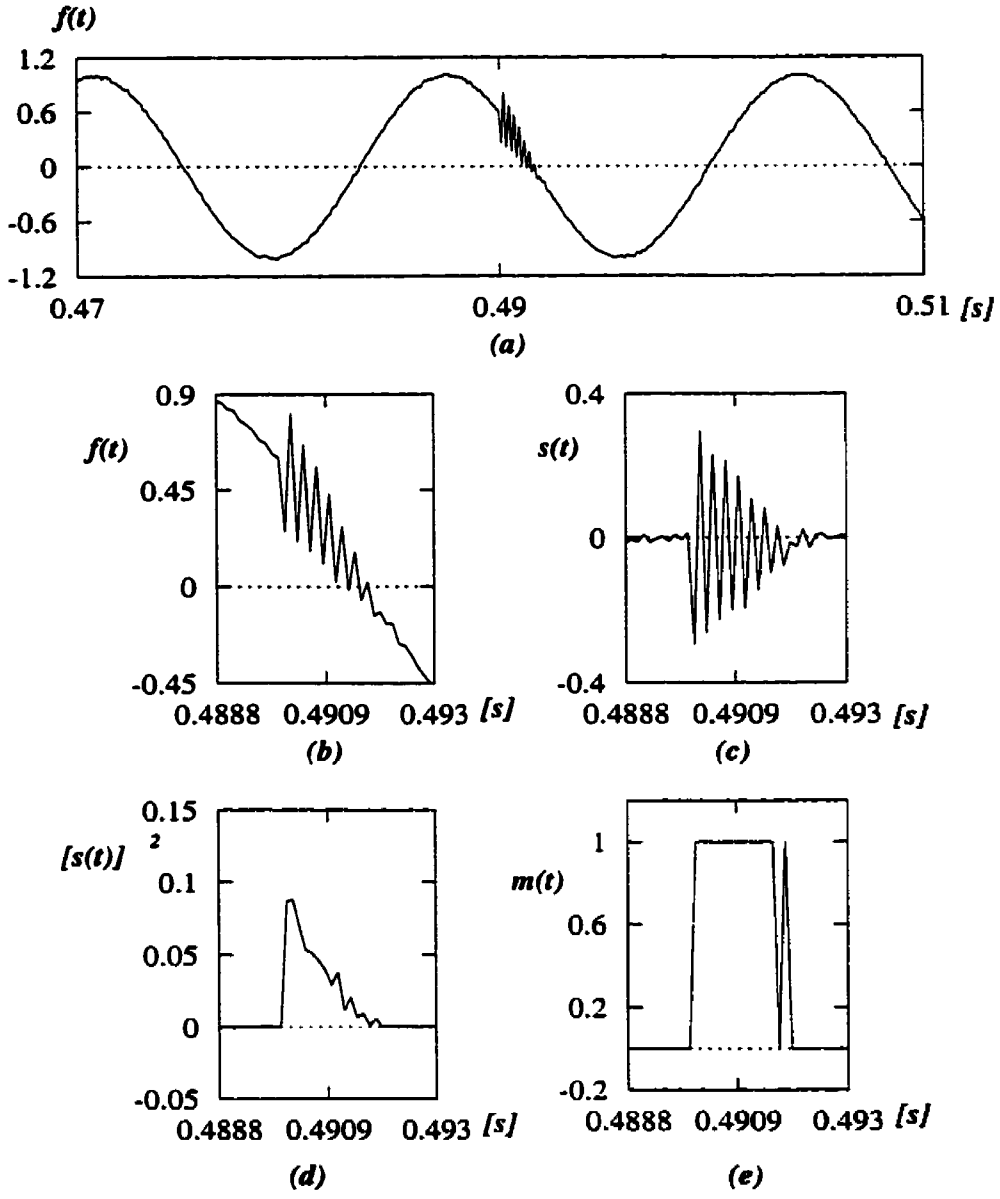

Figure 5.6: Detection and localization of a transient phenomenon in a noisy environment

a- Distorted signal

b- Zooming version of the distorted signal

c- Distortion extraction

d- The square of the reconstructed approximated version of the distortion event

e- Distortion duration

Table 5.2 presents the estimated starting and ending time of the capacitor-switching phenomenon with noise level variation from 0% to 1.2%. It can be seen that the estimated time error is increased considerably as the noise level magnitude was increased beyound 1.0%. However, higher values of noise level larger than 1.0% are not normally expected in power systems [2].

Table 5.2: Estimated starting and ending time of a transient phenomenon with noise level between 0 – 1.2%

Noise Level	Starting time [s]	Starting Error %	Ending Time [s]	Ending Error %
0.0 %	0.4901	0.0	0.4919	0.1239
0.5%	0.4901	0.0	0.4919	0.1239
1.0%	0.4901	0.0	0.4919	0.1239
1.1%	0.4901	0.0	0.8604	74.671
1.2%	0.1838	62.490	0.4919	72.961

5.5.3 Sag phenomena

Figure 5.7 shows a signal distorted with high and low frequency components and a sag phenomenon to 0.85 p.u. (of peak value). The total harmonic distortion (THD) is equal to 18.24%. MRA was applied and the distorted signal was decomposed at different resolution levels. The duration for the sag phenomenon was detected and localized in the first detailed level for 14.6 cycles as shown in Figure 5.8.

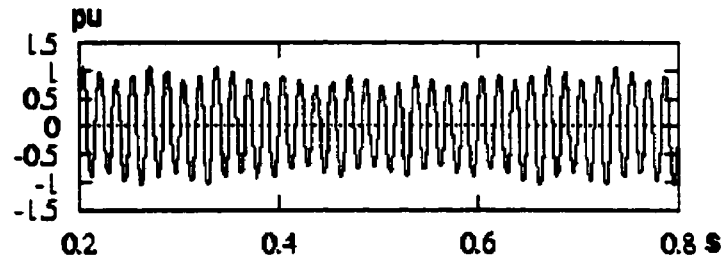

Figure 5.7: Harmonic distorted signal with sag phenomenon

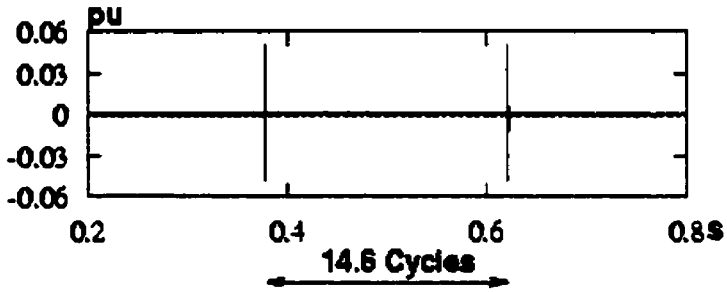

Figure 5.8: The first detail version of the distorted signal

5.5.4 Sag in noisy environment

The same technique was applied for detecting and localizing a one-cycle simulated sag phenomenon, Figure 5.9a. The simulated signal was further distorted with harmonic and had a high noise level. The actual starting time of the distortion was 0.4917 s and the ending time was 0.5083 s. Due to the high noise level, 1.0%, the first resolution level D_1, Figure 5.9b, could not be used to detect and localize the distortion event. The distortion event $s(t)$ was synthesized by ignoring the high-resolution levels, $F = 9$ and $J = 13$, for de-noising purposes, Figure 5.9c. The threshold measure Equation 5.13 was applied on $[s(t)]^2$ and $m(t)$ was constructed to estimate the time information of the distortion, Figure 5.9d and 5.9e.

Table 5.3 presents the estimated RMS value and the starting and ending time of a sag phenomenon with noise level variations from 0% to 2.0%.

Table 5.3: Estimated RMS value and starting and ending time of sag phenomena.

Noise Level	Derived Sag (RMS)	Error %	Derived Starting (s)	Error %	Derived Ending (s)	Error %
0.00%	0.1798	0.0150	0.4921	0.0745	0.5082	0.0240
0.25%	0.1814	0.0240	0.4921	0.0745	0.5081	0.0480
0.50%	0.1840	0.0384	0.4921	0.0745	0.5082	0.0240
0.75%	0.1895	0.0706	0.4921	0.0745	0.5082	0.0240
1.00%	0.1954	0.1014	0.4921	0.0745	0.5082	0.0240
1.25%	0.2058	0.1622	0.4922	0.0993	0.5082	0.0240
1.50%	0.2179	0.2331	0.4921	0.0745	0.5081	0.0480
1.75%	0.2284	0.2926	0.4921	0.0745	0.5081	0.0480
2.00%	0.2382	0.3400	0.4922	0.0993	0.5082	0.0240

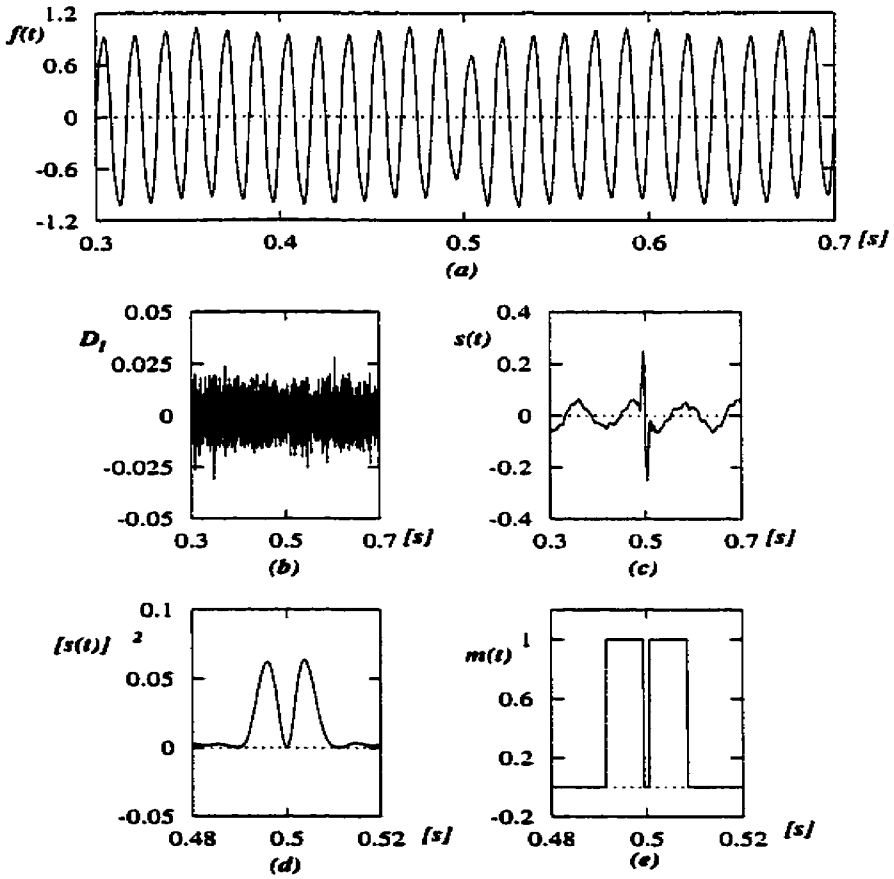

Figure 5.9: Detection and localization

a- Sag phenomenon in a noisy environment, b- First detail version, c- Distortion extraction

d- The square of the approximated version of the distortion, e- Distortion duration

5.7 Chapter Assessment

In this chapter a new wavelet multi-resolution analysis technique is proposed. This technique has the ability to detect and localize any disturbance in an electric power system. The first detail version of the decomposed signal can give accurate information about any variation in its pattern. As the noise level increases, the de-noising property of the wavelet-MRA can be implemented to detect and localize the distortion event.

On-line classification is another feature that must be considered to monitor power quality disturbances. The classification procedure for different disturbances will be discussed in the following chapter.

Chapter 6

Distortion Classification

6.1 Introduction

Energy companies rely on power quality monitoring data to ensure the reliability and enhanced delivery of their product. These monitoring devices allow energy companies to continually evaluate the quality of their supply, assisting them in spotting and correcting system weaknesses before they create problems. The ability to extract information rather than just data from monitored signals is an important requirement for modern disturbance monitors. This information is essential to design an automated classification system for different power quality disturbances.

A new technique is proposed in this Chapter that has the ability to decompose any distorted signal into different building blocks and extract time-frequency features simultaneously from each block. The feature extraction method maps a d dimensional vector into a d' dimensional vector, where $d' << d$ whilst, at the same time retaining as much discriminatory information as possible. The proposed feature extraction method is based on the distribution of the energy of the distorted signal in different frequency bands by utilizing wavelet multi-resolution analysis (MRA). The dimensionality of data is mapped into a small unmber of interpretable features. These features are proven to be very efficient in auto-classifying different power quality problems that overlap in time and frequency. This technique can be used to design an on-line

automated power quality monitoring system that has the ability to detect, localize, and classify different disturbances. It also can be used to auto-cluster large amount of data or classify it according to IEEE Std.1159. The results of the proposed technique suggest that it will be able to be implemented on-line "in real time" for classifying different power quality disturbances.

This chapter is organized as follows. After a brief introduction of this chapter, Section 6.2 presents the MRA tool and its ability to distribute the energy of different distorted power signals (voltages or currents) at different resolution levels. The standard deviation of each detail version of the decomposed signal can be used to classify different disturbances. The proposed Wavelet-based methodology for feature extraction is discussed in Section 6.3. Section 6.4 utilizes pattern recognition techniques to design an automatic classifier based on the wavelet features. Evaluation of the proposed wavelet-based features is discussed in Section 5.5. Application of the proposed automatic classification technique is presented and evaluated in Section 6.5. Finally assessment of this chapter is presented in Section 6.7.

6.2 Distribution of distorted signal energy in the wavelet domain

Disturbance in any signal can be considered as a result of change in the energy status of that signal. If one can detect by a proper method these changes then he can identify the disturbance type and magnitude. It is a known fact that for each type of disturbance there are some associated energy changes with the signal. The energy of the distorted signal will be partitioned at different resolution levels in different ways according to the power quality problem at hand. Therefore, having a tool that can decompose the energy of the signal and localize it in the time and frequency domains could be used in classifying different disturbances.

Using MRA, any distorted signal can be decomposed into different resolution levels. The energy of the detail coefficients at each resolution level is equivalent to the energy of the constructed version of the signal at that level. This is because the selected wavelet function is orthonormal and therefore satisfies Parsival's theorem (Section 4.9). The distribution of energy of the

coefficients at different resolution levels can be presented in terms of the standard deviation of the detail versions at each resolution level. This feature will be defined as the std-MRA curve.

To illustrate the efficiency of MRA in detecting and classifying power quality problems, different disturbances is simulated using Matlab code and mapped into the wavelet domain. The distribution of the energy for each detail version (standard deviation) is computed for each resolution level. The results are used to detect, localize and classify different phenomena based on the following rules:

6.2.1 Pure sine wave

Figure 6.1 shows the pure sine wave (Figure 6.1a) and the three finer decomposition levels (Figures. 6.1b, 6.1c, and 6.1d). The horizontal axis presents the time in seconds and the vertical axis presents the magnitude in volts. The std-MRA curve is shown in Figure 6.1e. The horizontal axis presents the different resolution levels and the vertical axis presents the magnitude of the standard deviation of the detail versions at different resolution levels.

In this case, all the finer resolution levels (Figures. 6.1b, 6.1c, and 6.1d) do not detect any changes. The pure sine wave std-MRA curve will be used as a reference in comparison with other cases. It will appear as a dotted line in each of the following cases.

6.2.2 Sag in a pure sine wave

The sag is detected and localized in all the finer three decomposition levels Figures 6.2b, 6.2c, and 6.2d. It is clear from the Figure that the duration of the sag can be easily measured, and hence determined if the sag phenomenon is instantaneous, momentary, or temporary. The maximum value of the std-MRA curve is decreased with an amount related to the sag magnitude and duration as shown in Figure 6.2e.

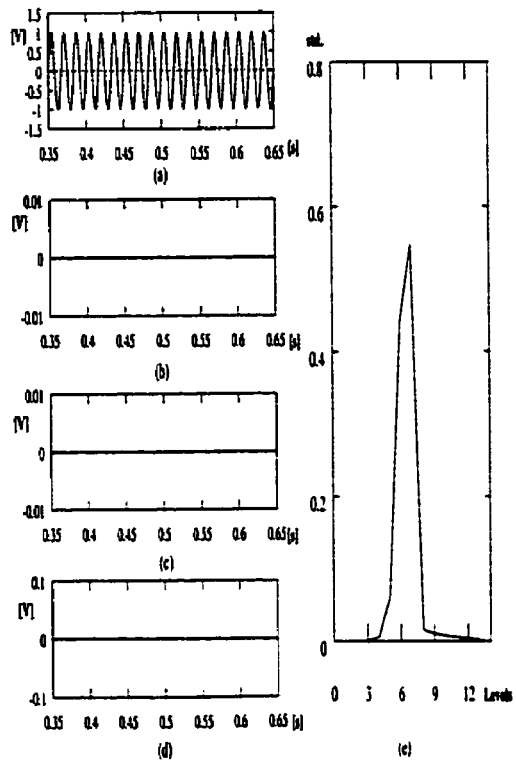

Figure 6.1: Detection, localization, and classification of a pure sine wave
a- Pure signal, b-First detail version, c- Second detail version, d- Third detail version, e- std_MRA curve

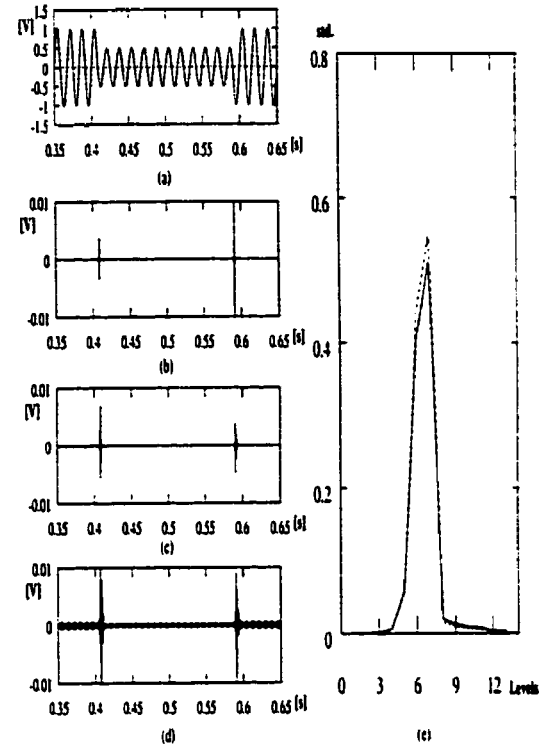

Figure 6.2: Detection, localization, and classification of a sag in a pure sine wave. a-Sag signal, b-First detail version, c-Second detail version, d- Third detail version, e- std_MRA curve

6.2.3 Swell in a pure sine wave

The swell is detected and localized in all the finer three decomposition levels, Figures 6.3b, 6.3c, and 6.3d. Similar to the sag case, the duration of the swell can be easily measured. The maximum value of the std-MRA curve is increased with an amount related to the swell magnitude and duration as shown in Figure 6.3e.

6.2.4 Harmonic distortion

Since harmonic distortion is stationary therefore, there is no localization property that can be detected at any of the finer levels, Figures 6.4b, 6.4c, and 6.4d. The lower left and right parts of the std-MRA curve is changed according to the harmonic content of the signal. As shown in Figure 6.4e, the lower left part is changed according to the high frequency content of the distorted signal and the lower left part is changed according to the low frequency content of the distorted signal compared with the power frequency (60 Hz).

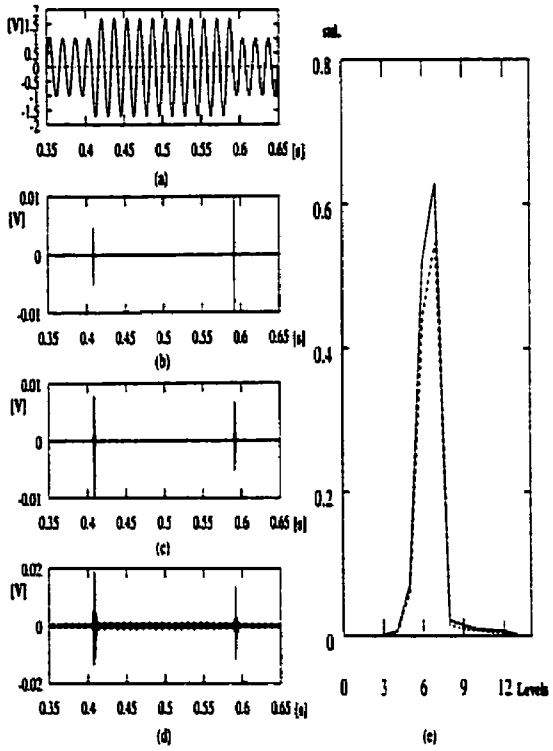

Figure 6.3: detection, localization, and classification of a swell in a pure sine wave. a-Swell signal, b-First detail version, c-Second detail version, d- Third detail version, e- std_MRA curve

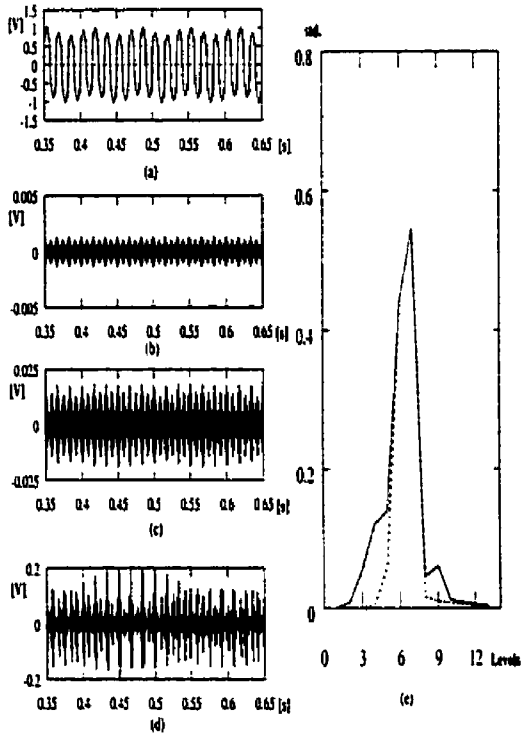

Figure 6.4: detection, localization, and classification of harmonic distorted signal a- Harmonic signal, b-First detail version, c- Second detail version, d- Third detail version, e- std_MRA curve

6.2.5 Sag in a harmonic distorted signal

The sag is detected and localized in the first finer level, Figure 6.5b. The number of decomposition levels can be increased to detect these phenomena at other finer levels. The amplitude of the decomposed signal is reduced during the sag interval compared by its magnitude before the sag, Figure 6.5c. The maximum value of the std-MRA curve is decreased with an amount related to the sag magnitude and duration as shown in Figure 6.5e. The lower left of the std-MRA curve is also changed according to the high frequency content of the signal.

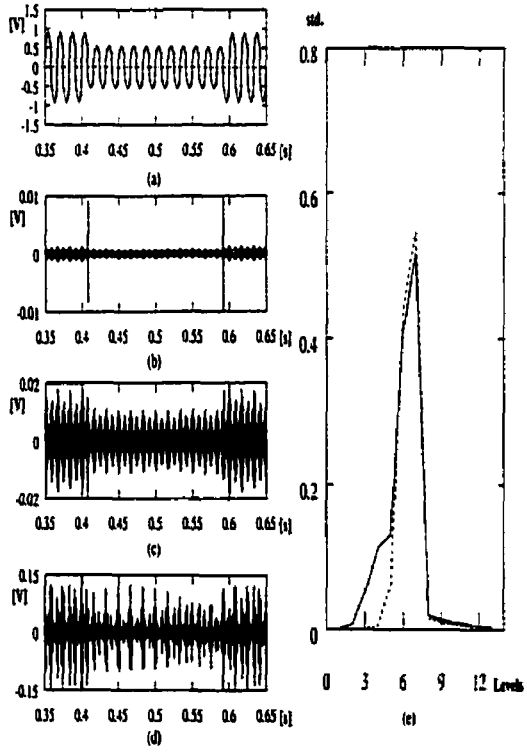

Figure 6.5: detection, localization, and classification of a sag in a harmonic distorted signal

a- Sag in harmonic signal, b-First detail version, c- Second detail version, d- Third detail version, e- std_MRA curve

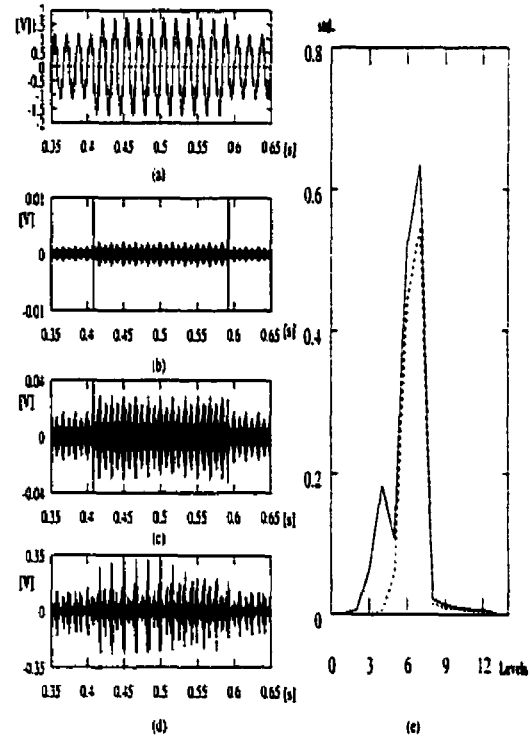

Figure 6.6: detection, localization, and classification of a swell in a harmonic distorted signal

a- Swell in harmonic signal, b-First detail version, c- Second detail version, d- Third detail version, e- std_MRA curve

6.2.6 Swell in harmonic distorted signal

The swell is detected and localized in the first finer level, Figure 6.6b. The amplitude of the decomposed signal is increased during the swell interval compared with its magnitude before the swell, Figure 6.6c. The maximum value of the std-MRA curve is increased with an amount related to the swell magnitude and duration as shown in Figure 6.6e. The lower left of the std-MRA curve is also changed according to the harmonic content of the signal.

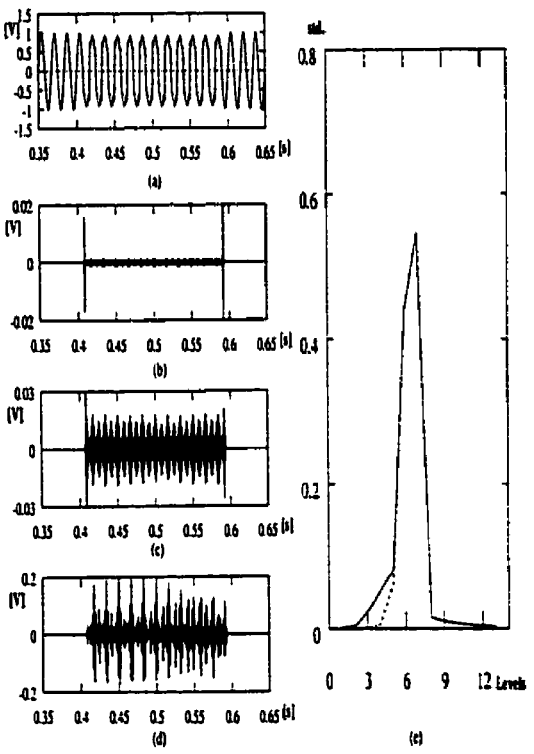

Figure 6.7: detection, localization, and classification the presence of non linear loads for short intervals
a- Distorted signal, b-First detail version, c-Second detail version, d- Third detail version, e- std_MRA curve

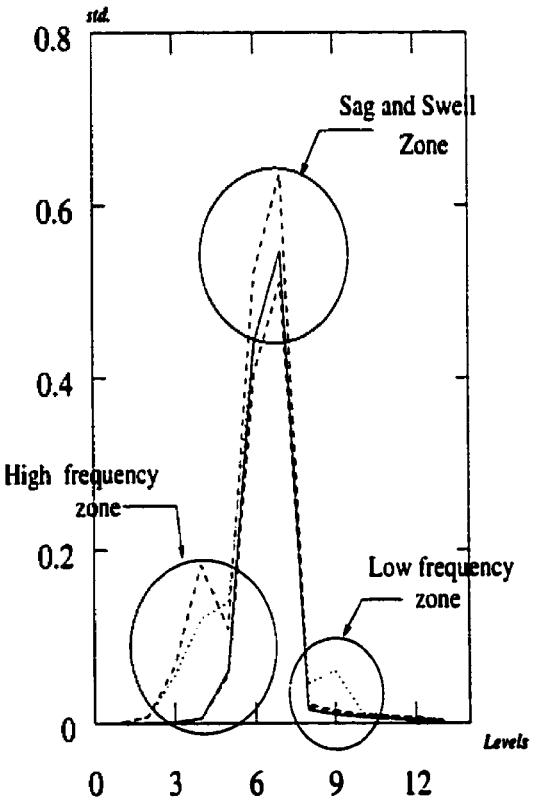

Figure 6.8: std-MRA curve for different Power quality problems.

6.2.7 Transient distortion in pure sine wave

This phenomenon is detected and localized at all the three finer decomposition levels, Figures 6.7b, 6.7c, and 6.7d. The magnitude of the coefficient outside the transient event interval is almost equal to zero for all the finer levels. The lower part of the curve will be changed according to the harmonic content of the transient.

Using the proposed rules extracted from the MRA technique at finer levels and the std-MRA curve one can detect, localize, and classify different power quality problems. This is clear from Figure 6.8, where the solid std-MRA curve is for a pure sine wave and the other curves are for:

A - Voltage swell in harmonic distorted signal, dashed curve above the pure sine wave curve.
B - Voltage sag in pure sine wave, dashed curve below the pure sine wave curve.
C - Harmonic distorted signal, dotted curve on the lower left and right parts of the pure sine wave curve.

These classification roles are so simple for the operator to detect, localize, and classify different power quality problems. The top part of the std-MRA curve is a good feature to classify the sag, swell, and interruption phenomena. The lower left part and the lower right part of the std-MRA curve are good indicators for any high or low frequency component embedded in the distorted signal.

6.3 The Proposed Classification Methodology

Feature extraction is a preprocessing operation that transforms a pattern from its original form to a new form suitable for further processing. Mapping the data of the distorted signal $s(t)$ into a wavelet domain is the first step in performing the proposed feature extraction process. The distribution of the distorted signal energy at different resolution levels is computed to generate the proposed translation invariant features. The term "translation invariant" denotes that the features remain unchanged if the power quality problem undergoes a change of position (translation). These features have the property of being able to effectively differentiate among different power quality problems.

According to Parseval's theorem, if the used scaling function and the wavelet function form an orthonormal basis, then Parseval's theorem relates the energy of the distorted signal to the energy in each of the expansion components and their wavelet coefficients. This means that the energy of the distorted signal can be partitioned in terms of the expansion coefficients. Therefore, the energy of the distorted signal, E^2_{Signal}, will be partitioned at different resolution levels in different ways according to the power quality problem at hand.

A set of discriminative, translation invariant features with small dimensionality that present the energy distribution of $f(t)$ at different resolution levels is generated. These features can be presented by computing the norm "$\| \cdot \|$" of the wavelet coefficients (C_{Signal} computed in Equation 5.5) that represent the distorted signal $f(t)$ at different resolution levels, as follows:

$$E_{Signal} = [\|c_o\| \ \|d_o\| \ \|d_1\| \ \ldots\ldots \|d_{J-1}\| \ ] \tag{6.1}$$

where,

$$\|c_o\|_2 = [\sum_{k=-\infty}^{\infty} |c_o(k)|^2 \ ]^{1/2} \tag{6.2}$$

$$\|d_j\|_2 = [\sum_{k=-\infty}^{\infty} |d_j(k)|^2 \ ]^{1/2} \tag{6.3}$$

In a similar way, the wavelet coefficients of a pure signal C_{pure} can be generated and used as a reference for the purpose of classification and measurements. These coefficients are:

$$C_{pure} = [c_{op} \mid d_{op} \mid d_{1p} \mid \ldots\ldots d_{(J-1)p} \mid] \tag{6.4}$$

and their energy distribution can be presented by the norm of the C_{pure}, using Equation 6.2 and Equation 6.3, the proposed feature vector x_o that is used to classify the distortion event can be generated by finding the difference ΔE that represent the energy distribution of the distortion event, where:

$$\Delta E = E_{signal} - E_{pure} \tag{6.5}$$

This feature vector can be represented in terms of the energy distribution of the distortion event on different resolution levels as:

$$x_o = [\ \Delta E_{Co}\ \ \Delta Ed_{do}\ \ \Delta E_{d1}\ \ .....\Delta E_{d(J-1)}\ ] \tag{6.6}$$

Or x_o can be mathematically represented as:

$$\begin{bmatrix} x_{01} \\ x_{02} \\ \vdots \\ x_{(0,j)} \\ \vdots \\ x_{(0,J+1)} \end{bmatrix} = \begin{bmatrix} \Delta E_{c(o)} \\ \Delta E_{d(o)} \\ \vdots \\ \Delta E_{d(j)} \\ \vdots \\ \Delta E_{d(J-1)} \end{bmatrix} = \begin{bmatrix} \| c_{od} \|_2 \\ \| d_{od} \|_2 \\ \vdots \\ \| d_{jd} \|_2 \\ \vdots \\ \| d_{(J-1)d} \|_2 \end{bmatrix} \tag{6.7}$$

$$x_{01} = \Delta E_{c(o)} = \| c_{od} \|_2 = [\ \sum_{k=-\infty}^{\infty} | c_{od}(k) |^2\ ]^{1/2} \tag{6.8}$$

$$x_{(0,j)} = \Delta E_{d(j)} = \| d_{jd} \|_2 = [\ \sum_{k=-\infty}^{\infty} | d_{jd}(k) |^2\ ]^{1/2} \tag{6.9}$$

Another component is added to the feature vector, $\Delta\tau$, that represents the duration of the distortion event. Using the first decomposition level of the distorted signal one can detect and localize any disturbance in the signal. The duration measurement of the distortion event is presented in the Chapter 5. The modified feature vector can then be presented as:

$$\begin{matrix} \textit{Feature} \\ \textit{Vector} \end{matrix} \quad \begin{matrix} \textit{Distorted} \\ \textit{Signal} \end{matrix} \quad \begin{matrix} \textit{Pure} \\ \textit{Signal} \end{matrix}$$

$$\begin{bmatrix} x_{01} \\ x_{02} \\ \vdots \\ x_{(0,j)} \\ \vdots \\ x_{(0,J+1)} \\ x_{(0,J+2)} \end{bmatrix} = \begin{bmatrix} E_{c(o)} \\ E_{d(o)} \\ \vdots \\ E_{d(j)} \\ \vdots \\ E_{d(J-1)} \\ \tau_{distortion} \end{bmatrix} - \begin{bmatrix} E_{c(o)} \\ E_{d(o)} \\ \vdots \\ E_{d(j)} \\ \vdots \\ E_{d(J-1)} \\ \tau_{pure} \end{bmatrix} = \begin{bmatrix} \Delta E_{c(o)} \\ \Delta E_{d(o)} \\ \vdots \\ \Delta E_{d(j)} \\ \vdots \\ \Delta E_{d(J-1)} \\ \Delta\tau \end{bmatrix} \tag{6.10}$$

where J represents the total number of resolution levels.

Figure 6.10 shows the difference in energy distribution (ΔE) at different resolution levels for 1200 distorted signals with the following power quality problems:

- Sag in a pure sine wave,
- Swell in a pure sine wave,
- Sag in a harmonic distorted signal,
- Swell in a harmonic distorted signal.

The sag and swell duration and magnitudes were randomly varied to cover the variation range indicated in IEEE std. 1159. The effective values of the harmonic distortion were also chosen randomly and all the signals were further corrupted by the addition of white gaussian noise. As the noise level increases from 0.5% to 3.5%, the proposed classification technique will provide a translation invariant feature vector as shown in Figures 6.9 and 6.10.

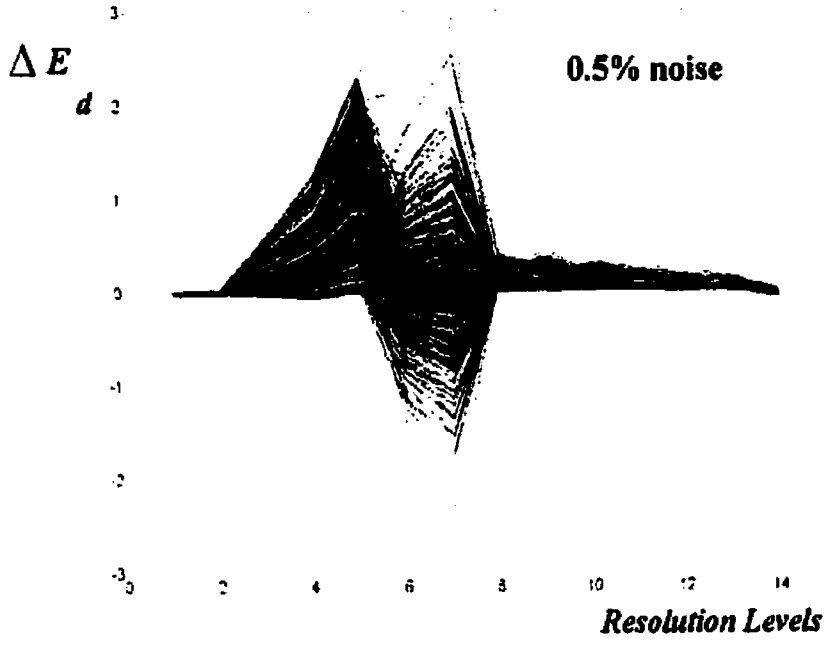

Figure 6.9: Feature vector for different power quality problems with noise level 0.5%

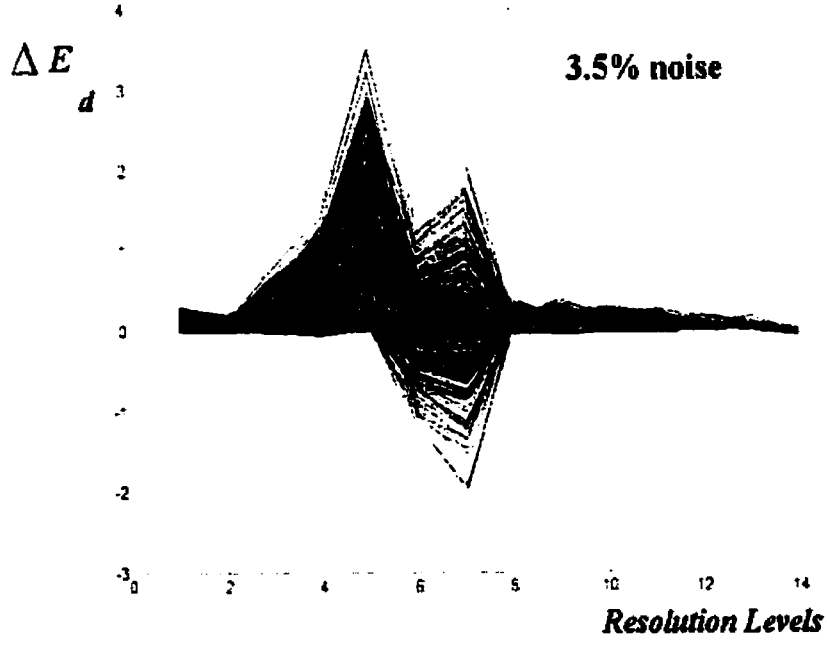

Figure 6.10: Feature vector for different power quality problems with noise level 3.5%

6.4 Automatic classification of different disturbances

Different pattern recognition techniques were used with the proposed features to design an automated recognition system. This system can be installed on-line to classify different disturbances according to IEEE std. 1159. The following sections give an introduction to different pattern recognition techniques that were implemented with the proposed features to classify different disturbances. Using the mentioned features one can classify power quality problems in noisy environment with or without dc offset. The proposed technique shows its ability to classify steady state and transient phenomena. It can be implemented to classify non-stationary signals or signals that are distorted with more than one power quality problem.

6.4.1 Pattern Recognition Techniques

Pattern recognition techniques are automated tools for decision-making processes. One of the important applications of pattern recognition is in waveform classifications, which is to predict the class membership of a distorted signal and to minimize the risk of misclassification. In this section, a comprehensive study of the effectiveness of the proposed translation invariant features using the following pattern recognition techniques is studied in order that we can use them in the proposed automated disturbance classifier [71-78]:

1. Minimum Euclidean distance Classifier

2. k – nearest neighbor Classifier

3. Neural network Classifier

4. Rule-Based Classifier

6.4.1.1 Minimum Euclidean Distance Classifier (MED)

For MED classification, the unknown feature x_o is more likely to belong to the class r_l if and only if the distance between x_o and a prototype (mean μ) of class r_l is less than the distance between x_o and other class prototype. This is can be formulated as follows:

$$x_o \in r_l \quad iff \quad d_E(x_o, \mu_l) < d_E(x_o, \mu_k) \tag{6.11}$$

where, the Euclidean distance is:

$$d_E(x_o, \mu_l) = \left[\sum_{i=1}^{n} (x_{oi} - \mu_l)^2 \right]^{1/2} \tag{6.12}$$

6.4.1.2 K-nearest neighbour (kNNR) Classifier

The nearest neighbour (NNR) is a classification technique that assigns unknown pattern x_o to the class of its nearest neighbour. The NNR can be formulated as [71-72]:

$$x_o \in r_l \quad iff \quad d(s_l, x_o) = min_l (d(s_l, x_o)) \tag{6.13}$$

where d is the distance between the set of classified learning data samples, $s_l = \{s_1, s_2, \ldots\ldots s_N\}$, and the unknown sample to be classified x_o. The k-nearest neighbour (kNNR) is an extension of the NNR, where the unknown sample x_o, is assigned to the class of the majority among the k-nearest neighbours.

6.4.1.3 Neural Network Classifier (NN)

A Neural network is a powerful pattern recognition tool [77-78]. It is defined as software algorithms that can be trained to learn the relationships that exist between input and output data, including non-linear relationships. Once they have learned by examples they can generalize. Figure 6.11 shows a three layers feed-forward neural network classifier. The NN utilizes the proposed feature vector as an input to classify different power quality problems according to IEEE std. 1159.

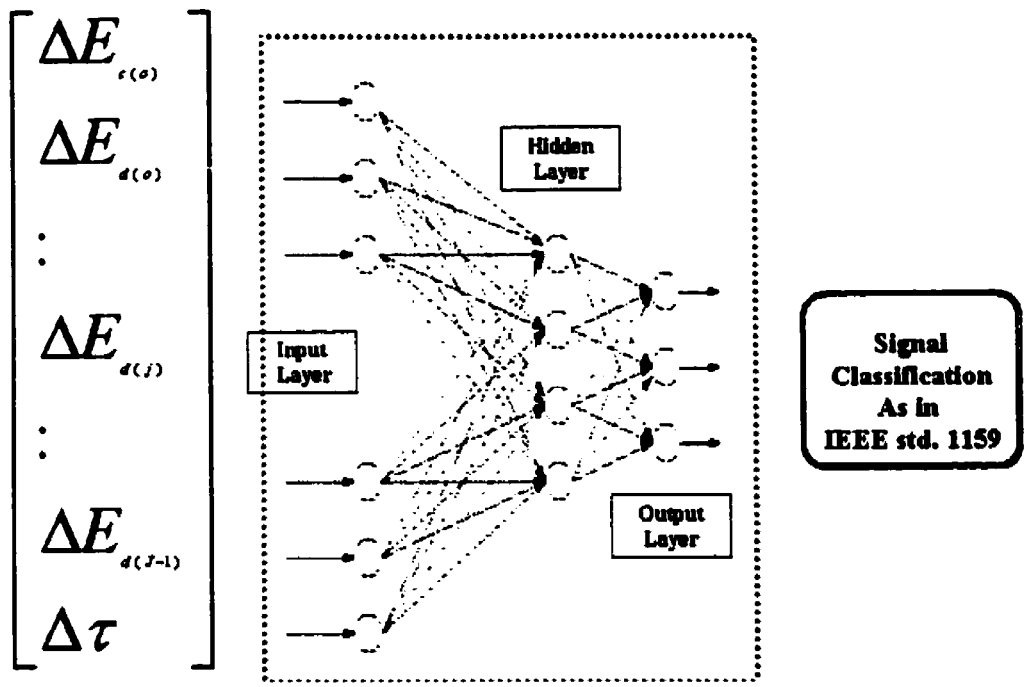

Figure 6.11: Automatic power quality classification using Neural Net classifier

6.4.1.4 Rule-Based Classifier (RBC)

A set of rules is constructed to classify different power quality problems. These rules are simple combinations of propositions that can be evaluated to be either true or false. Each decision rule is associated with a particular class, and a rule that is satisfied, i.e., is evaluated as true, is an indication of particular class. These rules are as follows:

IF	C_1 AND C_2 AND C_3 AND C_4	Then	Pure Signal
IF	C_5	Then	High Frequency Content
IF	C_6 OR C_7	Then	Low Frequency Content
IF	C_8	Then	Sag
IF	C_9	Then	Swell
IF	C_{10}	Then	DC Offset

The propositions are constructed using a set of conditions (C_1-C_{10}). Each condition that enters into the propositions making up a decision rule involves a simple logical operation (Anding, Oring).

These conditions are as follows:

C_1	x_{014} *And* x_{013} *And* x_{012} *And* x_{011} *And* x_{010}	$\leq$	Θ_5
C_2	x_{09} *And* x_{08}	$\leq$	Θ_4
C_3	x_{07} *And* x_{06}	$\leq$	Θ_3
C_4	x_{05} *And* x_{04} *And* x_{03} *And* x_{02}	$\leq$	Θ_2
C_5	x_{014} *Or* x_{013} *Or* x_{012} *Or* x_{011} *Or* x_{010}	$>$	Θ_5
C_6	x_{07} *Or* x_{06}	$>$	Θ_3
C_7	x_{05} *Or* x_{04} *Or* x_{03} *Or* x_{02}	$>$	Θ_2
C_8	x_{08}	$<$	0.0
C_9	x_{08}	$>$	0.0
C_{10}	x_{01}	$>$	Θ_1

Where x_{0i} represents the feature vector i extracted as indicated in Equation 6.10.

The different threshold values ($\Theta_1 - \Theta_5$) are computed using the following equation:

$$\begin{matrix} \text{Threshold} \\ \begin{bmatrix} \Theta_1 \\ \Theta_2 \\ \Theta_3 \\ \Theta_4 \\ \Theta_5 \end{bmatrix} \end{matrix} = \begin{matrix} \text{Threshold} \quad \text{Vector} \\ \begin{bmatrix} \Delta E_{ct(o)} & \\ Max(\Delta E_{dt(j)}) & j = 0,\ldots,3 \\ Max(\Delta E_{dt(j)}) & j = 4,5 \\ Max(\Delta E_{dt(j)}) & j = 6,7 \\ Max(\Delta E_{dt(j)}) & j = 8,\ldots,12 \end{bmatrix} \end{matrix} \tag{6.14}$$

where,

$$\begin{bmatrix} \Delta E_{ct(o)} \\ \Delta E_{dt(o)} \\ \vdots \\ \Delta E_{dt(j)} \\ \vdots \\ \Delta E_{dt(J-1)} \end{bmatrix} = \begin{matrix} \text{Pure with noise and phase shift} \\ \begin{bmatrix} E_{ct(o)} \\ E_{dt(o)} \\ \vdots \\ E_{dt(j)} \\ \vdots \\ E_{dt(J-1)} \end{bmatrix} \end{matrix} - \begin{matrix} \text{Pure Signal} \\ \begin{bmatrix} E_{ct(o)} \\ E_{dt(o)} \\ \vdots \\ E_{dt(j)} \\ \vdots \\ E_{dt(J-1)} \end{bmatrix} \end{matrix} \tag{6.15}$$

According to Equation 6.14 and 6.15, all threshold values are equal to zero in the case of a pure signal. To generate the worst condition, a pure signal contaminated with noise and phase shift angle is used. The maximum noise level was selected equal to 2.0% and the phase shift angle was varied between 0 and $\pi/2$. The selected threshold values are shown in Table 6.1.

Table 6.1: The threshold values at different levels

Features	Threshold	
	Θ_i	mag.
x_{01}	Θ_1	0.001
$x_{02} - x_{05}$	Θ_2	0.08
$x_{06} - x_{07}$	Θ_3	0.15
$x_{08} - x_{09}$	Θ_4	0.015
$x_{010} - x_{014}$	Θ_5	0.085

6.5 Feature Evaluation using Different Classifiers

A confusion matrix M is used as a measure for the classification accuracy. This type of measure is used to summarize both overall accuracy of classification and the relative levels of various types of misclassification. The number of correct classification falls along the diagonal of the matrix M and all off-diagonal elements represent miss-classifications [70-71].

The classification accuracy or error percentage is computed as follows:

$$Accuracy = \frac{N_{correct}}{N_{Total}} * 100 \tag{6.16}$$

$$Error = \frac{N_{error}}{N_{Total}} * 100 \tag{6.17}$$

$$N_{correct} = \sum diag(M) = \sum_{i=1}^{p} m_{ii} \tag{6.18}$$

$$N_{error} = \sum_{j=1}^{p} \sum_{i=1}^{p} m_{ij} \qquad \forall\ i \neq j \tag{6.19}$$

where N_{Total} is the total number of samples, $N_{correct}$ is the number of correctly classified samples, N_{error} is the number of errors, and p is the number of classes.

6.6 Application and Results

6.6.1 Oscillatory Transient phenomenon

The proposed classification technique is applied to classify the simulated oscillatory transient indicated by Equation 2.2 and shown in Figure 6.12. As indicated in Section 2.10 neither the STFT technique nor the point-by-point comparison technique can monitor exactly the duration or classify the oscillatory transient event.

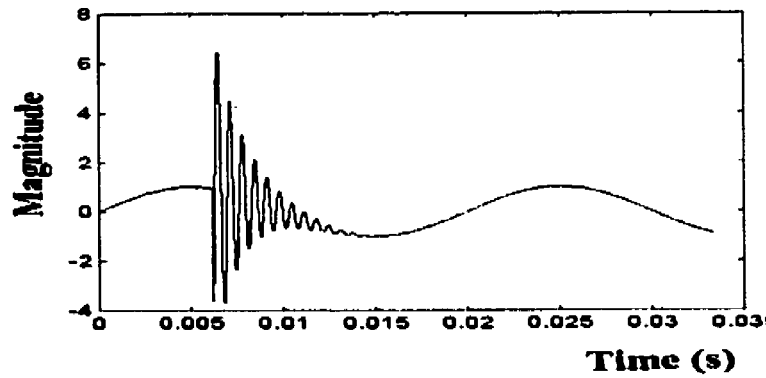

Figure 6.12: Simulated oscillatory distorted signal

Utilizing MRA, the signal is mapped into 2D and decomposed into 12 resolution levels (Table 6.2) covering the frequency band from 0 to f_{max} (=120kHz).

Due to convolution with the wavelet filter followed by decimation by two the resulted spectrum will cover the frequency band ($f_{max}/2$ *to* f_{max}). Therefore, implementing the proposed technique, the First Detail Version D_1 (Figure 5.5) of the distorted signal (in frequency band 60 – 120 kHz.) can be used to localize the distortion event in time as indicated in Section 5.5.1.

Table 6.2: Different resolution levels and their frequency bands

Resolution Level	Frequency Band (Hz)	Resolution Level	Frequency Band (Hz)
1	60 – 120 k	7	937.5 – 1875
2	30 – 60 k	8	468.75 - 937.5
3	15 – 30 k	9	234.35 – 468.7
4	7.5 – 15 k	10	117.17 – 234.35
5	3.75 – 7.5 k	11	58.58 – 117.17
6	1.875-3.75 k	12	29.29 – 58.58

Figure 6.13 shows the feature vector of the distorted signal compared to the feature vector of a pure undistorted signal. The 7th resolution level (in frequency band 937.5-1875 Hz) shows a high-energy content ($\| d_d \|_2 \cong 60$); note that the 7th resolution level includes the 1500 Hz component previously imbedded in the simulated signal $f(t)$ as in Equation 2.2. Part of the distortion event energy is leaked to the adjacent 6th (frequency band 1875-3750 Hz) and 8th (frequency band 468.75-937.5 Hz) resolution levels. However, the magnitude of this leakage energy is very small compared with that in the 7th resolution level due to the sharp cut-off frequency of the selected wavelet filter (Daubechies 40). This leads to an important criterion in selecting the mother wavelet to be used for the analysis, which will be presented in Appendix B.

The results of MRA technique, where the energy of the distortion event concentrated at the 7th resolution level (frequency band = 937.5-1875 Hz) and duration= 12ms, are compared with the categories of electromagnetic phenomena presented by IEEE Std.1159 and shown in Table 6.3. The distortion event is then classified as oscillatory transient with low frequency content.

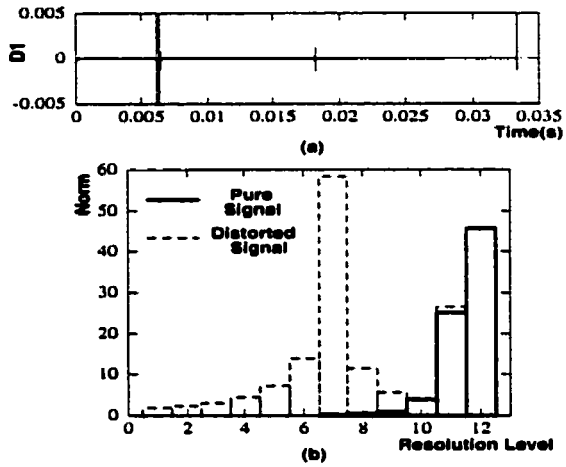

Figure 6.13: Discrete Wavelet Transform

Table 6.3: Typical characteristics of transient phenomena in power systems (Part of Table 2 -IEEE Std.1159-1995)

A – Impulsive Transient	**Typical Spectral**	**Typical Duration**	**Typical Magnitude**
1 – Nanosecond	5 *n* s rise	< 50 *n* s	
2 – Microsecond	1 μ s rise	50 *n* s - 1 ms	
3 – Millisecond	0.1 ms rise	< 1 ms	
B – Oscillatory Transient			
1 – Low Frequency	***< 5 kHz***	***0.3 - 50 ms***	***0-4 pu***
2 – Medium Freq.	5-500 kHz	20 μ s	0-8 pu
3 - High Frequency	0.5 - 5 M Hz	5 μ s	0-4 pu

6.6.2 Feature extraction of a transient event

Utilizing MRA, the distorted signal, a capacitor switching phenomena shown in Figure 6.14, is decomposed into several detail versions (building blocks). Some of these building blocks that have important parts of the energy of the distorted signal are shown in Figure 6.15. The shown resolution levels include detail versions of the first D_1, second D_2, sixth D_6, seventh D_7, eighth D_8, tenth D_{10}, eleventh D_{11}, and twelve D_{12} as shown in Figure 6.15a-i respectively. These versions of the signal are easier to study and interpret.

The capacitor switching phenomena is sampled at 165 kHz and a 3 cycles window size is selected (8266 sampling point). These sampling points (c_{j+1}) are used as input for MRA and decomposed into 13 resolution levels. The frequency bands that represent each resolution level are summarized in Table 6.4. Using the first detail version D_1 (Figure 6.15a), any changes in the pattern of the signal can be detected and localized. The duration of the distortion event can be measured from the detail coefficients (d_j) at this resolution level. The size of the coefficients (d_j) is equal to zero for a pure signal and they will have certain values for any disturbance event. MRA shows that most of the distortion event energy is concentrated at seventh resolution level D_7 (645-1289 Hz) as shown in Figure 6.15d. The eleventh resolution level (40-80 Hz) presents the 60Hz power signal as shown in Figure 6.15g.

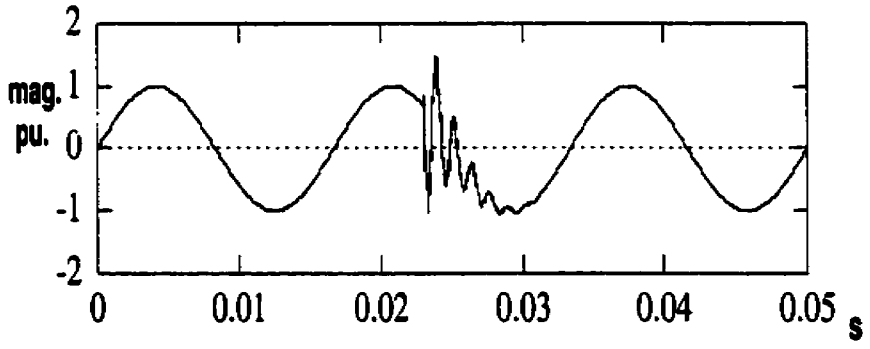

Figure 6.14: Capacitor switching phenomena

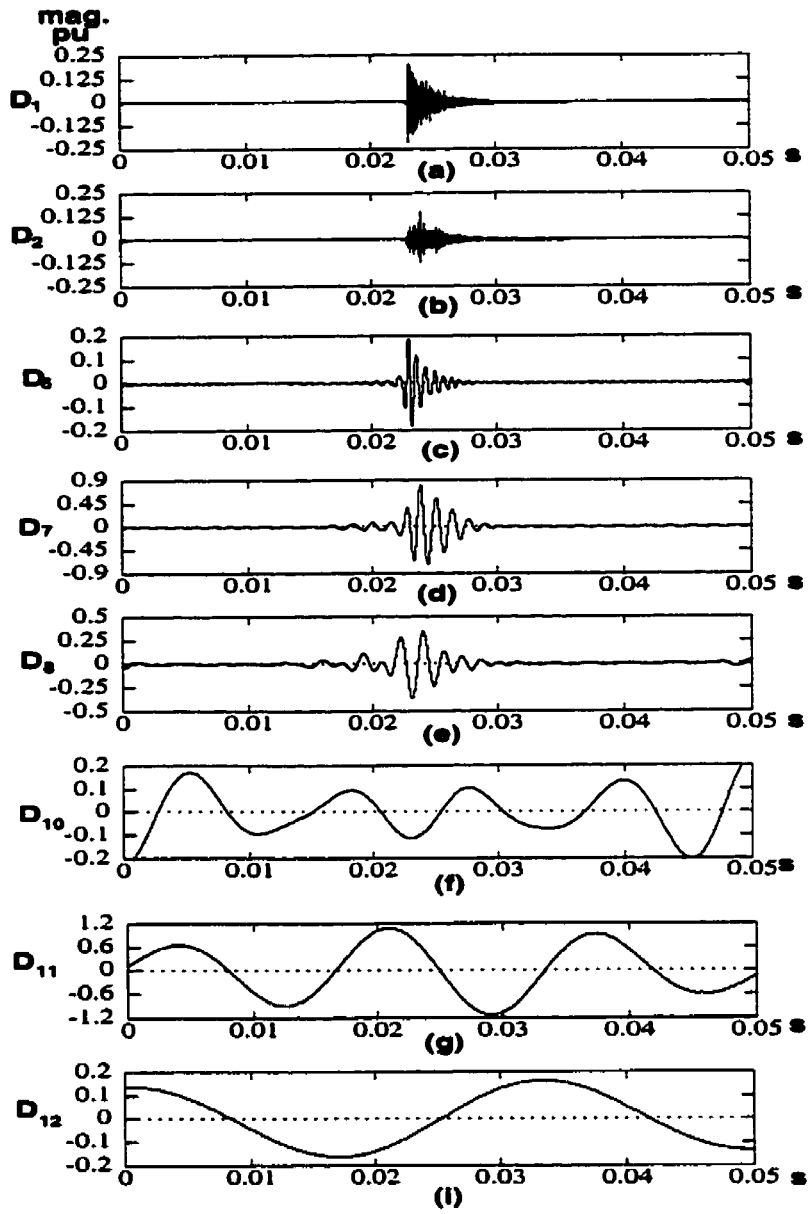

Figure 6.15: Building blocks " different resolution levels" of the distorted signal

a- First detail version, b- Second detail version, c- Sixth detail version, d- Seventh detail version, e- Eighth detail version, f- Tenth detail version, g- Eleventh detail version, i- twelfth detail version

Leakage of the signal energy will be seen at adjacent resolution levels. For example, part of the 60Hz energy of the signal, Figure 6.15g, will be leaked to the adjacent resolutions; Figure 6.15f and Figure 6.15i. This is due to the non-sharp cut-off frequencies of the wavelet filters. However, the magnitude of this leakage energy is very small compared with that in Figure 6.15g. The selection of the filters will help in reducing this leakage. As the number of filter coefficients n

increases, the cut-off frequency will become more sharp and the leakage energy is reduced. This is an important criterion in selecting the mother wavelet to be used for the analysis.

Table 6.4: Different resolution levels and their frequency bands

Resolution Level	Frequency Band kHz	Resolution Level	Frequency Band kHz
1	41.25 - 82.50	8	0.322 – 0.645
2	20.62 - 41.25	9	0.161 – 0.322
3	10.31 - 20.62	10	0.081 – 0.161
4	5.150 - 10.31	11	0.040 – 0.081
5	2.570 - 5.150	12	0.020 – 0.040
6	1.289 - 2.570	13	0.010 – 0.020
7	0.645 - 1.289		

The distribution of signal energy at different resolution levels (building blocks) can be used to extract important features that help in classifying different power quality problems. Furthermore, the localization property of the wavelet transform coefficients of the first resolution level can give accurate information on classifying the type of distortion as continuous or transient, and stationary or non-stationary.

The proposed feature extraction technique is applied on the distorted signal $f(t)$ in Figure 6.14 (capacitor switching phenomena). The energy distribution for both the distorted signal (dashed line) and pure one (solid line) is shown in Figure 6.16a. The extracted feature vector for $f(t)$ is shown in Figure 6.16b. The distorted signal (8266 sampling points) is mapped into a small number of features (13 numbers). This feature vector extracts the energy of the distortion event and distributes it across different resolution levels. Figure 6.16b shows that the distortion event energy is distributed across resolution levels 1 to 8. Most of the distortion energy is concentrated in the 7^{th} resolution level (645–1289 Hz). The time information of this distortion event is measured from the first resolution level and found to be 7 ms as shown in Figure 6.15a. These results; resolution level =7, frequency band = 645-1289 Hz, and duration= 7ms, are compared with the categories of electromagnetic phenomena presented by IEEE Std.1159. The distortion event is then classified as oscillatory transient with low frequency content.

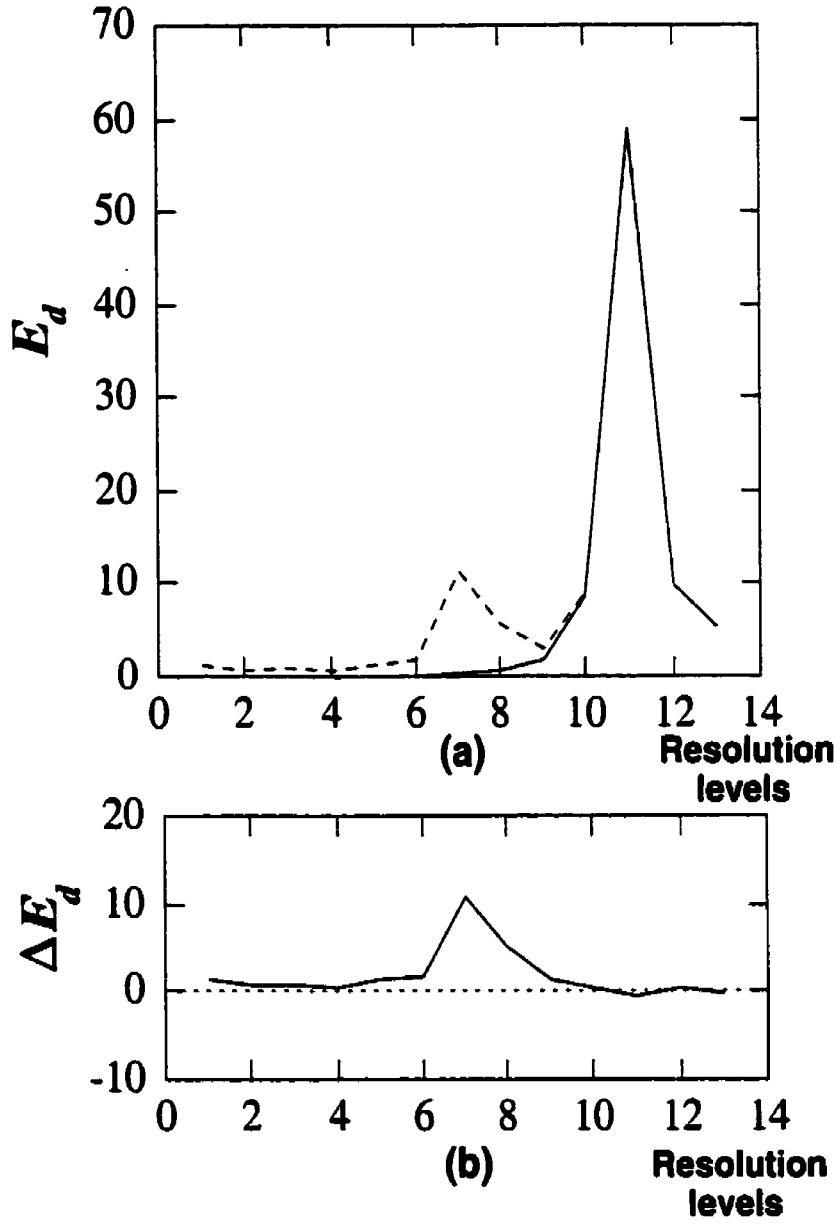

Figure 6.16: Distribution of energy of the signal at different resolution levels

6.7 Wavelet Based Automated Recognition System

In order to test the ability of the proposed classifier to distinguish between frequently encountered power quality problems, a set of pure signal and five different disturbances have been simulated using Matlab, in particular:

1. Sags
2. Swells
3. Harmonics
4. Sags and harmonics
5. Swells and harmonics
6. Pure signal

6.7.1 Data Generation

For each type of disturbance, a subset of 200 different signals was generated. Each signal is one-second long, sampled at 8.192 kHz, which corresponds to 8192 samples. The parameters of these disturbances were chosen according to IEEE std. 1159 [16]. The sag and swell duration was randomly varied from 12.5 ms to 0.985 s. Their voltage magnitudes were selected randomly to cover the variation range from 0.9 to 1 pu and from 1.1 to 1.8 pu respectively. The effective values of the harmonic distortion was chosen randomly between 2.5% and 60% and include harmonic components up to the 15^{th} harmonic. All signals were further corrupted by the addition of white gaussian noise with zero-mean and one-standard deviation and magnitude that vary between 0% and 3.5%.

6.7.2 Simulated Results

Three classification methods that can learn from data and make prediction on new cases are applied. The performance of the different classification methods, using the proposed wavelet-feature extraction technique to recognize the mentioned power quality problems, is presented in

this section. The variance methods were compared relative to each other using the confusion matrix and the error rate.

6.7.3 Minimum Euclidean Distance Classifier

Several data sets were generated for learning and testing purpose. A learning set of 1200 signals was divided into 6 subsets each of 200 signals. Each subset represents one of the mentioned power quality problems with different variables. The noise level for the learning set was equal to 0.5%. Using the proposed feature extraction technique, each signal (8196 points) was mapped into a, discriminative and translation invariant, feature vector of 15 elements. Using the learning set a prototype (mean μ_i) for each class r_i was computed.

Another five sets, each of 6 subsets with similar size as the ones in the learning set, were generated for the purpose of testing. The noise level for each testing set was increased to 0.5%, 1.0%, 1.5%, 2.5%, and 3.5%. Features were extracted from each signal and used to classify different power quality problems. The performance of MED classifier for 0.5% noise level testing data is presented in Table 6.5.

Table 6.5: Confusion matrix using MED Classifier

True Class	Classification Results					
	Pure	Sag	Swell	Har.	Sag & Har.	Swl & Har.
Pure	200	0	0	0	0	0
Sag	83	117	0	0	0	0
Swell	95	0	105	0	0	0
Har.	71	0	0	128	0	1
Sag& Har	14	46	0	64	76	0
Swell & Har	20	0	24	55	0	100
Classifier Accuracy	60.50 %					

The MED classifier takes a small computation time compared with the other methods, however it shows low classification performance. This is due to the non-spherical shape of the feature space. The confusion matrix shows a misclassification of the data that have mixed characteristics such as sag-harmonic and swell-harmonic cases.

6.7.4 k-Nearest Neighbour (k-NNR) Classifier

The same learning and testing sets were used for this classifier. The 31-nearest neighbours were selected to classify the unknown feature x_o to the class of the majority r_i among the 31-nearest neighbours as indicated in Equation 6.13. The performance of k-NNR classifier for 0.5% noise level testing data is presented in Table 6.6.

The k-NNR classifier takes more computation time compared to the MED. The method shows high classification accuracy for 0.5% noise level. The accuracy of the classifier was reduced as the noise level increased beyond 0.5%, see Table 6.9. The k-NNR shows good classification accuracy for mixed power quality problems such as the swell-harmonic case.

Table 6.6: Classification Results using KNNR Classifier

True Class	Classification Results					
	Pure	Sag	Swell	Har.	Sag & Har.	Swl & Har.
Pure	200	0	0	0	0	0
Sag	0	197	0	0	3	0
Swell	0	0	196	0	0	4
Har.	2	0	0	194	1	3
Sag &Har	0	8	0	18	174	0
Swell & Har	0	0	7	2	2	189
Classifier Accuracy				95.8333 %		

6.7.5 Neural Network Classifier (NN)

A three layers feed-forward neural network was used to classify different power quality problems. The single hidden layer is constructed using 4 units. The NN classifier was trained on a large set of data consisting of 6 subsets each of 400 signals. The parameters for each subset were changed randomly. The noise level was also randomly varied between 0-5%. The feature vectors for different power quality problems (6 subsets) were extracted and used as an input data for training the NN classifier.

Using the same testing data that was used for MED and k-NNR classifiers, the NN classifier shows high accuracy. The random noise level was increased from 0.5% to 3.5% and the NN classifier still gave accurate results. The results of the classification process using NN for 1.0% noise level data is presented in Table 6.7.

Table 6.7: Classification Results using NN classifier

True Class	Classification Results					
	Pure	Sag	Swell	Har.	Sag & Har.	Swl & Har.
Pure	200	0	0	0	0	0
Sag	2	198	0	0	0	0
Swell	11	3	185	0	1	0
Har.	0	1	0	199	0	0
Sag &Har	0	0	0	1	197	2
Swell & Har	0	1	3	19	12	165
Classifier Accuracy	95.333 %					

6.7.6 Rule Based Classifier (RBC)

Using the extracted features, each signal (8196 points) was mapped into a discriminative and translation invariant feature vector of 15 elements. Applying the classification rules, different power quality problems were classified. Table 6.8 shows the classification results for six subsets

(1200 signals, 200 each class) that present the above mentioned power quality problems where the noise level is 1%.

Table 6.8: The confusion matrix and the classification results

True Class	Classification Results					
	Pure	Sag	Swell	Har.	Sag & Har.	Swl & Har.
Pure	200	0	0	0	0	0
Sag	0	196	1	0	3	0
Swell	0	0	200	0	0	0
Har.	6	0	0	194	0	0
Sag &Har	0	0	0	0	199	1
Swell & Har	0	0	8	0	0	192
Classifier Accuracy	98.4167 %					

6.7.7 Performance Comparison

While speed of computation and simplicity of solution may help in deciding which methods should be applied, the accuracy of the performance will always remain the primary criterion in choosing the classifier. The error rate (Equation 6.17) is used in measuring the performance of each classifier. The results of the error rate at different noise levels are presented in Table 6.9.

From the tabulated results shown in Table 6.9, it is clear that the error rate for Neural Network classifier is generally better than that for the others. From the tabulated results shown in Table 6.9, it seems that the error rate for the RB classifier is small particularly when the noise level is below 2.5%. This is due to the fact that when the noise level is increased beyond 2.5% the proposed threshold values listed in Table 6.1 can no longer distinguish among different power quality problems. Furthermore, high noise level will cause problems in measuring the duration of the transient event from the three higher resolution levels. The NN classifier shows higher overall performance even with high noise levels. The NN classifier is the least sensitive to noise level variation in the input data. The k-NNR classifier also shows a good performance for 0.5% noise

level. The MED classifier shows low classification performance due to the non-spherical shape and the overlap in the features space. The MED classifier cannot classify an unknown sample that has several characteristics of mixed classes such as sag-harmonic or swell-harmonic, while the k-NNR and NN classifiers can classify such cases.

Table 6.9: comparison the classification accuracy
for different data groups using different classifiers

Noise Level	Error %			
	MED Classifier	KNNR Classifier	Neural Net Classifier	RB Classifier
0.5%	39.50	4.17	4.67	1.59
1.0%	36.17	15.66	4.67	1.59
1.5%	38.17	11.92	6.00	2.00
2.5%	38.50	15.33	5.17	7.34
3.5%	36.58	11.58	7.18	47.92

6.8 Chapter Assessment

In this chapter a new technique to extract important features for distortion events that overlaps in time and frequency are proposed. This technique is based on both a wavelet multi-resolution analysis for feature extraction and pattern recognition techniques for automated classification. This technique can be implemented as a new tool to overcome the limitations in the existing disturbance analyzers. The following points summarize the finding of this chapter:

- MRA is used to generate a translation invariant feature vector that can be used to classify different power quality problems. The advantage of this technique lies in the feature vector which shows the same characteristics at different noise levels.

- The size of the feature vector is very small compared with that of the original signal.

- The performance of the pattern recognition techniques, which is based on the generated features show excellent results in classifying different power quality problems, especially with RBC technique.

The detection, localization, and classification capability of the proposed technique presents encouraging results which can be used to modify the present monitoring techniques in order to give superior capabilities for measuring different disturbances. This new measuring technique will be discussed in Chapter 7.

Chapter 7

The New Measurement Technique

7.1 Introduction

This chapter presents a new measurement technique that can measure accurately a wide range of different power quality problems. The distortion event is mapped into the wavelet domain and extracted from the raw data. The wavelet coefficients of the distortion event are then used combined with the measured duration (Chapter 5) to quantify the true RMS. The proposed technique is implemented to measure the RMS, total harmonic distortion, dc content, and the phase shift angle. The coefficients are also used to compute the active and reactive power in any system under steady state conditions.

This chapter also introduces a new wavelet-based procedure to monitor the fast variation of RMS value in the signal. This procedure will help in monitoring the non-rectangular variations of the sag phenomena. It can also be used to assist the quality of service presented in the distribution systems, as well as the quality of the mitigation devices, and the characteristics of any load during RMS variations. The new measurement technique can be also implemented to monitor any new variations of the distortion event before it elapses. This information will help in finding the rectangular or non-rectangular voltage-tolerance curves for different equipment.

The proposed techniques can be executed by transforming the distorted signal into the wavelet domain and extracting the distortion event. Knowing the wavelet coefficients that represent the distortion event we can calculate its energy. Furthermore, using the detail version of the first

resolution level we extract the duration of the distortion event. Using this information one can measure the magnitude of the distortion event.

The proposed measurement technique is implemented in two different ways. In the first measurement technique, the maximum change in the energy of the resolution level that represents the power frequency and the duration of this disturbance are used to construct a set of curves. These curves can be used to monitor and measure any changes in the magnitude of the signal. In the second proposed measurement technique, the coefficients that represent the signal in the wavelet domain are used to extract the distortion event and calculate its indexes.

The proposed measurement technique, which is based on wavelet multi-resolution analysis, has the ability to give indices of signals that are distorted by more than one power quality event that overlap in time and frequency. The proposed measurement technique is used to measure and studying the following parameters under noisy conditions and multi-distortion events:

- Peak value during short duration variations (SDV)
- Root mean square (RMS) and total harmonic distortion (THD)
- Active and Reactive power and power factor
- Non-rectangular RMS variations

This chapter is organized as follows. After a brief introduction to the measurement in the wavelet domain, a proposed technique that utilizes the maximum value of std-MRA curves is presented in Section 7.2. A set of curves is generated to measure short duration variations (SDV) in electrical systems. In Section 7.3, the wavelet expansion coefficients are introduced as a measure of the RMS, THD, active, and reactive power, and the power factor. A new wavelet based monitoring technique for the non-rectangular RMS variations is discussed in Section 7.5. The applications and results of the proposed measuring techniques are presented in Sections 7.6. Finally an assessment of the proposed measurement technique is presented in Section 7.7.

7.2 Measurements of Short-duration variations Using std-MRA curves

Measuring the magnitude of the distortion within the signal is an important factor in assisting the quality of the power and in making a decision to store the signal or discard it.

During short duration variations (SDV), the energy of the distorted signal will show changes in its magnitude for certain period of time. Therefore the std_MRA curve will present these variations at the resolution level that covers the power frequency (60Hz) and the duration of this variation can be monitored in the first detail version of the distorted signal. By monitoring the changes in the maximum point of the std-MRA curve, we can quantify the magnitude of the SDV of the signal. As the magnitude or duration of the signal changes during the SDV event, the maximum value of the std-MRA curve will also change. Figure 7.1 shows the variation in the magnitude of the std-MRA curve for four signals:

- Pure sine wave of the power frequency signal
- 10-cycle sag in a pure sine wave
- 10-cycle swell in a pure sine wave
- 30-cycle interruption in a pure sine wave

The changes in magnitude and duration of the short duration variation (SDV) events can be calculated by generating a set of curves that represent the variation in the std-MRA curve as the magnitude and duration of the SDV event changes, as seen in Figure 7.2. The measurement curves are generated as follows:

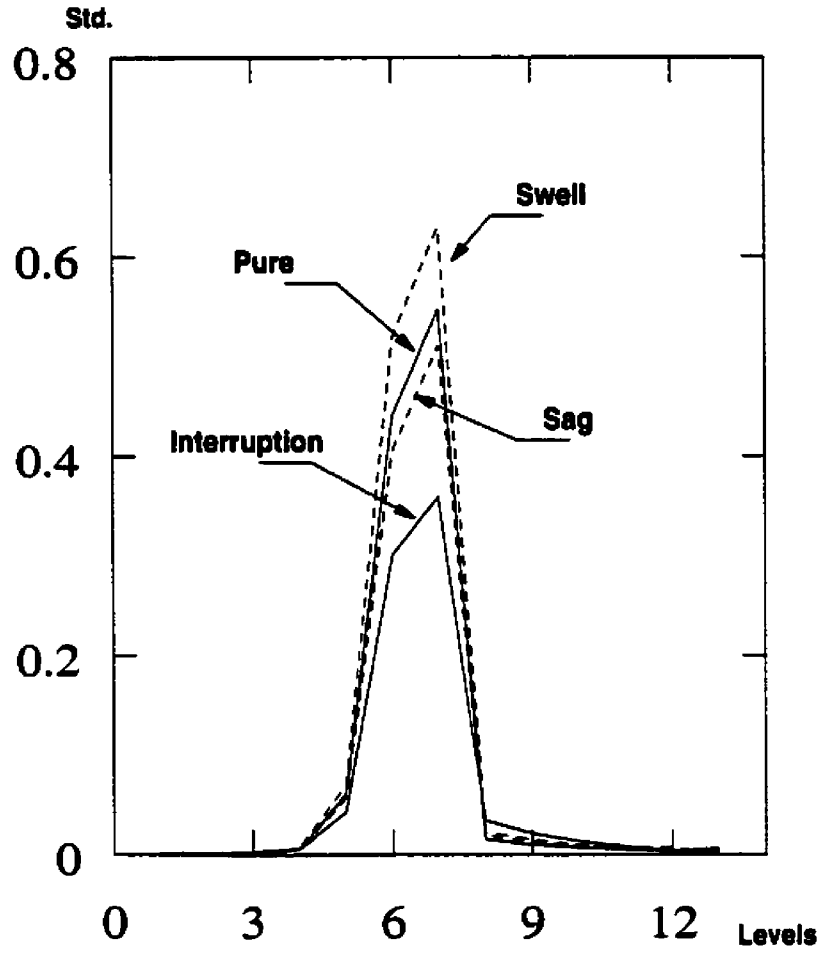

Figure 7.1: Changes in the std-MRA curve for
different short duration variation events

- Generate a group of signals distorted with sag phenomena started from pure wave to complete interruption with fixed duration (number of cycles).
- Apply multi-resolution analysis on each signal and find the standard deviation multi-resolution analysis curve (std-MRA).
- For each case find the maximum value of the std-MRA curve.
- Using a curve fitting technique, find the best curve to fit the generated curve.
- Change the number of cycles of the SDV distorted signal and repeat the process again to generate other curves for different duration.

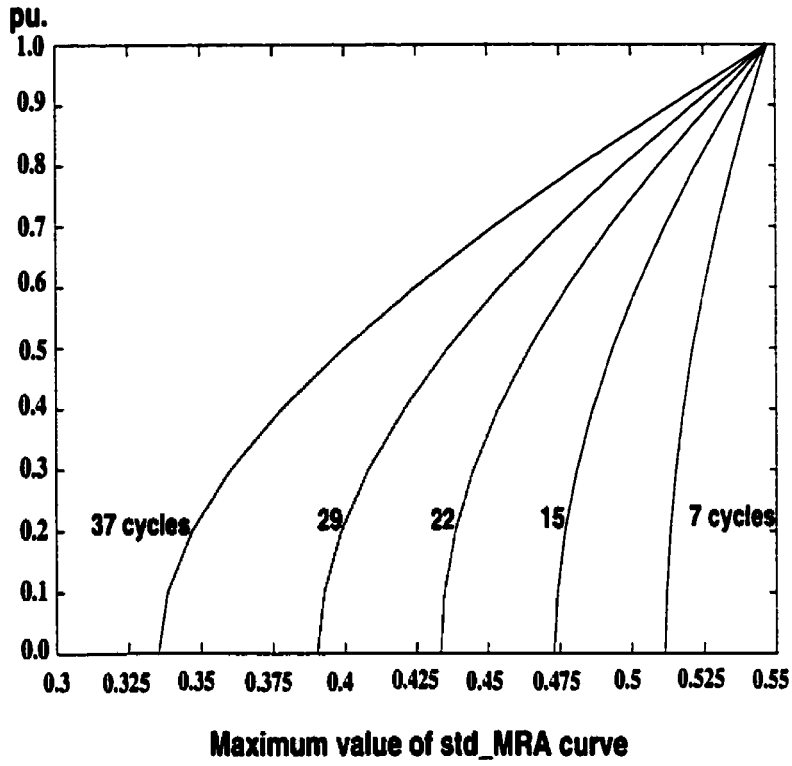

Figure 7.2: The variation of signal magnitude during different sag intervals with the changes in the maximum value of the std-MRA curve

Using a curve fitting technique, we found the polynomials that represent these curves; this is shown in Table 7.1. These polynomials are generated for different intervals to cover all the expected intervals of the voltage sag phenomenon.

When the monitored signal is distorted with sag phenomena, the std_MRA curve will show reduction in its maximum value and the first detail version will give a measure of the sag duration. Knowing the duration we select the best polynomial and substitute the maximum value of the std_MRA curve to calculate the sag magnitude. The flow chart in Figure 7.3 shows the general steps used to generate the measurement curves.

Table 7.1: Polynomial coefficients using curve fitting technique

Coef.#	7 cycles	15 cycles	22 cycles	29 cycles	37 cycles
1	-1.5189e+010	-1.8333e+008	-1.6292e+007	-1.9944e+006	-3.1674e+005
2	4.8308e+010	5.6309e+008	4.8196e+007	5.6646e+006	8.5144e+005
3	-6.4011e+010	-7.2034e+008	-5.9345e+007	-6.6890e+006	-9.4938e+005
4	4.5233e+010	4.9126e+008	3.8931e+007	4.2036e+006	5.6206e+005
5	-1.7978e+010	-1.8838e+008	-1.4351e+007	-1.4828e+006	-1.8635e+005
6	3.8105e+009	3.8511e+007	2.8184e+006	2.7836e+005	3.2814e+004
7	-3.3649e+008	-3.2790e+006	-2.3039e+005	-2.1731e+004	-2.3981e+003

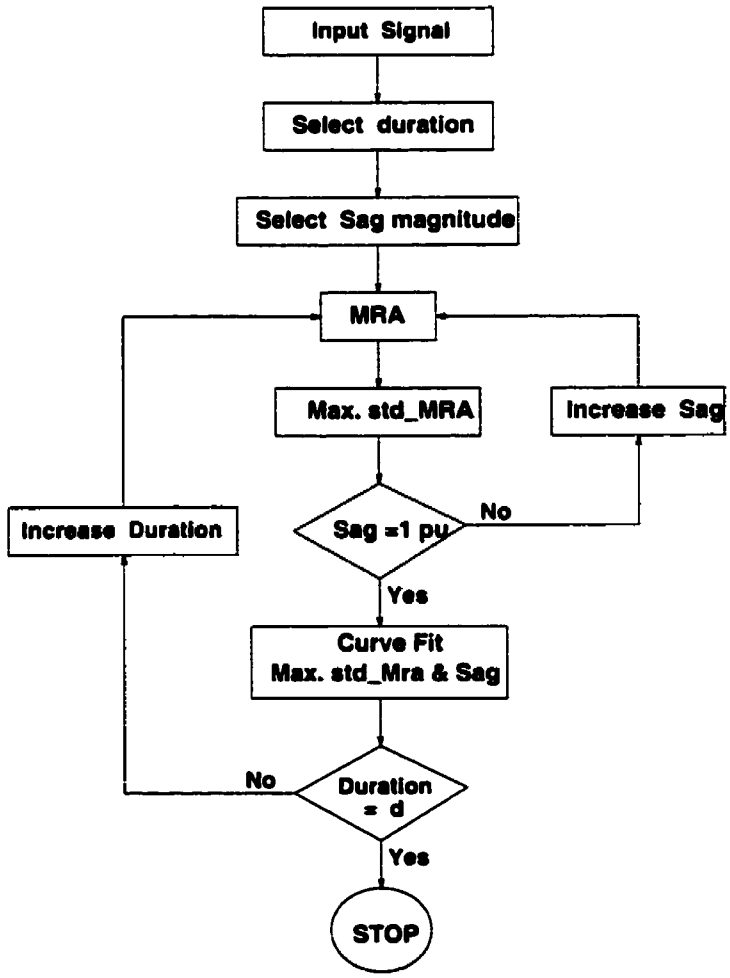

Figure 7.3: Flow chart for the generated curves used in the measurement

7.3 Measurement Using Wavelet expansion Coefficients

If the monitored signals (current $i(t)$ and the voltage $v(t)$) represent square-integrable density functions, then their wavelet transform can be formulated as follows:

$$i(t)=\sum_k c_{i,o}(k)\phi(t-k)+\sum_k\sum_{j=0}^{J-1} d_{i,j}(k)2^{j/2}\psi(2^j t-k) \tag{7.1}$$

and

$$v(t)=\sum_k c_{v,o}(k)\phi(t-k)+\sum_k\sum_{j=0}^{J-1} d_{v,j}(k)2^{j/2}\psi(2^j t-k) \tag{7.2}$$

$$c_{i,j-1}(k)=\langle i(t),\phi_{j,k}(t)\rangle=\sum_m h(m-2k)\,c_{i,j}(m) \tag{7.3}$$

$$d_{i,j-1}(k)=\langle i(t),\psi_{j,k}(t)\rangle=\sum_m h_1(m-2k)\,c_{i,j}(m) \tag{7.4}$$

$$C_i=[c_{i,o}\mid d_{i,o}\mid d_{i,1}\mid \ldots\ldots d_{i(J-1)}\mid] \tag{7.5}$$

$$C_v=[c_{v,o}\mid d_{v,o}\mid d_{v,1}\mid \ldots\ldots d_{v(J-1)}\mid] \tag{7.6}$$

The RMS value of the current (i_{RMS}) is:

$$i_{RMS}=\sqrt{\frac{1}{T}\int i^2(t)dt}$$

$$\int i^2(t)dt=\int\left[\sum_k c_{i,o}(k)\phi(t-k)+\sum_k\sum_{j=0}^{J-1} d_{i,j}(k)2^{j/2}\psi(2^j t-k)\right]^2 dt$$

Due the orthonormality (orthogonal and normalized), then,

$$i_{RMS} = \sqrt{\frac{1}{T}\sum_{k} c_{i,o}^{2}(k) + \frac{1}{T}\sum_{k}\sum_{j=0}^{J-1} 2^{j} d_{i,j}^{2}(k)} \tag{7.7}$$

$$v_{RMS} = \sqrt{\frac{1}{T}\sum_{k} c_{v,o}^{2}(k) + \frac{1}{T}\sum_{k}\sum_{j=0}^{J-1} 2^{j} d_{v,j}^{2}(k)} \tag{7.8}$$

The energy can be calculated as:

$$W = \int i(t)\, v(t)\, dt = \sum_{k} c_{i,o}(k)\, c_{v,o}(k) + \sum_{j=0}^{J-1} 2^{(j+1)} \sum_{k} d_{i,j}(k)\, d_{v,j}(k)$$

For a periodic wave, the average power is:

$$P_{av} = \frac{1}{T}\int i(t)\, v(t)\, dt$$

$$P_{av} = \frac{1}{T}\sum_{j=0}^{J-1} 2^{(j)}\, \langle C_{i,j}(k), C_{v,j}(k) \rangle$$

$$C_i = [c_{i,o} \mid d_{i,o} \mid d_{i,1} \mid \ldots\ldots d_{i,(J-1)} \mid] \tag{7.9}$$

$$C_v = [c_{v,o} \mid d_{v,o} \mid d_{v,1} \mid \ldots\ldots d_{v,(J-1)} \mid] \tag{7.10}$$

Using the wavelet coefficients of the current and the voltage signals, then the phase shift angle can be presented as:

$$\cos(\alpha) = \left[\frac{\langle C_i, C_v \rangle}{\| C_i \| \| C_v \|}\right] \tag{7.11}$$

According to Parseval's theorem, if the used scaling function and the wavelets form an orthonormal basis, then Parseval's theorem relates the energy of the distortion in the signal $s(t)$ to the energy in each of the expansion components and their wavelet coefficients C_{dist}. This means that the energy of the distortion W_{dist} can be represented in terms of the expansion coefficients.

In terms of the wavelet coefficients, the energy of the distortion W_{dist} is equal to the square of the norm of the wavelet coefficients C_{dist}.

$$W_{dist} = \| C_{dist} \|_2^2 \tag{7.12}$$

where, $\| C_{dist} \|_2$ is the norm of the distortion coefficients and can be mathematically represented as:

$$\| C_{dist} \|_2 = \sqrt{|\langle C_{dist} , C_{dist} \rangle|} \tag{7.13}$$

$$\| C_{dist} \|_2 = \left[\sum_{k=-\infty}^{\infty} | c_{od}(k) |^2 + \sum_{j=0}^{\infty} \sum_{k=-\infty}^{\infty} | d_{jd}(k) |^2 \right]^{1/2} \tag{7.14}$$

Therefore, the true RMS value of the distortion $s(t)$ can be calculated using the wavelet coefficients as follows:

$$RMS_{s(t)} = \left[\frac{1}{\Delta\tau} \| C_{dist} \|_2^2 \right]^{1/2} \tag{7.15}$$

where $\Delta\tau$ is the duration of the distortion event measured from the localization process as mentioned in Chapter 5.

In terms of the wavelet coefficients, the total harmonic distortion (THD) can be computed as follows:

$$THD\ \% = \frac{\| C_{dist} \|_2}{\| C_{pure} \|_2} x100\ \% \tag{7.16}$$

where, $\| C_{pure} \|_2$ is the norm of the pure signal.

Therefore, transforming the distorted signal into a set of coefficients in the wavelet domain can be used to construct a monitoring device to measure different distortion events.

7.4 Non-Rectangular RMS Variation

The previous part of this chapter assumes that RMS variation changes in a rectangular form for a certain period of time. This phenomenon is not true when a large part of the load consists of induction motors, or synchronous motors, or generators. It has been documented in [1] and [19] that there are other RMS-variations with non-rectangular envelopes. These variations are difficult to characterize because there is no single magnitude and duration that can characterize them, see Figure 7.4a.

There are two existing techniques for presenting the non-rectangular variations in the RMS value. The following is the summary of these existing techniques [1]:

1. The first technique defines the magnitude as the minimum RMS voltage during the disturbance. The duration is defined as the time during which the RMS voltage is below a certain threshold, typically 90% of the nominal voltage. This method is used in most power quality monitors. The disadvantage of this method is that the non-rectangular RMS variations are considered more severe than what they actually are.

2. The second technique characterizes the voltage quality by the number of times the voltage drops below a given value for longer than a given time. This technique became part of the IEEE std. 493 [23]. Using this method we can quantify the number of sags, however, we cannot characterize each sag event individually. Furthermore, implementing this method to assess the influence of non-rectangular sages on a piece of equipment is prone to uncertainties no matter which definition of magnitude and duration is used.

In the following proposed technique we present a method that can measure non-rectangular RMS variations and simultaneously detect and classify any disturbances that may exist.

7.5 Proposed technique for the of Measurement Non-Rectangular RMS Variations

In this section, a new wavelet-based procedure is proposed to characterize RMS variations. This procedure can help in assessing the quality of service presented in a distribution system, the quality of the mitigation devices, and the characteristics of any load during RMS variations. It can also give important information about any new variations of the distortion during its elapse. This information will help in finding the rectangular or non-rectangular voltage-tolerance curves for different equipment. This can help in the design of a new CPEMA curve that considers non-rectangular RMS variations and other power quality problems that may take place simultaneously. A flow chart showing the executing steps of the proposed procedure is shown in Figure 7.5:

- Any changes in the pattern of the signal can be detected and localized at the finer resolution levels as presented in Chapter 5. The set of coefficients $d_{(J-1)}(k)$ is used to monitor the number of changes in the signal during the selected window duration.
- The distorted signal is segmented into window frames with respect to a fixed time interval as shown in Figure 7.4b.
- For each frame, we find the wavelet coefficients C and C_{dist}, where

$$C_{dist} = C - C_{Ref} \tag{7.18}$$

and C are the wavelet coefficients of the signal, C_{dist} are the wavelet coefficients of the distortion event and C_{Ref} are the reference wavelet coefficients computed from C_{pure};

$$C_{Ref} = Pk_{new} * C_{pure} \tag{7.19}$$

where Pk_{new} is the peak value of the distortion event. The initial value of Pk_{new} is selected to be equal to 1 for a pure signal.

- We use C_{dist}, the new $RMS_{s(t)}$ and its peak value (Pk) of the distorted signal is estimated.
- We use the energy measure $\Delta E_{Ref}(L_f)$ of the resolution level (L_f), that covers the power frequency band, to monitor the direction of variation in the $RMS_{s(t)}$ of the distortion event, as shown in Figure 7.4d, where

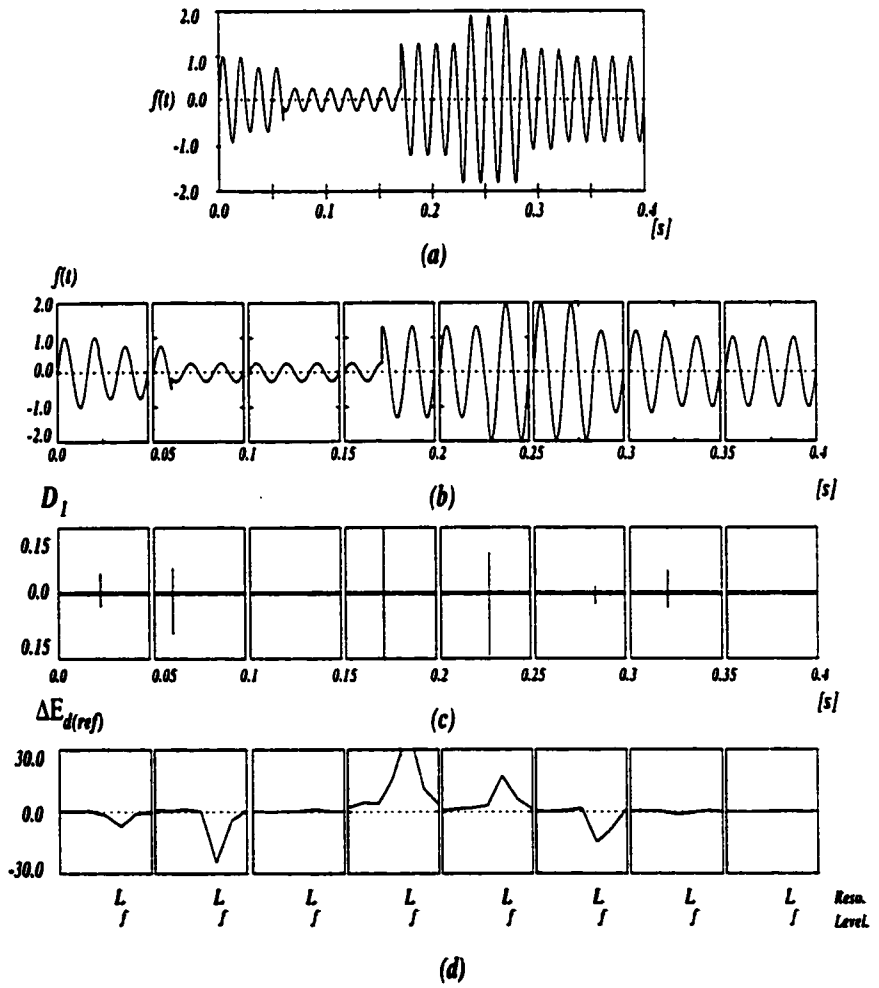

Figure 7.4: RMS variation monitoring

a- Distorted signal, b- Windowing the distorted signal,

c- First detail version, d- Energy distribution

$$\Delta E_{Ref}(L_f) > 0 \Leftrightarrow \text{increasing in RMS value}$$

$$\Delta E_{Ref}(L_f) < 0 \Leftrightarrow \text{decreasing in RMS value}$$

$$\Delta E_{Ref}(L_f) = 0 \Leftrightarrow \text{no change in RMS value}$$

and

$$\Delta E_{Ref}(L_f) = E_{signal}(L_f) - Pk_{new} * E_{pure}(L_f) \tag{7.20}$$

- The Pk_{new} value is updated to be used for monitoring the new variation in RMS value in the second window frame.

$$Pk_{new} = Pk_{new} + T * Pk \tag{7.21}$$

and

$$T = \begin{cases} 1 & \Delta E_{Ref}(L_f) > 0 \\ 0 & \Delta E_{Ref}(L_f) = 0 \\ -1 & \Delta E_{Ref}(L_f) < 0 \end{cases} \tag{7.22}$$

- We use the proposed feature vector (Equation 6.10) to classify the type of distortion in the signal.

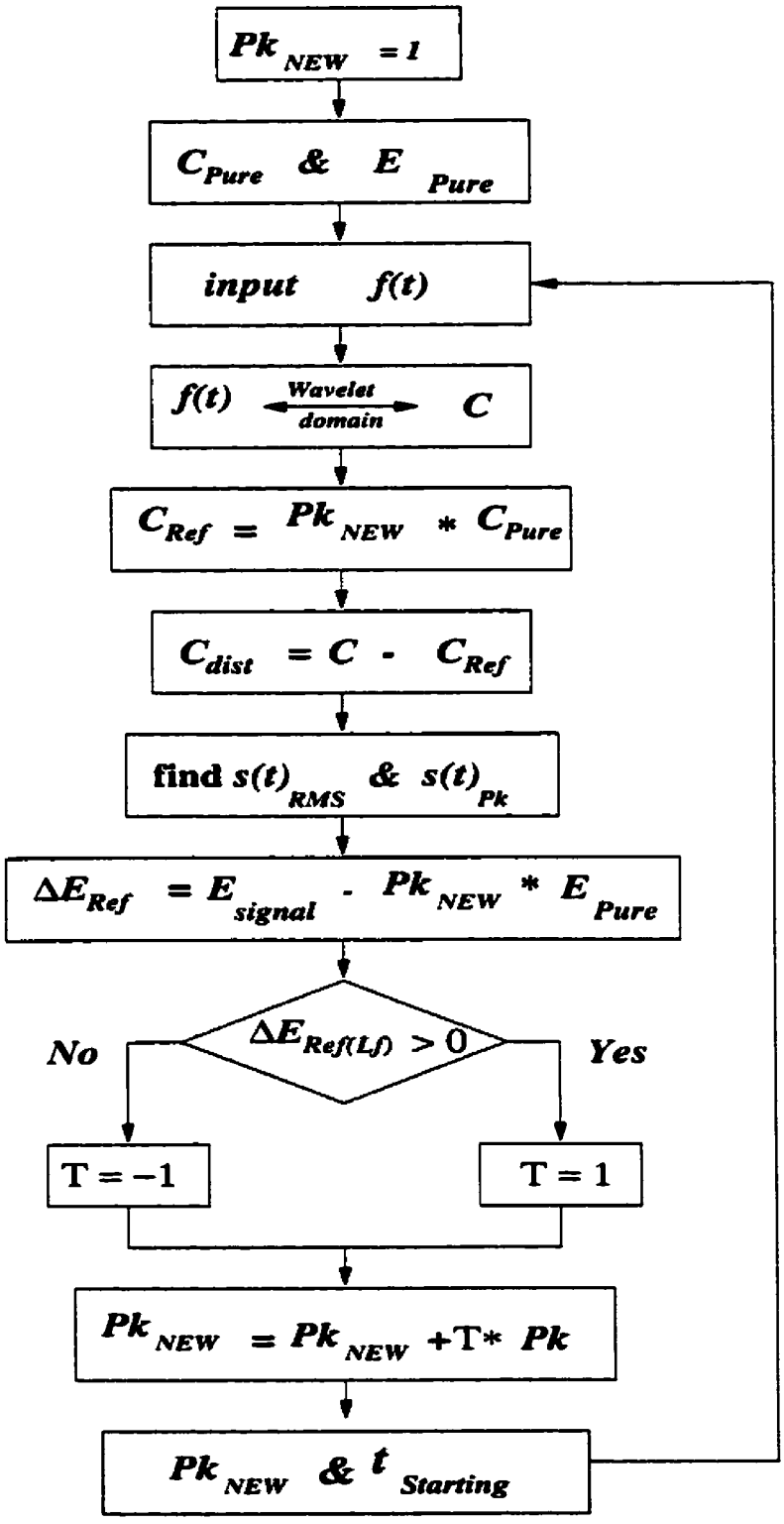

Fig 7.5: Monitoring flow chart for RMS variation

7.6 Applications And Results

7.6.1 Measurement of Short-duration variations using std-MRA curves

Figure 7.6 shows an example of using the maximum value of the std-MRA curve to measure the voltage sag in the signal in a harmonic distorted environment. The signal is distorted with sag to 0.85 pu (in peak value) as shown in Figure 7.6 a and the total harmonic distortion (THD) is equal to 18.24%. MRA is applied and the distorted signal is decomposed at different resolution levels. The sag phenomenon is detected due to the changes in the std-MRA curve in zone "B" as a reduction in its maximum value compared with that of a pure sine wave (dotted line). The high and low harmonic distortions are detected in zones "A" and "C". The duration for the sag phenomenon is detected and localized in the first detailed level for 14.6 cycles (Figure 7.6 b). The maximum value of the std-MRA curve is 0.5303 (Figure 7.6 c). Using the polynomials for the generated curves for sag measurements (Figure 7.6 d), the peak value of the signal during the sag phenomenon is equal to 0.8643 pu. On the other hand, the std_MRA curve shows the existing of high and low frequency components. The value of the harmonic distortion can be also measured.

The main advantage of the proposed method, compared to previous methods, comes from its ability to separate power quality problems that overlap in both time and frequency. It has the ability to separate the pure signal from any high or low frequency content, dc content, and noise distortion. The energy distribution of the distorted signal will be localized in time and presented at different frequency bands. This time-frequency picture of the energy of the distorted signal will be used as a classification feature vector (std-MRA) that has small dimensionality. The std-MRA feature vector presents a simple classification rule for the operator to detect, localize, and classify different power quality problems or to give an accurate measurement for the magnitude and duration of the signal during short duration variation events. Furthermore, using the std-MRA,

we can distinguish between similar power quality problems and help in finding the source of the disturbance.

The same procedure is applied on signals distorted with different magnitude and duration of swell phenomenon. The relation between the maximum value of the std-MRA curve and the magnitude of the voltage swell is plotted at different intervals. These curves can be used to measure the magnitude of the voltage swell in the signal. Figure 7.7 shows an example using the maximum value of the std-MRA curve to calculate the voltage swell in the signal.

The proposed technique was applied to measure different cases of voltage sag and swell phenomenon. The actual values and the derived ones are presented in Tables 7.2 and 7.3.

Table 7.2: The actual and derived values of the voltage sag for different intervals

Case no.	No. of cycles	Maximum std-MRA	Derived Voltage	Actual Voltage
1	14.82	0.498	0.57	0.5649
2	36.5	0.476	0.78	0.7815
3	22.6	0.511	0.82	0.8176
4	29.35	0.429	0.45	0.465

Table 7.3: The actual and derived values of the voltage swell for different intervals

Case no.	No. of cycles	Maximum std-MRA	Derived Voltage	Actual Voltage
1	15.16	0.7099	1.91	1.9146
2	37.14	0.6892	1.39	1.3939
3	30.29	0.7332	1.62	1.605
4	14.53	0.6132	1.42	1.438

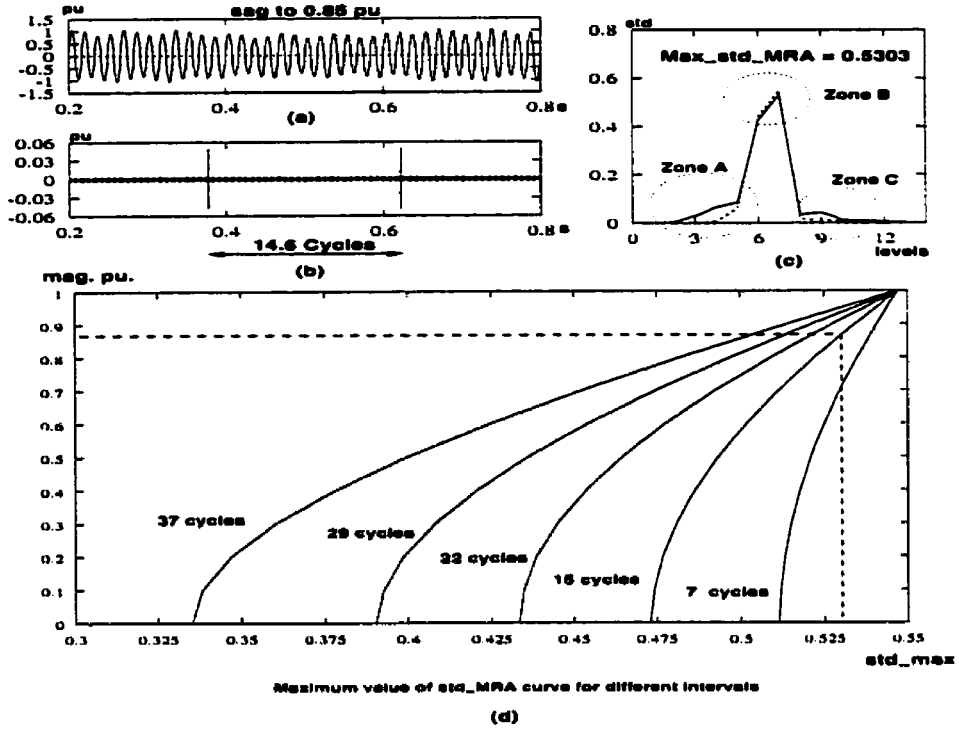

Figure 7.6: Measuring the voltage sag

a- Input signal, b- First detail level,

c- std-MRA curve, d- Measurement curves.

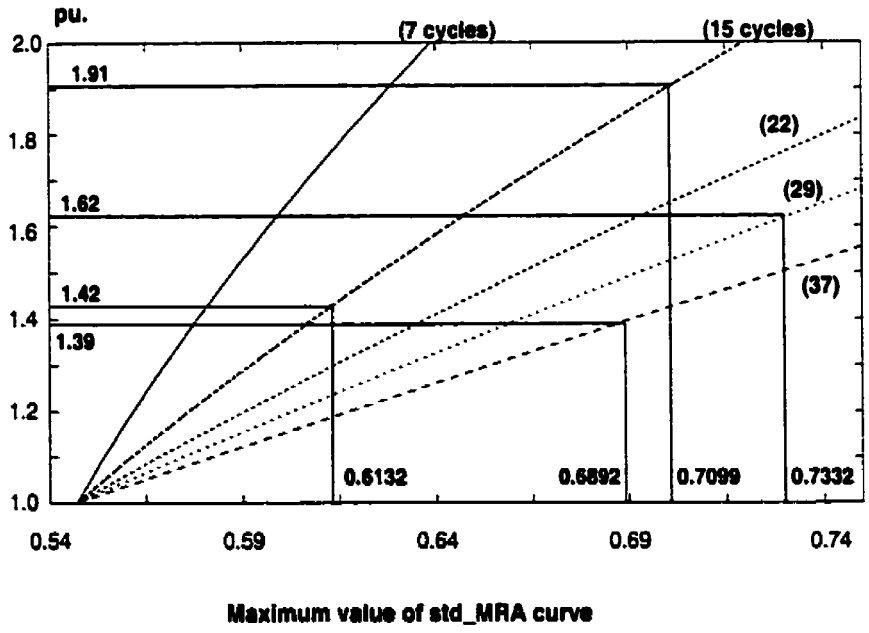

Figure 7.7: Measurement of the voltage swell magnitude

for different distorted signals

7.6.2 Measurement under Steady State Conditions

The CIGRE benchmark within the Electromagnetic Transient Simulation Program EMTDC was utilized as a tentative model of a typical HVDC system. For each signal, a window size of 8 cycles was selected. Each signal is sampled at 4 kHz and decomposed into 9 resolution levels that represent several frequency bands. PSCAD simulation results on the CIGRE benchmark was utilized to measure currents, voltages, and active and reactive power at the inverter side as shown in Figure 7.8.

Table 7.4: Comparison the PSCAD and Wavelet-based proposed technique

Inverter side measurements	**PSCAD**	**Proposed Technique**
Phase A Current (RMS) kA	2.82441	2.843
Phase A Voltage (RMS) kV	129.6895	129.450
Power Factor	- 0.8607	- 0.8658
Active Power (kW)	981.5279	956.141
Reactive Power (kVAR)	551.3008	552.544

The proposed MRA technique was implemented and similar results to those of the PSCAD simulator were achieved using the wavelet coefficients. A comparison between the PSCAD results and the computed parameters in the wavelet domain are presented in Table 7.4. The proposed technique shows accurate results for measuring different variables in the HVDC system.

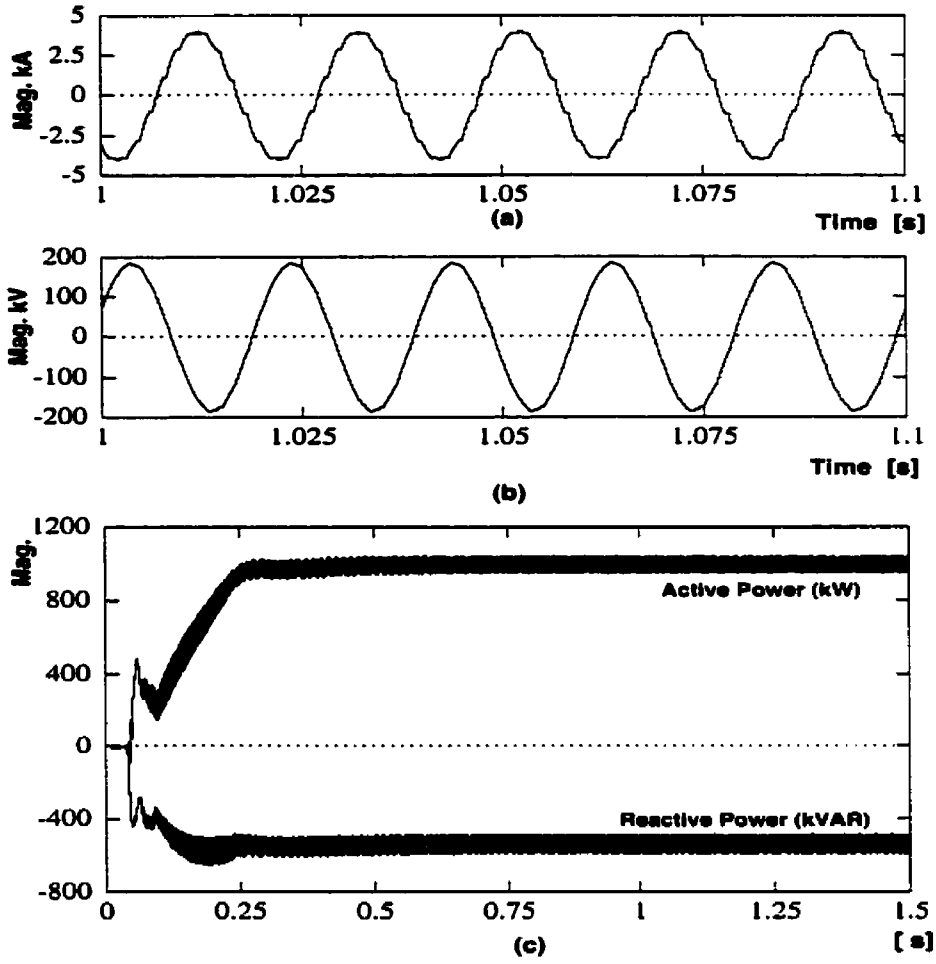

Figure 7.8: Monitoring HVDC system

a- Inverter phase A current, b- voltage, and c- power

7.6.3 Measurements of Sag magnitude in noisy environment

The same technique was applied for measuring a one-cycle simulated sag phenomenon. The simulated signal is further distorted with harmonic and has a high noise level. The actual starting time of the distortion is detected and localized as indicated in Chapter 5. The wavelet coefficients are used, as indicated in Equation 7.15 to compute the RMS value of the sag phenomena. Table 7.5 presents the estimated RMS value of the sag phenomenon with noise level variation from 0% to 2.0%.

Table 7.5: estimated RMS value and starting and ending time of a sag phenomena in a noisy environment

Noise Level	Derived Sag (RMS)	Error %
0.00%	0.1798	0.0150
0.25%	0.1814	0.0240
0.50%	0.1840	0.0384
0.75%	0.1895	0.0706
1.00%	0.1954	0.1014
1.25%	0.2058	0.1622
1.50%	0.2179	0.2331
1.75%	0.2284	0.2926
2.00%	0.2382	0.3400

The proposed technique shows accurate results of measuring the RMS value of the sag phenomena up to noise level 1%, which is the maximum noise expected in power systems.

7.6.4 Measurement of Non-Rectangular RMS Variation

A 21-cycle distorted signal $f(t)$ was simulated. This signal under went six variations in its magnitude and duration. The distorted signal was segmented into 3-cycle window frames. The features extracted from each window frame were used to classify the type of distortion. The energy distribution $\Delta E(L_f)$ was used to classify the distortion event

$$\Delta E(L_f) < 0 \Leftrightarrow E_{signal}(L_f) < E_{Pure}(L_f) \Leftrightarrow \text{Sag}$$

$$\Delta E(L_f) > 0 \Leftrightarrow E_{signal}(L_f) > E_{Pure}(L_f) \Leftrightarrow \text{Swell}$$

$$\Delta E(L_f) = 0 \Leftrightarrow E_{signal}(L_f) = E_{Pure}(L_f) \Leftrightarrow \text{Pure Signal}$$

The proposed technique, section (7.5), was used to monitor the RMS-variation during the distortion event and $\Delta E_{Ref}(L_f)$ was used to monitor the direction of the variation (increased or decreased).

Figure 7.9 shows the process of classifying and monitoring the RMS-variations during any distortion event. This process starts with inputting the distorted signal. Figure 7.9a shows the distorted signal contaminated with the RMS-variations that are shown in Table 7.6. Then we construct suitable window frames. Figure 7.9b shows the different window frame; each frame presents 3 cycles of the distorted signal. The third step is the extraction phase. The time localization property for different variations was extracted from the detail version of the distorted signal D_1 for each frame as shown in Figure 7.9c. As the noise level increased, the proposed algorithm for the noisy environment (section 5.4) was used to localize the distortion event. In the last phase, we monitored the energy variation in the resolution level of the power signal (60 Hz). Figure 7.9d shows the variation of distorted signal energy distribution ΔE with respect to the power frequency resolution level L_f. The four lines in Figure 7.9d are:

1. $E_{signal}(L_f)$ the solid line on the top.
2. $E_{Pure}(L_f)$ the dotted line on the top
3. $\Delta E(L_f)$ the dashed line on the top.
4. $\Delta E_{Ref}(L_f)$ the solid line on the bottom.

The first frame in Figure 7.9d shows that the signal $\Delta E(L_f)$ and $\Delta E_{Ref}(L_f)$ are coincident with each other. $\Delta E(L_f)$ is greater than zero which represents a swell phenomenon and $\Delta E_{Ref}(L_f)$ also greater than zero which represents an increase in the RMS value. The second frame shows $\Delta E_{Ref}(L_f)$ is less than zero, representing a reduction in the RMS of the signal and

$\Delta E(L_f)$ is greater than zero, representing a swell phenomenon. The third frame represents a reduction in RMS value and sag phenomenon.

The proposed technique is implemented in different sets of simulated data. The results of applying the technique to the distorted signal, shown in Figure 7.9a, are summarized in Table 7.6. The results of the table indicate very clearly the effectiveness of applying our proposed technique for monitoring and classifications. The errors between the actual and the measured using the proposed technique are very small for both the magnitudes and durations.

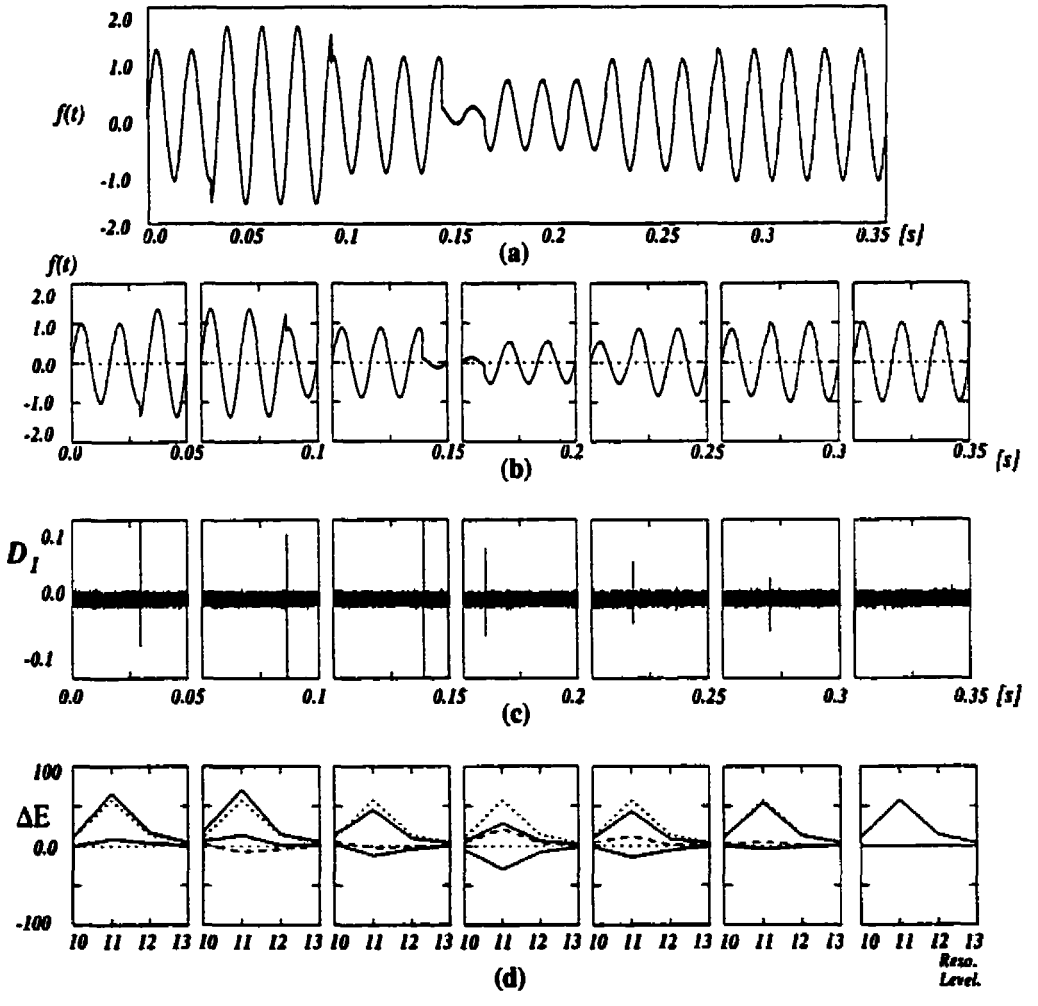

Figure 7.9: Monitoring of the RMS variation

a-Distorted signal, b- Windowing the distorted signal,

c- First detail version, d- Energy distribution

Table 7.6: Non-Rectangular RMS- variation measurements

Frame #	Actual Variation		Estimated Variation	
	Mag. (peak)	Time (s)	Mag. (peak)	Time (s)
1	1.3500	0.0296	1.3614	0.0296
2	0.8775	0 .0864	0.8287	0.0864
3	0.1316	0.1391	0.1192	0.1391
4	0.5265	0 .1599	0.5429	0.1600
5	0.8424	0.2180	0.8588	0.2184
6	1.0000	0.2702	1.0068	0.2703
7	1.0000	0.3000	0.9966	0.3010

The proposed technique is utilized for monitoring non-stationary variation in the RMS values of the following two cases shown in Figures 7.10 and 7.11. The estimated variations in the RMS values are monitored and instances of these variations are detected as indicated in Tables 7.7 and 7.8.

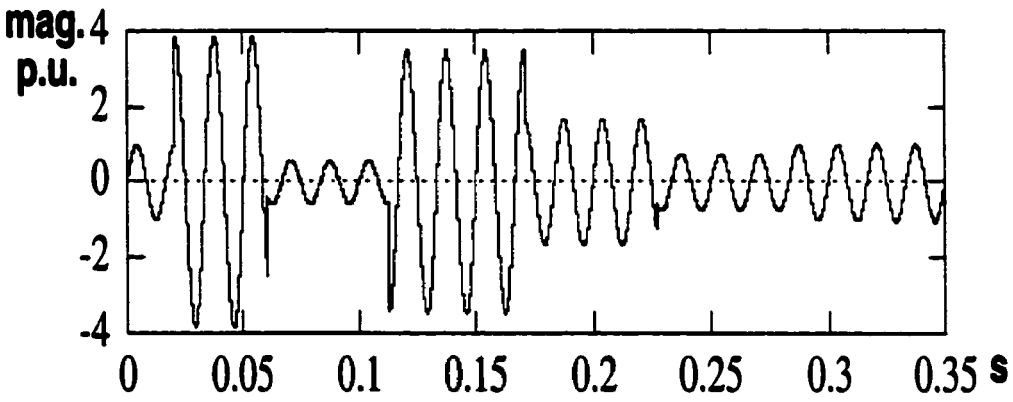

Figure 7.10: Monitoring of the RMS variation (case 1)

Table 7.7: Non-Rectangular RMS - variation measurements (case1)

Frame #	Actual Variation		Estimated Variation	
	Mag. (peak)	Time (s)	Mag. (peak)	Time (s)
1	3.8500	0.0207	3.9448	0.0207
2	0.5775	0.0102	0.4410	0.0103
3	3.4650	0.0129	3.5265	0.0129
4	1.6632	0.0207	1.6016	0.0207
5	0.7484	0.0271	0.6855	0.0272
6	1.0067	0.0336	1.0549	0.0349

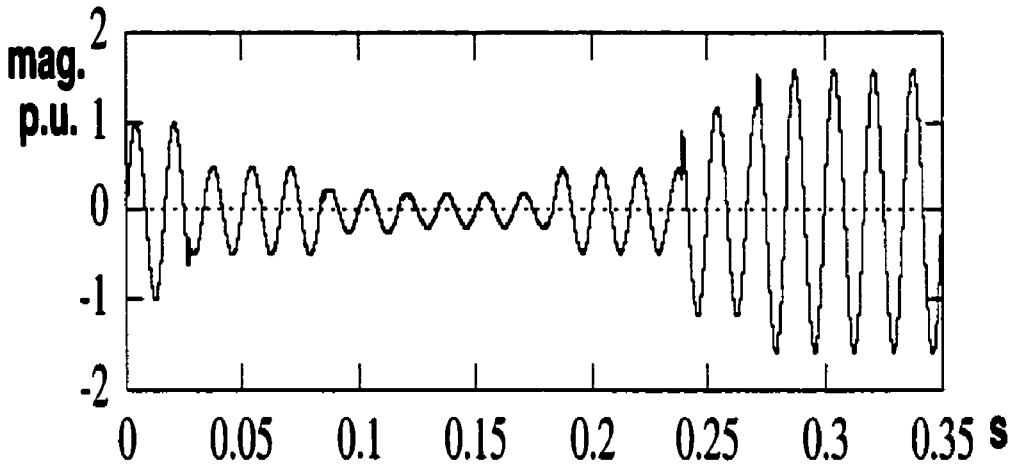

Figure 7.11: Monitoring of the RMS variation (case 2)

Table 7.8: Non-Rectangular RMS- variation measurements (case2)

Frame #	Actual Variation		Estimated Variation	
	Mag. (peak)	Time (s)	Mag. (peak)	Time (s)
1	0.5000	0.0268	0.4653	0.0269
2	0.2500	0.0346	0.2214	0.0349
3	0.1875	0.0190	0.1880	0.0020
4	0.4688	0.0329	0.4998	0.0349
5	1.1719	0.0393	1.1777	0.0393
6	1.5762	0.0214	1.5849	0.0214

7.7 Chapter Assessment

In this chapter a new technique is proposed to measure effectively and accurately the different distortion events under both steady state and short-duration disturbances.

The main contribution in this chapter is that it provides a reliable procedure to measure the disturbances in a wavelet-based environment. This is an important feature that will assist in achieving our final goal of developing an automated classifier for the different power system disturbances.

The localization property of the wavelet transform (presented in Chapter 5) and the detail coefficients are used to measure the distortion event magnitude. The proposed technique is further modified to give a measure of the RMS value during non-rectangular variations.

A new wavelet-based procedure to characterize RMS variations is presented in this Chapter. This procedure can help in assessing the quality of service presented in a distribution system, the quality of the mitigation devices, and the characteristic of the load during RMS variation. Utilizing this procedure, a clear picture of any further changes in the harmonic distortion, noise level, or RMS variations can be detected, localized, classified, and quantified inside the distortion event.

Chapter 8

Wavelet-Based Data Reduction

8.1 Introduction

As we mentioned in Chapter 1, the goal of this thesis is to design a reliable, accurate and wide-scale power quality monitoring system with superior characteristics. This chapter is devoted to develop a new procedure that will compress and store the distortion event efficiently. This procedure is based on wavelet analysis, where a small set of wavelet coefficients represents the disturbances to assist in achieving this goal. This procedure will replace the existing technique of storing all sampling points of the disturbance.

The proposed data reduction technique is presented in Section 8.2. Section 8.3 illustrates the performance evaluation of the proposed technique. The Application and Chapter assessments are presented in Sections 8.4 and 8.5, respectively.

8.2 Data Reduction and Representation

The feature vector presented in Equation 6.10 and the rapid drop off in the number of the coefficients are two important characteristics that can be used for reducing the amount of data to be stored. The feature vector shows that the energy of the signal is concentrated at certain resolution level (i^{th}). Due to the rapid drop off in the size of the coefficients, the information in this resolution level can be represented by only a small number of detail coefficients. These coefficients can be stored and used, when needed, to reconstruct the original signal. Figure 8.1 shows the reduction in the size of detail $d_j(k)$ and approximated $c_j(k)$ expansion coefficients from (N) to $(N+n-1)/2$ in the first resolution level. Where N is the size of the sampling points of the input signal and n is the size of the selected wavelet filter coefficients. The size of these coefficients is further reduced to $(\approx N/2^{resolution\text{-}level})$ as the input signal is decomposed into different resolution levels.

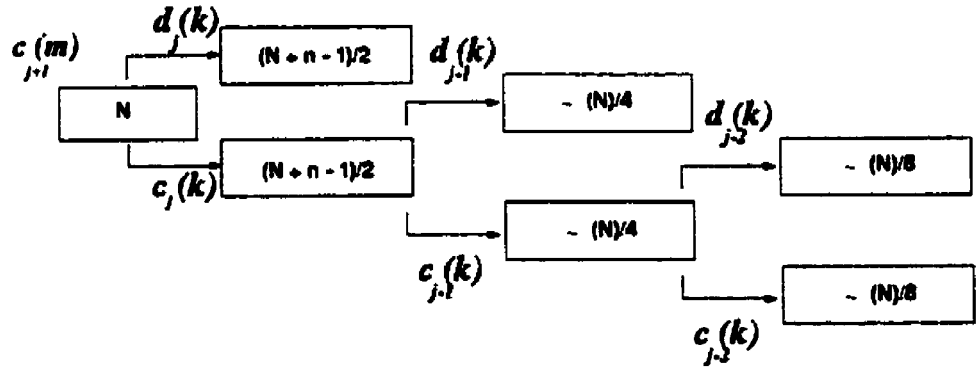

Figure 8.1: The rapidly drop off in the size of the coefficients in the wavelet domain

The proposed data representation technique is summarized in the following steps and also shown in Figure 8.2:

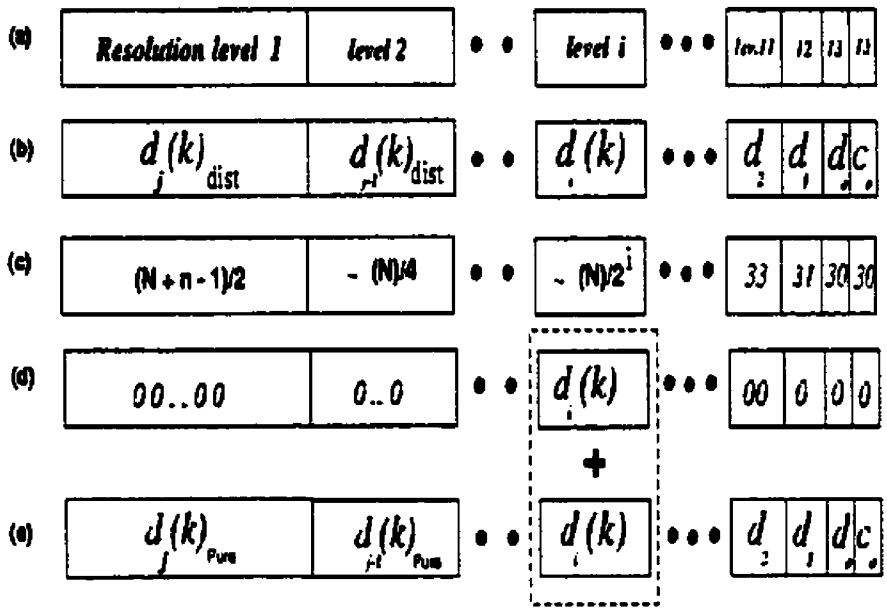

Figure 8.2: Data reduction and presentation

Step 1: We use MRA to decompose the distorted signal (N sampling points) at different resolution levels as presented in Figure 8.2a.

Step 2: We find the difference (C_{dist}) between the wavelet coefficients of the distorted signal (C_{Signal}) and that for a pure one (C_{Pure}) as shown in Figure 8.2b,

where

$$C_{dist} = C_{Signal} - C_{Pure} \tag{8.1}$$

The number of these coefficients at different resolution level is shown in Figure 8.2c.

Step 3: We use the proposed feature vector to find the resolution level (i) where most of the energy of the distortion event is concentrated. This resolution level (i) will present all the important information that characterizes the distortion event.

Step 4: We ignore all the other coefficients and store only the coefficients of the (i^{th}) resolution level where the size of these coefficients is equal to $(\approx N/2^i) << (N)$ as shown in Figure 8.2c and d.

$$d_j(k) = \begin{cases} 0 & resolution \quad level \neq i \\ \\ d_i(k) & resolution \quad level = i \end{cases} \tag{8.2}$$

Step 5: We add the stored set of detail coefficients $d_i(k)$ to similar set of a pure signal at the same resolution level.

$$\tilde{d}_j(k) = \begin{cases} d_j(k)_{Pure} & resolution \quad level \neq i \\ \\ d_i(k)_{dist} + d_i(k)_{pure} & resolution \quad level = i \end{cases} \tag{8.3}$$

Step 6: We use the new set of the coefficients $\tilde{d}_j(k)$ to reconstruct the distorted signal $\tilde{f}(t)$. Figure 8.2f shows the reconstructed version of the distortion event by storing only $(N/2^i)$ coefficients.

By applying the above steps we store only the detail coefficients that represent the distortion event. And since the number of detail coefficients is reduced as the number of resolution levels increases, then the number of coefficients to be stored to represent the distortion event will be very small compared with the number of sampling points of the distorted signal.

8.3 Performance Evaluation

In many cases one can compress and store the data by very simple algorithms. However, the ultimate judgement of how effective these techniques will depend on how much information is

lost in storing the data. This is can be examined by reconstruction the original data from the compressed one. Mathematically we measure the quality of compression by calculating the normalized mean squared error (NMSE) of the reconstructed data.

We will examine the performance of our proposed method by evaluating the reconstructed signal $\tilde{f}(t)$ and then calculating the normalized mean square error $(NMSE)$ between the original signal $f(t)$ and the reconstructed one $\tilde{f}(t)$. Where $NMSE$ is computed as follows:

$$NMSE = \frac{\| f(t) - \tilde{f}(t) \|^2}{\| f(t) \|^2} \tag{8.4}$$

Where $\| f(t) \|^2$ is the square of the norm for the original signal, which represents the energy of the signal.

8.4 Application and Results

The proposed technique was used to compress the data of the following power quality problems, and the effectiveness of the technique was examined by calculating the NMSE using Equation 8.4.

8.4.1 Case 1: Capacitor Switching Phenomena

Step 1: Utilizing MRA, the distorted signal (Figure 8.3) was decomposed into several detail versions (building blocks). Some of these building blocks that have important parts of the energy of the distorted signal are shown in Figure 8.4. The shown resolution levels include detail versions of the first D_1, second D_2, sixth D_6, seventh D_7, eighth D_8, tenth D_{10}, eleventh D_{11}, and twelve D_{12} as shown in Figures 8.4a-i respectively. These versions of the signal are easier to study and interpret. The capacitor switching phenomena (Figure 8.3) was sampled at 165kHz and a 3 cycles window size was selected (8266 sampling point). These sampling points (c_{j+1}) were used as input for MRA and decomposed into 13 resolution levels. The frequency bands that represent each resolution level are summarized in Table 8.1.

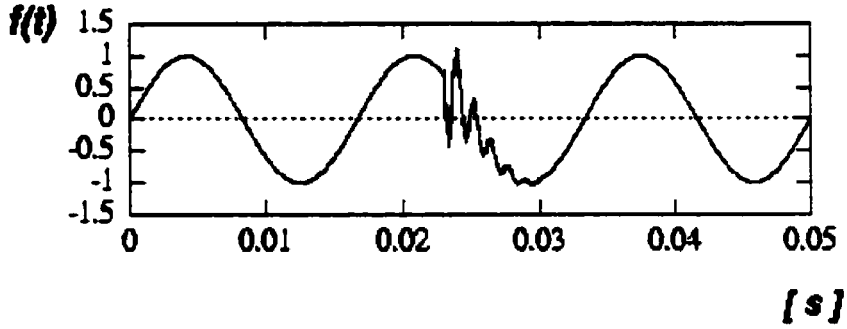

Figure 8.3: Distorted Signal with a capacitor switching phenomena

Table 8.1: Different resolution levels and their frequency bands

Resolution Level	Frequency Band kHz	Resolution Level	Frequency Band kHz
1	41.25 - 82.50	8	0.322 – 0.645
2	20.62 - 41.25	9	0.161 – 0.322
3	10.31 - 20.62	10	0.081 – 0.161
4	5.150 - 10.31	11	0.040 – 0.081
5	2.570 - 5.150	12	0.020 – 0.040
6	1.289 - 2.570	13	0.010 – 0.020
7	0.645 - 1.289		

MRA shows that most of the energy in the distortion event is concentrated in the seventh resolution level D_7 (645-1289 Hz) as shown in Figures 8.4d. The eleventh resolution level (40-80 Hz) presents the 60Hz power signal as shown in Figures 8.4g. Leakage of the signal's energy is seen at adjacent resolution levels. For example, part of the 60Hz energy of the signal, Figures 8.4g, will be leaked to the adjacent resolutions; Figures 8.4f and Figures 8.4i. This is due to the non-sharp cut-off frequencies of the wavelet filters. However, the magnitude of this leakage energy is very small compared with that in Figures 8.4g. The selection of the filters will help in reducing this leakage. As the number of filter coefficients n increases, the cut-off frequency will become more sharp and the leakage energy is reduced. This is an important criterion in selecting the mother wavelet to be used for the analysis. This will be discussed in Appendix B "Selection of the mother wavelet".

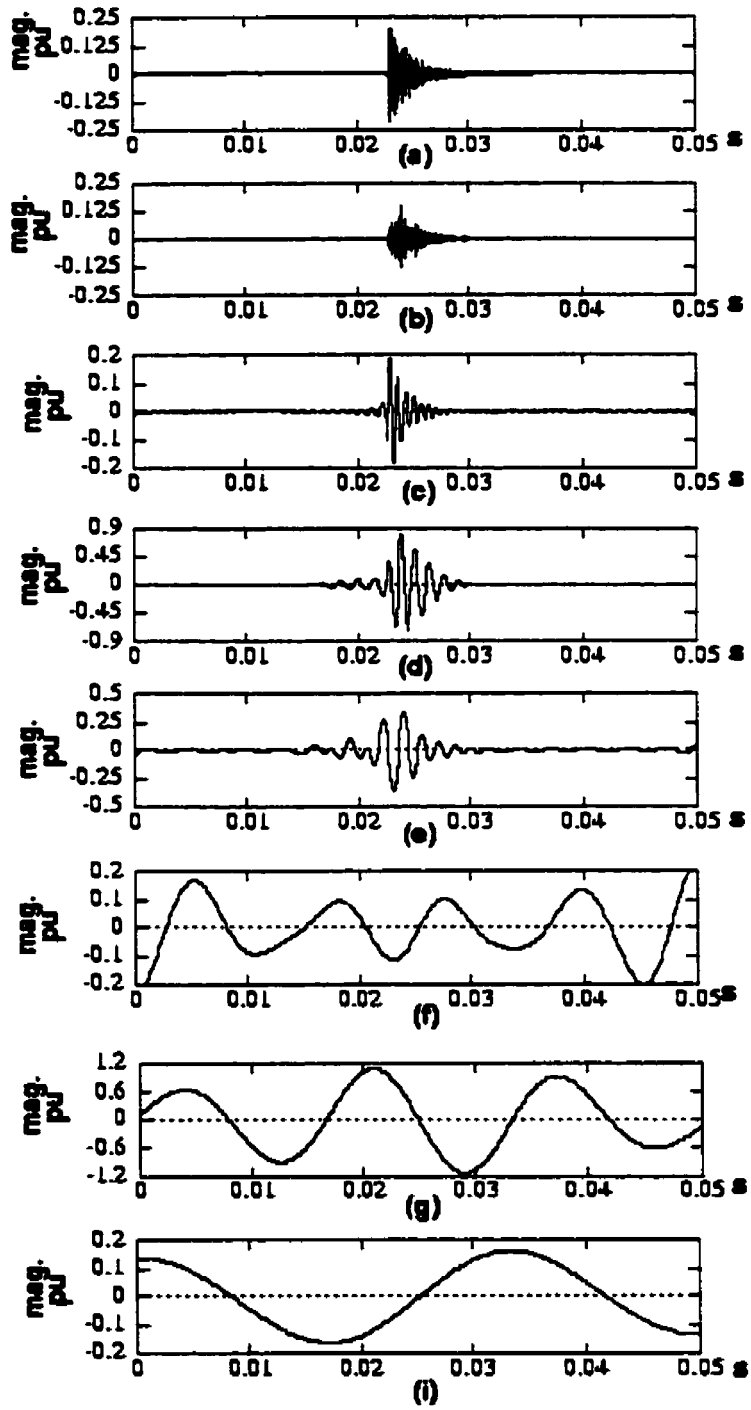

Figure 8.4: MRA of the distorted signal

Step 2: The distribution of distortion event energy at different resolution levels (building blocks) can be used to extract important features that help in selecting the coefficients to be stored to reconstruct the distortion event. Figure 8.5 shows that most of the energy of the distortion event is concentrated on the 7th resolution level. The sold line in Figure 8.5a represents the feature vector of a pure signal and the dashed line represents the distorted signal. The energy distribution of the distortion event is shown in Figure 8.5b.

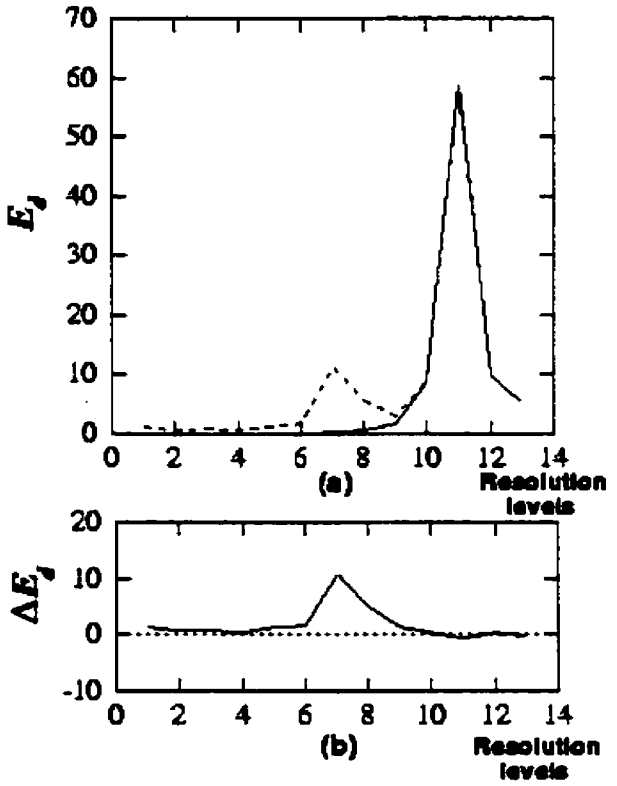

Figure 8.5: Feature vector of the distorted signal

Step 3: This feature vector indicates that most of the important information resides in the 7th resolution level. This resolution level can be represented using 93 detail coefficients.

Step 4: Ignore all the other coefficients and store only the coefficients of the 7th resolution level (93 coefficients << 8266) as indicated in Equation 8.2.

Step 5: Using the new set of the coefficients $\tilde{d}_j(k)$, one can reconstruct the new set of wavelet coefficients that represent the distorted signal $\tilde{f}(t)$ as indicated in Equation 8.3.

Step 6: Reconstruct the distorted signal $\tilde{f}(t)$ using the new set of wavelet coefficients. The reconstructed version of the signal $\tilde{f}(t)$ is shown in Figure 8.6, which was generated from only the 93 coefficients stored to represent the distortion event.

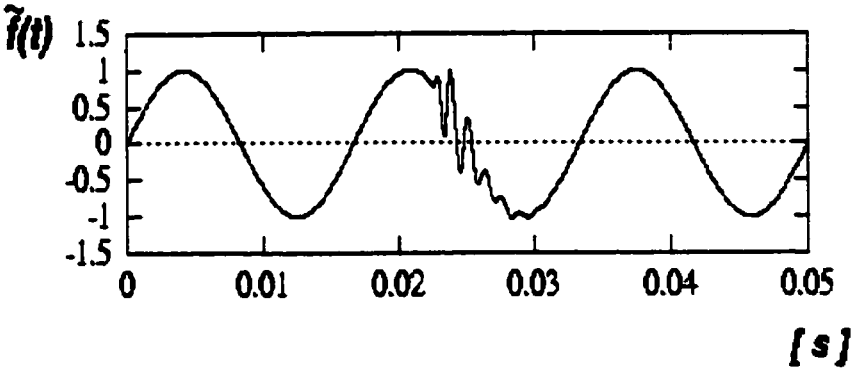

Figure 8.6: Reconstructed version of the distorted signal

The performance of the reconstructed signal $\tilde{f}(t)$ is evaluated by calculating the normalized mean square error $(NMSE)$ between the original signal $f(t)$ and the reconstructed one $\tilde{f}(t)$. The $NMSE$ is computed and found equal to 0.00487, which shows that the constructed signal is very close to the original signal.

8.4.2 Case 2: Harmonic Distorted Signal

The proposed data representation technique is implemented on a harmonic distorted signal shown in Figure 8.7a. The energy of the distortion event is concentrated on the 9th resolution level. Using the new set of the coefficients $\tilde{d}_j(k)$, one can reconstruct the distorted signal $\tilde{f}(t)$ from storing

only (45 coefficients << 8266). The reconstructed version of the signal $\tilde{f}(t)$ is shown in Figure 8.7b.

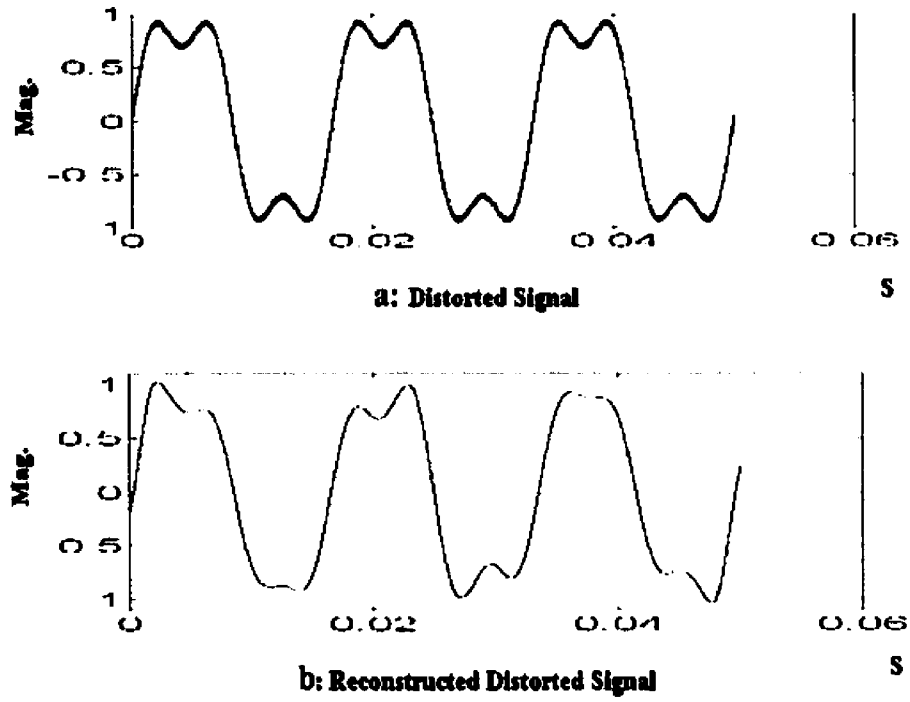

Figure 8.7: Data representation, a: harmonic distorted signal,
b: Reconstructed version of the distorted signal

The performance of the reconstructed signal $\tilde{f}(t)$ is evaluated by calculating the normalized mean square error (*NMSE*), which is to 0.0224.

8.5 Chapter Assessment

In this chapter, a new data compression technique is proposed, which is based on wavelet analysis. This technique can be used to store only a small number of coefficients that can be used to reconstruct the original signal. The proposed technique will help in designing a comprehensive

power quality automated recognition system that has the ability to detect, localize, classify, measure and store different distortion events.

Chapter 9

Conclusions and Future Research

9.1 Introduction

In this thesis new automated power quality detection, classification, measuring, de-noising and data compression techniques are proposed. These techniques are based on wavelet theory and multi-resolution analysis. The localization property of the wavelet transform is used to detect and classify different disturbances. Any distorted event can be decomposed into different resolution levels. The energy of each resolution level can generate a translation invariant feature vector with small dimensionality that can be used to classify different disturbances according to IEEE std. 1159.

Different monitoring devices are available that can measure the duration of a disturbances. The sensitivity of these devices depends on selected threshold levels that may result in missing desired disturbances or capturing large numbers of waveforms. The existence of noise can further mislead the monitoring devices to capture and measure certain disturbances. In the proposed monitoring system, the duration of a distortion event can be measured using the information extracted from the first resolution level, which has the ability to detect any changes in the pattern of the signal and can be utilized to purify the signal from any noise content. Chapter 5 shows a set of newly proposed techniques that detect and measure the duration of any transient event in a noisy or clean power system environment without the need to specify certain thresholds.

Using the available monitoring devices, it is often difficult to determine on an on-line basis the characteristics of transient, oscillatory, or non-stationary disturbances. It is imperative to have in these monitoring devices a waveform capture capability for a detailed off-line analysis of different stored disturbances, which is a very time consuming process. This off-line analysis delays the mitigation control process that may lead to catastrophic damage.

In this thesis, the on-line based automated classification methodology of a distortion event is presented in Chapter 6. A wavelet-based feature extraction technique that reduces the size of the monitoring signal to a small set of numbers contained in a feature vector is also proposed. The feature vector is used to classify different disturbances and it yields excellent results. The main advantage of the proposed technique comes from its ability to extract the distortion events that overlap in time and frequency domains. Because of the small dimension of this feature vector an on-line automated classifier can be designed. This classifier can classify on-line different disturbances according to IEEE std. 1159, efficiently and accurately.

The RMS value of the distortion event magnitude represents an important factor in designing an automated power quality recognition system. A wavelet-based technique is utilized in this thesis to measure different distortion events. The wavelet expansion coefficients are used to compute the magnitude of the distorted signal and the root-mean-square (RMS) value. This technique is presented in Chapter 7 and it is implemented to measure the RMS value of a steady-state distortion event or during short duration variations as indicated in IEEE std. 1159.

The variations of the RMS value during a distortion event are also monitored and measured. A new wavelet-based technique is proposed to monitor the non-rectangular RMS variations. This technique is implemented for monitoring different signals that have non-stationary variations in their magnitudes. The proposed measurement technique shows its superiority compared with exiting techniques in terms of:

- Its ability to measure a large number of power quality problems such as sag, swell, harmonics, flickers, etc.
- Its ability to measure non-stationary disturbances that may overlap in the time and frequency domains.

- Its ability to give a measure of more than one power quality problem that may take place simultaneously.
- Its ability to monitor and measure a low frequency disturbance and localize it in time.
- Its ability to measure and determine other power system parameters such as the phase shift angle, active and reactive power and total harmonic distortion.

Another problem that exists in the available monitoring devices is the large dimensionality of the stored data and the complicity of the discrimination process. This leads to a substantial deterioration in the performance of traditionally favoured classifiers.

Data reduction is one of the main design factors for developing the automated recognition system. A wavelet-based technique is proposed to represent the distortion events by using small set of coefficients. This set of coefficients can be stored to represent the original distorted signal rather than storing a large size vector of the sampling points of the distortion event. The proposed data reduction technique is utilized to store and reconstruct the original distorted signals of steady state and transient events. The proposed data reduction technique is presented in Chapter 8.

The research in this thesis shows the capability of the wavelet-based technique for designing an automated wide-scale power quality monitoring system with the following characteristics:

- Fast detection and localization of disturbances that may overlap in time and frequency in a noisy environment.
- On-line classification by extracting discriminative, translation invariant features with small dimensionality, which can represent efficiently the voluminous amount of distorted data.
- Analysis of different non-stationary disturbances and measure of their indices.
- De-noising ability and high efficiency in data compression and storing.

A wavelet-based power quality automated recognition system is proposed in this thesis. This system can be implemented on-line for detecting, classifying, measuring and storing different power system disturbances. This system can overcome many of the drawbacks of existing monitoring devices.

9.2 Contributions

The contribution of this work comes from its ability to represent a single tool that can be used to construct an automated monitoring system. The design of the proposed automated monitoring system depends on five building blocks. These blocks can be constructed in parallel or sequentially to design a real time on-line automated monitoring system. Each block in the constructed system can perform superior better than existing monitoring systems.

The original contribution of the work done in this thesis is summarized in the following points:

Part A: Detection and duration measurement under noisy environment

Any distortion in the signal can be detected and localized using wavelet coefficients at the highest resolution level. However, as the noise level increases and the transient event magnitude decreases, the coefficients that represent the noise will merge with those that represent the distortion, the wavelet detection and localization property will no longer be valid at this resolution level. In general the noise level in power system is low, which is about 1.0%. This proposed method is very adequate in this range. For higher noise levels a new wavelet-based technique is proposed for detection and duration measurement.

The first step in the detection and duration measurement process in a noisy environment is to determine the noise level. An assessment of the noise level is measured by computing the energy of the coefficients at the highest resolution level. For high noise levels, the duration of the distortion event can be measured by reconstructing an approximated version of the distortion event using a selected set of the wavelet expansion coefficients.

Part B: Disturbance Classification

The energy of the distortion event at different resolution levels is used in this new technique as a feature vector that can classify different disturbances. These discriminative, translation invariant features with small dimensionality are used to classify different power quality problems that overlap in time and frequency. State of the art pattern recognition techniques were employed to evaluate the extracted features and classify different events.

Part C: Distortion Measurement

Since the energy of the distorted event is represented by a set of coefficients in the wavelet domain. Therefore, the norm of these coefficients is used to measure the energy in the distorted event. Combining the energy of the distortion event and its duration as measured in part A, the RMS value, dc content, phase shift and the THD% of the distorted signal can be computed. This technique is new and was implemented for the first time in measuring the RMS for power quality problems.

Part D: Non-Rectangular RMS variation Measurement

A new wavelet-based procedure to characterize non-rectangular RMS variations is presented in this thesis. This procedure can help in assessing the quality of service presented in a distribution system, the quality of the mitigation devices, and the characteristic of the load during RMS variation. Utilizing this procedure, a clear picture of any further changes in the harmonic distortion, noise level, or RMS variations can be detected, localized, classified, and quantified inside the distortion event.

Part E: Data Reduction

The feature vector presented in Equation 6.10 and the rapid drop off in the size of the coefficients are two important characteristics that can help in reducing the amount of data to be stored for the distortion event, as described in chapter 8.

The proposed techniques in this thesis can be implemented in hardware and installed on the system to give automatic detection, localization, and classification of any power quality phenomena according to IEEE std. 1159. These techniques are accurate, efficient, fast and reliable compared with the existing techniques. Additionally, the proposed technique has the ability to reduce the size of the data of the distorted event to a small size and store it. This technique can be implemented *on-line* and in *real-time* in the case of non-transient power quality problems. It can also be implemented in *real-time* for transient events by utilizing parallel processors, where each processor will take care of a specified resolution level. A general outline version of the automated power quality monitoring system is shown in Figure 9.1.

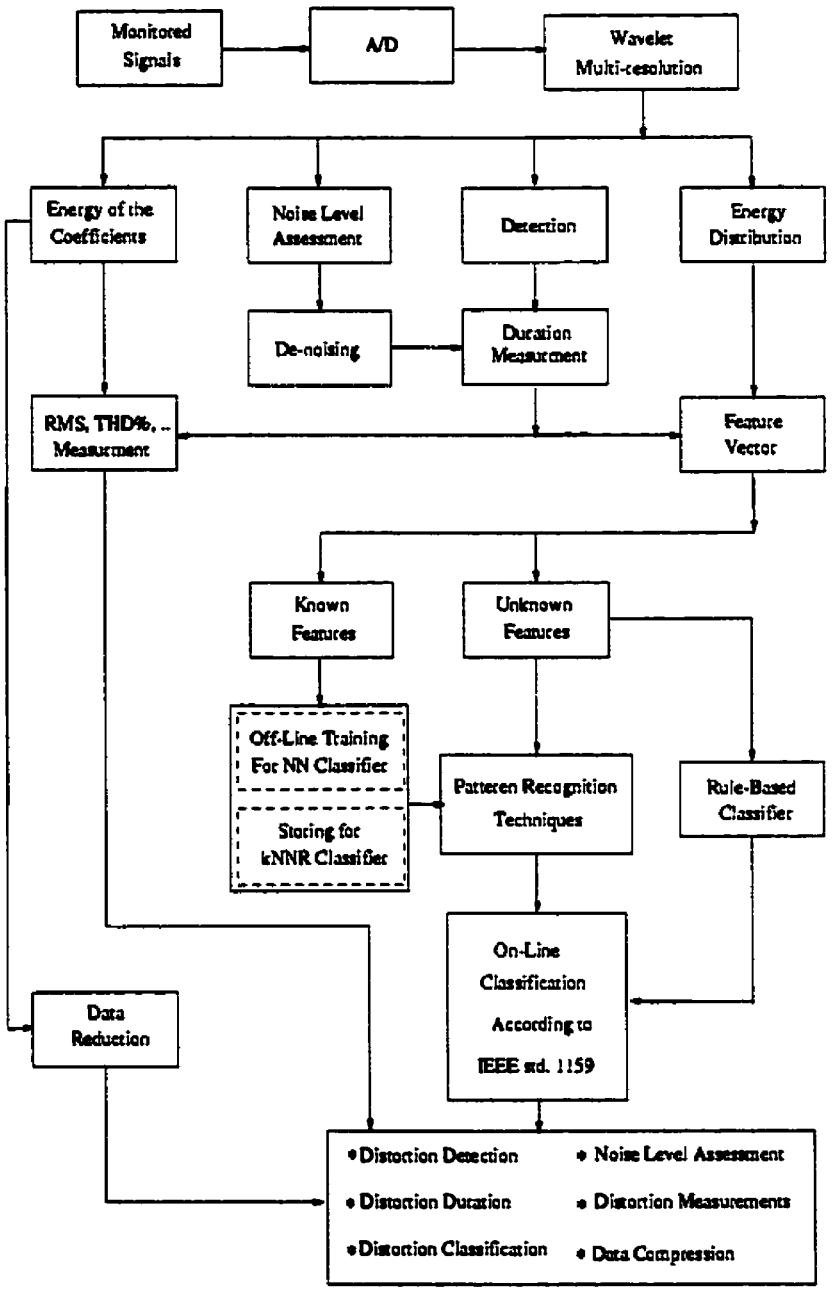

Figure 9.1: Wavelet-Based Automated Recognition System for Power Quality Monitoring

9.3 Future Research

The distinguished advantage of this automated system is its ability to be used readily in monitoring other complicated power quality problems that will arise from the deregulation of the power industry, such as:

1. Monitoring and control of different disturbances that may take place in HVDC systems. A preliminary result of this application is presented in [65].

2. Monitoring the disturbances in multi-ownership generation-transmission-distribution chain and identifying the source of any disturbance under an open market environment.

3. Monitoring and control of the mitigation devices and assessing their quality.

4. Monitoring the load characteristics during any variations.

5. Modifying voltage tolerance curves "CBEMA curve" to include high frequency content components and non-rectangular RMS variations.

6. Using the MRA technique to control the switches for designing active filters.

7. Using the feature vector to design a smart control and protection systems.

Appendix A

A.1 General Properties For Wavelet Multi-resolution:

In order to develop a multilevel representation of a signal $f(t)$ that belongs to $L^2(R)$ we seek a sequence of embedded subspaces V_j with the following properties:

1 - Containment property:

$$\underset{\text{Low-resolution}}{\{0\}} \subset \ldots V_{-2} \subset V_{-1} \subset V_0 \subset V_1 \subset V_2 \ldots \subset \underset{\text{High-resolution}}{L^2(R)}$$

$$\text{LessDetail} \qquad\qquad \text{MoreDetail}$$

The containment property imposes the subspace V_{j-1} be completely contained in subspace V_j. Since subspace V_{j-1} is embedded in subspace V_j, it follows that a signal in V_{j-1} is blurrier than the one in subspace V_j.

The containment property also implies that going to a finer subspace (higher resolution), one needs to add details to a signal and going to a coarser scale (lower resolution) one must give up details of the signal. This implies that in order to move a signal from one subspace to another subspace, one should add or take out details from the signal.

2 - Completeness property:

$$\bigcap_{j\in Z} V_j = \{0\} \quad \text{And} \quad \bigcup_{j\in Z} V_j = L^2(R)$$

The completeness property indicates that the union of each subspace V_j will form $L^2(R)$ and each subspace completely characterizes a signal in its subspace. Each subspace is spanned by integer translates of a single function, $\phi(t)$ such that

$$\phi(t) \in V_o \Leftrightarrow \phi(t+1) \in V_o$$

3 -Scaling properties:

$$\phi(t) \in V_j \Leftrightarrow \phi(2t) \in V_{j+1} \qquad \text{For any function } \phi \in L^2(R)$$

The scaling property relates how a function dilates or scales from one subspace to another. If $\phi(t)$ resides in V_j then $\phi(2t)$ exists in V_{j+1}. This means that elements in a space are simply scaled versions of the elements in the next space. Figure A.1 shows that the subspace V_1 is spanned by integer translates of a single function $\phi(2t)$, and the elements in the subspace V_o are a scaled and translated combination of the elements in space V_1.

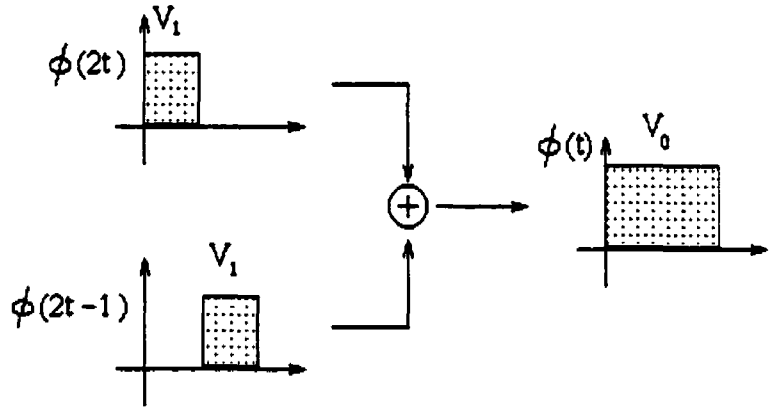

Figure A.1: The completeness and scaling properties

4- Basis property:

There exists a scaling function $\phi(t) \in V_o$ such that the translated and scaled version set $\phi_{j,k}(t)$ forms an orthonormal basis that spans V_m, i.e.

$$<\phi_{j,k}(t),\ \phi_{j,l}(t)> = \delta(k-l) = \begin{cases} 0 & k \neq l \\ 1 & k = l \end{cases}$$

A.2 The Multi-resolution Analysis process:

Using the scaling and wavelet functions a signal is analyzed from fine to coarser scale. Removing the details from the approximated versions at different resolution levels can decompose the signal at different resolutions.

The mathematical representation of the scaling function is given by the following Equation.

$$\phi(t) = \sum h(n)\sqrt{2}\phi(2t-n), \qquad n \in Z$$

Scaling and translating the time variable ($t = 2^j t - k$), we get :

$$\phi(2^j t-k) = \sum h(n)\sqrt{2}\phi(2(2^j t-k)-n),\ n \in Z$$

$$= \sum_n h(n)\sqrt{2}\phi(2^{j+1}t-2k-n)$$

let $m=2k+n$

$n=m-2k$

then

$$\phi(2^j t-k) = \sum_m h(m-2k)\sqrt{2}\phi(2^{j+1}t-m)$$

The subspace V_{j+1} can be denoted as:

$$V_{j+1} = span_k\{2^{(j+1)/2}\phi(2^{j+1}t-k)\}$$

The approximated version of $f(t) \in V_{j+1}$ can be expressed at scale $J+1$, as:

$$f(t) = \sum_k c_{j+1}(k)2^{(j+1)/2}\phi\,(2^{j+1}t-k)$$

Where only the scaling function is used, without the wavelet function, to approximate the signal. At one scale lower resolution j, the wavelet function is necessary to represent the details that are not available at scale j.

Therefore:

$$f(t)=\underbrace{\sum_k c_j(k)2^{j/2}\phi(2^j t-k)}_{\text{Approximated version}}+\underbrace{\sum_k d_j(k)2^{j/2}\psi(2^j t-k)}_{\text{Detail version}}$$

Where the term $2^{j/2}$ maintains the unit norm of the basis functions at various scales. For orthonormal scaling and wavelet functions, the expansion coefficients $c_j(k)$ and $d_j(k)$ can be calculated using the inner product as follows:

$$c_j(k)=\langle f(t),\phi_{j,k}(t)\rangle \;=\langle f(t),2^{j/2}\phi(2^j t-k)\rangle$$

$$c_j(k)=\langle f(t),\phi_{j,k}(t)\rangle=\int f(t)2^{j/2}\phi(2^j t-k)dt$$

From the previous calculation one must construct $f(t)$ to calculate the coefficient $c_j(k)$, however, one can obtain the coefficients $c_j(k)$ and $d_j(k)$ without constructing $f(t)$. This can be accomplished as follows:

We have

$$\phi(2^j t-k) \;=\sum_n h(m-2k)\sqrt{2}\phi(2^{j+1}t-m)\;, \qquad n\in Z$$

Therefore,

$$c_j(k)=\langle f(t),\phi_{j,k}(t)\rangle=\int f(t)2^{j/2}\sum_m h(m-2k)\sqrt{2}\phi(2^{j+1}t-m)dt$$

$$=\sum_m h(m-2k)\int f(t)2^{(j+1)/2}\phi(2^{j+1}t-m)dt$$

And $$\int f(t)2^{(j+1)/2}\,\phi(2^{j+1}t-m)dt = c_{j+1}(m)$$

Therefore

$$c_j(k) = \langle f(t), \phi_{j,k}(t)\rangle = \sum_m h(m-2k)\, c_{j+1}(m)$$

By the same way the detailed version coefficient $d_j(k)$ can be presented without involving $f(t)$ in the calculation. Therefore, the wavelet coefficient at scale j can be presented as

$$d_j(k) = \langle f(t), \psi_{j,k}(t)\rangle = \sum_m h_1(m-2k)\, c_{j+1}(m)$$

From the other hand, the detailed $d_j(k)$ and approximated $c_j(k)$ versions of the coefficients can be used to reconstruct the signal.

Consider a signal $f(t) \in V_{j+1}$, then this signal can be expressed at scale $J+1$ by using only scaling function as:

$$f(t) = \sum_k c_{j+1}(k)2^{(j+1)/2}\phi\ (2^{j+1}t-k)$$

Or in terms of a next scale (which requires a wavelet function) as:

$$f(t) = \sum_k c_j(k)2^{j/2}\phi\ (2^j t-k) + \sum_l d_j(l)2^{j/2}\psi(2^j t-l)$$

Where the scaling and translating scaling function can be presented as

$$\varphi(2^j t-k) = \sum_m h(m)\sqrt{2}\varphi(2^{j+1}t-2k-m)$$

And the wavelet function can be presented as:

$$\psi(2^j t-l) = \sum_n h_1(n)\sqrt{2}\varphi(2^{j+1}t-2l-n)$$

Therefore,

$$f(t) = \sum_k c_j(k) 2^{j/2} \sum_m h(m)\sqrt{2}\varphi(2^{j+1}t - 2k - m)$$

$$+ \sum_l d_j(l) 2^{j/2} \sum_n h_1(n)\sqrt{2}\varphi(2^{j+1}t - 2l - n)$$

$$f(t) = \sum_k c_j(k) 2^{(j+1)/2} \sum_m h(m)\varphi(2^{j+1}t - 2k - m)$$

$$+ \sum_l d_j(l) 2^{(j+1)/2} \sum_n h_1(n)\varphi(2^{j+1}t - 2l - n)$$

Due to orthonormality, the approximated and detailed coefficients ($c_j(k)$ and $d_j(k)$) can be calculated using the inner product as follows:

$$c_{j+1}(k') = \langle f(t),\ 2^{(j+1)/2}\varphi(2^{j+1}t - k')\rangle$$

$$c_{j+1}(k') = \int f(t)\ 2^{(j+1)/2}\varphi(2^{j+1}t - k')dt$$

$$= \int \{\sum_k c_j(k) 2^{(j+1)/2} \sum_m h(m)\varphi(2^{j+1}t - 2k - m) +$$

$$\sum_l d_j(l) 2^{(j+1)/2} \sum_n h_1(n)\varphi(2^{j+1}t - 2l - n)\}\ \ 2^{(j+1)/2}\varphi(2^{j+1}t - k')dt$$

$$= \sum_k c_j(k) \sum_m h(m)\int 2^{(j+1)/2}\varphi(2^{j+1}t - 2k - m)\ 2^{(j+1)/2}\varphi(2^{j+1}t - k')dt$$

$$+ \sum_l d_j(l) \sum_n h_1(n)\int 2^{(j+1)/2}\varphi(2^{j+1}t - 2l - n)\ 2^{(j+1)/2}\varphi(2^{j+1}t - k')dt$$

$$= \sum_k c_j(k) \sum_m h(m)\langle 2^{(j+1)/2}\varphi(2^{j+1}t - 2k - m),\ 2^{(j+1)/2}\varphi(2^{j+1}t - k')\rangle$$

$$+ \sum_l d_j(l) \sum_n h_1(n) \langle 2^{(j+1)/2} \varphi(2^{j+1}t - 2l - n),\ 2^{(j+1)/2} \varphi(2^{j+1}t - k') \rangle$$

Due to orthonormality, the inner product terms will be equal to zero and will be only equal to one if and only if:

$$2k + m = k' \qquad \text{and} \qquad 2l + n = k'$$

$$m = k' - 2k \qquad \text{and} \qquad n = k' - 2l$$

Therefore,

$$c_{j+1}(k') = \sum_k c_j(k) \sum_m h(m) + \sum_l d_j(l) \sum_n h_1(n)$$

$$c_{j+1}(k') = \sum_k c_j(k)\ h(k'-2k) + \sum_l d_j(l)\ h_1(k'-2l)$$

For convenience let $k' = n$, *and* $l = k$,

Therefore,

$$c_{j+1}(n) = \sum_k c_j(k)\ h(n-2k) + \sum_k d_j(k)\ h_1(n-2l)$$

Appendix B

B.1 Choice of appropriate mother wavelet

Different disturbances can be modeled and presented using different wavelet $\psi(t)$ and scaling $\phi(t)$ functions. The accuracy of this presentation depends on the smoothness of the selected mother wavelet function. As the number of vanishing moments of the selected wavelet function increases, more smoothness can be achieved and more accurate representation of the distorted signal is obtained. It has been documented in [37] that the wavelet spectrum is meaningful only when the selected wavelet has enough vanishing moments. Furthermore, the FFT of the selected wavelet has to decrease faster near the origin. This will provide sharper cut-off frequency to the selected mother wavelet and reduces the amount of leakage energy to the adjacent resolution levels.

Therefore, the criteria for selecting a proper mother wavelet is to have a wavelet function with a sufficient number of vanishing moments in order to represent the salient features of the disturbance. At the same time, this wavelet should provide sharp cut-off frequencies. Furthermore, the selected mother wavelet should be orthonormal.

The magnitude of the leakage energy of the analyzed pure signal at adjacent resolution levels due to utilizing different wavelets has been studied here with three types of orthonormal mother wavelets:

- Daubechies (db1, db4, db10, db40),
- Coiflet (coif1-coif5), and
- Symlet (sym2-sym8).

The frequency response of the Daubechies (db4, db10, db40) and Coiflet (coif5) wavelet functions (high pass filters) and scaling functions (low pass filters) are shown in Figure B.1. Daubechies 40

shows the sharper cut-off frequency compared with the others and hence the leakage energy between different resolution levels is reduced. The number of vanishing moments of the db40 wavelet is large, and hence it gives a meaningful wavelet spectrum of the analyzed signal.

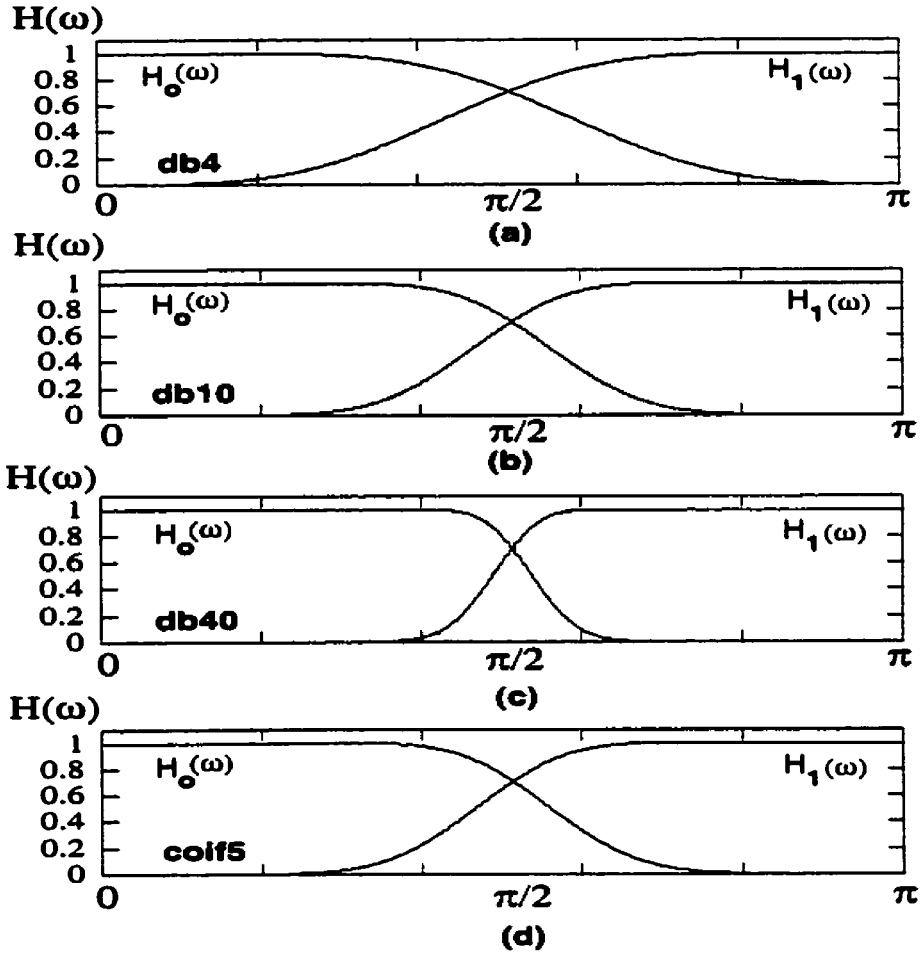

Figure B.1: Frequency response of the Wavelet filters

Comparison of the behavior of different wavelets for extracting the proposed features is implemented on the following signal:

Pure Signal: The 50 Hz power frequency pure signal is analyzed using different wavelets, (Figure B.2). Using db1, i.e. one vanishing moment, the energy of the pure signal is distributed over the different resolution levels (low and high frequency bands), Figure B.2a. This results from the wide

cut-off frequency of the selected filter shown in Figure B.1a. However, as the number of vanishing moments of the selected wavelet function increases (db40 with 40 vanishing moments), the energy of the analyzed pure signal is concentrated at the resolution level that covers the power frequency range (6^{th} resolution level), Figure B.2c. Only a small part of the signal energy is leaked to adjacent resolution levels 5^{th} and 7^{th}.

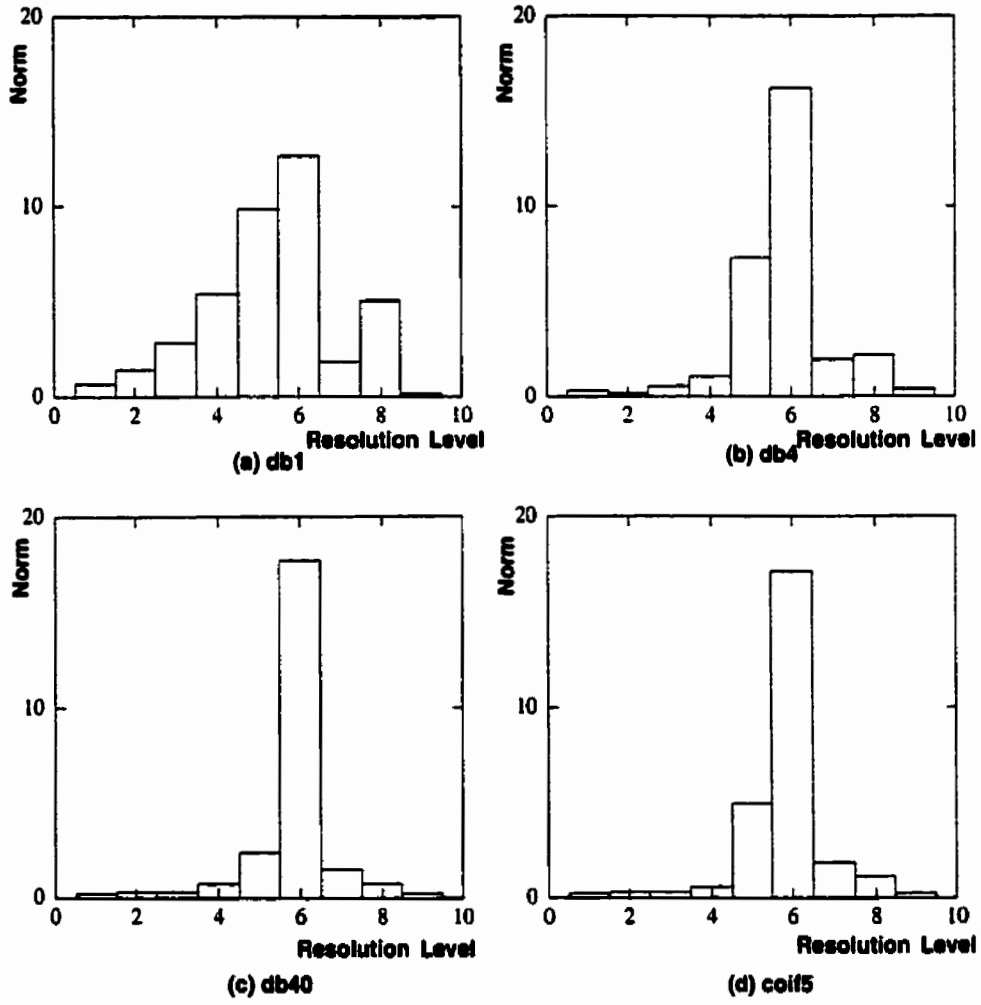

Figure B.2: Wavelet Transform Spectrum of 50Hz sine wave

Bibliography

[1] Math H. J. Bollen, "Understanding Power Quality Problems Voltage Sags and Interruptions," IEEE Press Series on Power Engineering, 2000.

[2] Roger C. Dugan, Mark F. McGranaghan, and H. Wayne Beaty, " Electric Power System Quality," McGraw-Hill 1996.

[3] G.T. Heydt, "Electric Power Quality," Stars in a Circle, 1994.

[4] Gregory J. Porter and J. Andrew Van Sciver, "Power Quality Solutions: Case Studies for Troubleshooters," The Fairmont press, Inc. 1999.

[5] Jos Arrillaga, Math H. J. Bollen, "Power Quality Following Deregulation," Proceedings of the IEEE, Vol. 88, No. 2, February 2000.

[6] J. Douglas, "Solving problems of power quality," in EPRI journal, Vol. 18, no. 8, pp. 6-15, Dec. 1993.

[7] A. Domijan, G.T. Hehdt, A.P.S. Meliopoulous, S.S. Venkata, S. West, "Directions of Research on Electric Power Quality," IEEE Transactions on Industry Applications, Vol. 8, No.1, 1993, p 429-436.

[8] Thomas S. Key, "Diagnosing power quality-related computer problems," IEEE Transactions on Industry Applications, Vol. IA-15, No.4, July/August 1979.

[9] W. Edward Reid, "Power Quality Issues – Standards and Guidelines," IEEE Transactions on Industry Applications, Vol. 32, No.3, May/June 1996, pp. 625-632.

[10] Erich W. Gunther and Harshad Mehta. "A survey of distribution system power quality- Preliminary Results," IEEE Transactions on Power Delivery, Vol. 10, No.1, Jan. 1995, pp 322-329.

[11] IEEE Working Group on Non-Sinusoidal Situations, "A Survey of North American Electric Utility Concerns Regarding Non-sinusoidal Waveforms," IEEE Transactions on Power Delivery Vol. 11, No.1, January 1996.

[12] Task Force on Harmonic Modeling and Simulation, " Modeling and Simulation of Propagation of Harmonics in Electric Power Networks, Part I: concepts, models, and simulation techniques," IEEE Transactions on Power Delivery Vol. 11, No.4, January 1996.

[13] Task Force on Harmonic Modeling and Simulation, "Modeling and Simulation of Propagation of Harmonics in Electric Power Networks, Part II: sample systems and examples," IEEE Transactions on Power Delivery Vol. 11, No.4, January 1996.

[14] IEEE task Force, "Effects of harmonics on equipment," IEEE transactions on industry applications, Vol. 38 No. 2, April 1993, p 672- 680.

[15] Jane M. Clemmensen "Estimating the cost of Power Quality," IEEE Spectrum, June 1993, pp 40-41.

[16] IEEE recommended practices for monitoring electric power quality, IEEE std. 1159-1995, New York: IEEE, 1995.

[17] Atish K. Ghosh, David L. Lubkeman "The classification of Power system disturbance waveforms using a neural network approach," IEEE Transactions on Power Delivery Vol. 10, No1, Jan.1995, pp. 109-115.

[18] S.J. Huang, C.L. Huang, and C.T. Hsieh, "Application of Gabor transform technique to supervise power system transient harmonics," IEE Proceeding of Generation, Transmission, and Distribution, Vol. 143, No. 5, September 1996.

[19] D.L. Brooks, R.C. Dugan, Marek Waclawiak, and Ashok Sundaram, "Indices for assessing utility distribution system rms variations," IEEE Transactions on Power Delivery Vol. 13, No1, Jan. 1998 pp.254-259.

[20] G.T. Heydt, W.T. Jewell, "Pitfalls of electric power quality indices," IEEE Transactions on Power Delivery Vol. 13, No2, Apr.1998., pp. 570-578.

[21] Girgis, A.A. and Ham, F., "A quantitative Study of Pitfalls in FFT," IEEE Trans. Aerosp. Electron. Syst., Vol. 16, No. 4, pp. 434-439, 1980.

[22] Jos Arrillaga, Bruce Smith, Neviller R. Watson and Alan R. Wood, "Power System Harmonic Analysis," John Wiley and Sons 1997.

[23] IEEE recommended practices for the design of reliable industrial and commercial power systems (The Gold Book), IEEE std. 493-1997.

[24] Jaideva C. Goswami and Andrew K. Chan "Fundamentals of wavelets: Theory, Algorithms, and Applications," John Wiley & Sons, inc. 1999.

[25] L. Prasad and S.S. Iyengar "Wavelet analysis with applications to image processing," CRC press 1997.

[26] Ingrid Daubechies, "Ten Lectures on Wavelets," Society for Industrial and applied mathematics, 1992.

[27] Olevier Rioul and Martin Vetterli, " Wavelets and signal processing," IEEE SP Magazine, Oct.1991.

[28] C. Sindney Burrus, Ramesh A. Gopinath, Haitao Guo, "Introduction to wavelets and Wavelet transform," Prentice Hall, New Jersey, 1997.

[29] Nikolaj Hess-Nielsen and Mladen Victor Wickerhauser "Wavelets and Time Frequency Analysis," Proceedings of the IEEE Vol.84, NO.4, pp 523-540, Apr.1996. "Invited Paper"

[30] Stephane G. Mallat "A Theory for Multiresolution Signal Decomposition: The Wavelet Representation," IEEE Transactions on Pattern Analysis and Machine Intelligence, Vol. 11, No.7, July 1989, pp674-693.

[31] John R. Williams and Kevin Amaratunga "Introduction to Wavelets in Engineering," International Jornal for Numerical Methods in Engineering, Vol.37, 2365-2388 (1994).

[32] A.W. Galli, G.T. Hydet, P.F. Riberio, "Exploring the power of wavelet analysis," IEEE Computer Applications in Power, Oct. 1996, pp 37-41.

[33] Andrew Bruce, David Donoho, and Hong-Ye Gao "Wavelet Analysis," IEEE Spectrum, pp 26-35, Oct. 1996.

[34] Albert Cohen and Jelena K. "Wavelets: The mathematical background," Proceedings of the IEEE, Vol.84, NO.4, Apr.1996.

[35] Les E Atlas, Garry D Bernard, and Siva Bala Narayanan, "Applications of Time-Frequency Analysis to Signals From Manufacturing," Proceedings of the IEEE, Vol.84, NO.9, pp 1319-1329 Sep.1996.

[36] Wim Sweldens "Wavelets: What Next," Proceedings of the IEEE, Vol.84, NO.4, pp 680-685, Apr.1996.

[37] Perrier, Philipovitch, and Basdevant, "Wavelet spectra compared to Fourier spectra," Journal of Mathematical Physics, Vol. 36, No. 3, March 1995, pp 1506-1519.

[38] Course Notes, Prof. George Freeman "Wavelets in Signal Processing," University of Waterloo, E&CE, Fall term, 1997.

[39] Hwei P. Hsu, "Applied Fourier Analysis," HBJ 1984.

[40] E. Oran Brigham, "The fast Fourier Transform and its applications", Prentice Hall International, 1988.

[41] S. Santoso, E.J Powers, W.M Grady, P. Hofmann, "Power quality assessment via wavelet transform analysis," IEEE Transactions on Power Delivery Vol. 11, No2, Apr.1996.

[42] S. Santoso, W.M. Grady, E.J. Powers, Jeff Lamoree, Siddhart C. Bhatt, "Characterization of Distribution Power quality events with Fourier and Wavelet Transforms," IEEE Transactions on Power Delivery Vol.15, No1, Jan. 2000, pp.247-254.

[43] David C, Robertson, Octavia I. Camps, Jeffrey S. Mayer, and William B. Gish, "Wavelets and Electromagnetic Power System Transients," IEEE Transactions on Power Delivery Vol. 11, No.2, April 1996, pp1050-1058.

[44] Christopher M. Johnson, Edward W. Page and Gene A. Tagliarini, "Signal Classification using Wavelets and Neural Networks," Proceedings SPIE, The International Society for Optical Engineering, International Symposium on Wavelet Applications III, 8-12 April 1996, Orlando, Florida.

[45] S.-J. Huang, C.-T. Hsieh, and C.-L. Huang, "Application of Morlet Wavelets to Supervise Power System Disturbances," IEEE Transactions on Power Delivery Vol. 14, No.1, January 1999, pp235-243.

[46] S.K. Pandey and L. Satish, "Multiresolution Signal Decomposition: A New Tool For Fault Detection In Power Transformers During Impulse Tests," IEEE Transactions on Power Delivery Vol. 13, No.4, October 1998, pp1194-1200.

[47] L. Angrisani, P. Daponte, M. D'Apuzzo, and A. Testa, "A measurement method based on the wavelet transform for power quality analysis," IEEE Transactions on Power Delivery, Vol. 13, No.4, October 1998.

[48] Weon-Ki Yoon and Michael J. Devaney, "Power measurement using the wavelet transform," IEEE Transactions on Instrumentation and Measurement, Vol. 47, No.5, Oct.1998, pp 1205-1209.

[49] P. Pillay, A. Bhattacharjee, "Application of wavelets to model short term power system disturbances," IEEE Transactions on Power Systems, Vol. 11, No.4, Nov.1996.

[50] W.A. Wilkinson, and M.D. Cox, "Discrete Wavelet analysis of power system transients," IEEE Transactions on Power systems, Vol. 11, No.4, Nov.1996.

[51] S. Santoso, E.J. Powers, W.M. Grady, "Power quality disturbance data compression using wavelet transform methods," IEEE Transactions on Power Delivery Vol.12, No3, July 1997, pp.1250-1257.

[52] T.B. Littler and D.J. Morrow, "Wavelets for the analysis and compression of Power system disturbances," IEEE Transactions on Power Delivery, Vol. 14, No.2, April 1999, pp. 358-364.

[53] G.T. Heydt, A.W. Galli, "Transient Power Quality Problems Analyzed Using Wavelets," IEEE Transactions on Power Delivery, Vol. 12, No.2, April 1997.

[54] A.P. Sakis Meliopoulos, Chien_Hsing Lee, "Wavelet Based Transient Analysis," North American Power Symposium, Oct. 1997, pp 339-346.

[55] Tongxin Zheng, Elham B. Makram, and Adly A. Girgis, "Power System Transient and Harmonic Studies Using Wavelet Transform," IEEE Transactions on Power Delivery Vol. 14, No.4, October 1999, pp1469-1476.

[56] Oinis Chaari, Michel Meunier, and Francoise Brouaye, "Wavelets: A new tool For the Resonant grounding power distribution system relaying," IEEE Transactions on Power Delivery Vol. 11, No.3, July 1996.

[57] F.H. Magnago and A. Abur, "Fault location using traveling waves and wavelet transform," North American Power Symposium, Oct. 1997, pp 332-338.

[58] Shyh-Jier Huang and Cheng-Tao Hsieh, "High-Impedance Fault Detection Utilizing A Morlet Wavelet Transform Approach," IEEE Transactions on Power Delivery Vol. 14, No.4, October 1999, pp1401-1410.

[59] Moises Gomez-Morante, Denise W. Nicoletti, "A Wavelet-based Differential Transformer Protection, " IEEE Transactions on Power Delivery Vol. 14, No.4, October 1999, pp1351-1356.

[60] A.M. Gaouda, M.M.A. Salama, M. Sultan and A. Chikhani, "Application of Multi-resolution signal decomposition For Monitoring Short-duration variations in distribution Systems," IEEE Transaction on Power Delivery, Vol.15, No.2, April 2000, pp.476-485.

[61] A.M. Gaouda, M.M.A. Salama, M. Sultan and A. Chikhani, "Power Quality Detection and Classification using Wavelet-Multi-resolution Signal Decomposition," IEEE Transaction on Power Delivery, Vol.14, No.4, October 1999, pp-1469-1475.

[62] A.M. Gaouda, S.H. Kanoun, M.M.A. Salama, "On-line Disturbance Classification Using Nearest Neighbor Rule," The International Journal of Electric Power Systems Research.

[63] A.M Gaouda, M.M.A. Salama, A. Chikhani and V.K. Sood, "Automating the classification of Power System Disturbances," IASTED International Conference Power and Energy Systems (PES 2000) September 19-22, 2000 Marbella, Spain.

[64] A.M. Gaouda, S.H. Kanoun, M.M.A. Salama, and A. Chikhani, "Wavelet-Based Intelligent System For Monitoring Non-Stationary Disturbances" 2000 Electric Deregulation and Restructuring, and Power Technologies Conference, 4-7 April, 2000 London, United Kingdom, 84-89.

[65] A.M. Gaouda, E.F. El-Saadany, M.M.A. Salama, V.K. Sood, and A.Y. Chikhani, "Disturbance Monitoring in HVDC Systems Using Wavelet-Multi-resolution Analysis," 2000 Electric Deregulation and Restructuring, and Power Technologies Conference, 4-7 April, 2000 London, United Kingdom, pp 678-684.

[66] A.M Gaouda, M.M.A. Salama, M. Sultan "Automated Recognition System for classifying and quantifying The Electric Power Quality " 8th international conference on harmonic and quality of power, October 14-16, 1998, Athens – Greece, pp 244-248.

[67] A.M Gaouda, M.M.A. Salama, A. Chikhani, and M. Sultan, "Application of wavelet analysis for monitoring dynamic performance in industrial plants," North American Power Symposium, Oct. 1997, Laramie, Wyoming, pp325-331.

[68] Sanjit K. Mitra and James F. Kaiser, "Handbook for Digital Signal Processing," John Wiley & Sons, 1993.

[69] Emmanuel C. Ifeachor and Barrie W. Jervis, "Digital Signal Processing: A Practical Approach," Addison-Wesly, 1993.

[70] C. Sidney Burrus, James H. McClellan, A.V. Oppenheim, T.W. Parks, R.W. Schafer and H.W. Schuessler, "Computer-Based Exercises for Signal Processing using Matlab," Matlab Curriculum Series, Prentice hall, 1994.

[71] S.O. Belkasim, M. Shridhar, M. Ahmadi, "Pattern recognition with moment invarients: a comparative study and new results," Pattern Recognition, Vol.24, No.12, 1991, pp.1117-1138.

[72] S.O. Belkasim, M. Shridhar, M. Ahmadi, "Pattern classification using an efficient KNNR," Pattern Recognition, Vol.25, No.10, 1992, pp.1269-1274.

[73] Sholom M. Weiss and Casimir A. Kulikowski, "Computer Systems That Learn," Morgan Aufmann Publishers 1991.

[74] S. Theodoridis and K. Koutroumbas, "Pattern Recognition," Academic Press 1999.

[75] H. Mori, "An artificial neural network based method for power system voltage harmonics," IEEE Trans. On Power Delivery, Vol. 7, No. 1, pp. 402-409, 1992.

[76] R. K. Hartana, and G. G. Richards, " Harmonic source monitoring and identification using neural networks," IEEE Trans. on Power Systems, Vol. 5, No. 4, pp. 1098-1104, Nov. 1990

[77] Sonja E., David L.L., and Mark W., " A neural network approach to the detection of incipient faults on power distribution feeders", IEEE Transactions on Power Delivery, Vol. 5, No. 2, pp. 905-914, 1990.

[78] Dejan J. S., and Yoh-Han P., "Artificial neural net based dynamic security assessment for electrical power systems," IEEE Transactions on Power Systems, Vol. 4, No. 1, pp. 220-228, Feb.1989.